TECHNISCHE UNIVERSITÄT WIEN

D I S S E R T A T I O N

New approaches for elemental analysis of advanced solid materials using Laser-Assisted Plasma Spectrochemistry.

ausgeführt zum Zwecke der Erlangung des akademischen Grades eines Doktors der technischen Wissenschaften

unter der Leitung von

Univ.Prof. Dipl.Ing. Dr.tech. Andreas Limbeck

E164 - Institut für chemische Technolgie und Analytik

eingereicht an der Technischen Universität Wien Fakultät für Technische Chemie von

Dipl.Ing. Weiss Maximilian BSc

01326639

Wien am 16.03.2022

Dimidium facti, qui coepit, habet: sapere aude, / incipe!
Horaz, Epistulae 1,2,40

1 Abstract

To face the challenges of the 21st century, material science has made tremendous progress in the last years. To tailor materials to their supplication, it is crucial to understand the relationship between the composition of the material and the desired properties. This begins with the production process, over the understanding of degradation processes during the application until the disposal, where knowledge of the composition is necessary for proper recycling. To accomplish this, a throughout analytical characterization is necessary. One of the most promising classes of methods that have gained increasing attention in recent years are based on laser ablation. A small portion of the sample is vaporized by high power pulsed laser, and either the light emitted from the plasma formed by the ablated material is monitored, or the condensed material is transported into a hyphenated instrument such as an ICP-MS for elemental analysis.

These methods have several advantages, such as little sample consumption, practically no or only minor sample preparation, high sensitivity for most elements, and the possibility of spatially and depth resolved analysis. However, currently these methods face limitations, whose solution is this thesis's topic: The main problem in solid state analysis remains the quantification of the obtained signals, as for the correction of matrix effects matrix matched standards are required. The commercial availability of those reference materials is limited, especially for novel classes of materials, and the production of in-house standards is laborious. The second issue is the limited depth resolution obtained with standard nanosecond lasers due to the laser-sample interaction, which usually constrains the depth resolution to the micrometer range. Some elements,like fluorine, are not accessible with many methods, which can reasonably only be measured with laser-induced breakdown spectroscopy, but with a sensitivity not sufficient for many applications.
This thesis consists of four manuscripts, of which three are published in peer-reviewed journals and one to be submitted, in which the issues listed above are resolved:

- **Use of liquid standards to determine the stoichiometry of boride thin films:** To overcome the need for matrix-matched standards, two methods for using liquid standards are investigated for laser ablation: dried droplets for LIBS and self-aliquoting microgrooves for LA-ICP-MS. Using these as in-house standards, it was possible to gain insight into the stoichiometry of several ternary transition metal diboride systems.

- **Characterization of the platinum surface decoration with online-LASIL:**

To understand the decoration of cathode materials of solid oxide fuel cells with platinum enhanced the oxygen reduction kinetics. With the recently introduced online-LASIL method, a depth resolution of <50 nm was achieved, sufficient to quantify the platinum concentration only on the surface. With spatially resolved measurements, gradients in the sample could be uncovered, and the production process could be optimized.

- **Quantitative depth profiling using online-LASIL:**Online-LASIL is used to perform quantitative depth profiling on silicon doped chromium boride samples which underwent oxidation experiments. It was possible to gain insights into the composition of the oxide layer. The results were confirmed by data from a throughout material science characterization.

- **Spatially resolved molecular enhanced LIBS of fluorine:** Fluorine is an element only hardly accessible with LIBS. To overcome this limitation, molecular emission instead of atomic emission can be used. Two methods to apply a thin layer of an external element were investigated and compared to introduce a molecular forming element. Thereby for the first time spatially resolved analysis of fluoropolymers could be performed using this technique.

Using the findings in this thesis, it is possible to enhance the applicability of laser ablation-based methods to a broad spectrum of material-science related questions. The presented methods can flexibly be adapted to other material systems of interest.

2 Zusammenfassung

Um die Herausforderungen des 21.Jahrhunderts zu meistern, hat die Materialwissenschaft in den letzten Jahren enorme Fortschritte gemacht. Um Werkstoffe auf ihre Anforderungen zuzuschneiden, ist es entscheidend, die Beziehung zwischen der Zusammensetzung des Werkstoffs und den gewünschten Eigenschaften zu verstehen. Dies beginnt mit den Produktionsprozessen, über das Verständnis von Korrosion bis hin zur Entsorgung. Um dies zu erreichen, ist eine Analyse der elementaren Zusammensetzung notwendig. Die auf Laserablation basierenden Methoden LIBS, LA-ICP-MS und zuletzt online-LASIL haben in den letzten Jahren enorm an Bedeutung gewonnen und sind am Sprung routinemäßig eingesetzt zu werden. In der Laserablation wird ein kleiner Teil der Probe wird mit einem gepulsten Hochleistungslaser verdampft, und entweder wird das Licht, das von dem durch das abgetragene Material gebildeten Plasma emittiert wird, gemessen, oder das abgetragene Material wird in ein gekoppeltes Gerät, meist ICP-MS transportiert.

Zu den Vorteilen dieser Methoden zählen ein geringer Probenverbrauch, kaum Probenvorbereitung, eine hohe Empfindlichkeit für die meisten Elemente und die Möglichkeit orts- und tiefenaufgelöst zu messen. Allerdings stoßen diese Methoden derzeit auch an ihre Grenzen, die die Problemstellung dieser Arbeit sind: Einige Elemente sind kaum zugänglich, wie z.B. Fluor, das nur mit LIBS gemessen werden kann, allerdings mit einer für viele Anwendungen nicht ausreichenden Empfindlichkeit. Das Hauptproblem der direkten Festkörperanalytik ist nach wie vor die Quantifizierung der erhaltenen Signale, da zur Korrektur von Matrixeffekten angepasste Standards benötigt werden. Die kommerzielle Verfügbarkeit solcher Referenzmaterialien ist begrenzt, insbesondere für neue Materialklassen, und die Herstellung eigener Standards inhouse ist arbeitsaufwendig. Das dritte Problem ist die begrenzte Tiefenauflösung, die mit Nanosekundenlasern aufgrund normalerweise auf den Mikrometerbereich beschränkt ist. Diese Arbeit besteht aus vier Manuskripten, von denen drei bereits in peer-reviewten Fachzeitschriften veröffentlicht wurden und eines noch eingereicht wird, in denen die oben genannten Probleme gelöst werden:

- **Verwendung von Flüssigkeitsstandards zur Bestimmung der Stöchiometrie von Borid-Dünnschichten:** Um die Notwendigkeit eines matrixangepassten Standards zu überwinden, wurden zwei Methoden zur Verwendung von Flüssigkeitsstandards für die Laserablation untersucht: dried dropplets für LIBS und selbstaliquotierende Micro-grooves für LA-ICP-MS. Die Verwendung dieser als Inhouse-

Standards ermöglichte es, die Stöchiometrie mehrerer ternärer Übergangsmetall-Diborid-Systeme zu untersuchen.

- **Charakterisierung der Platin-Oberflächenbelegung mit Online-LASIL:** Die Beschictung von Kathodenmaterialien von Festoxid-Brennstoffzellen mit Platin verbessert die Sauerstoffreduktionskinetik. Mit der kürzlich eingeführten Online-LASIL-Methode wurde eine Tiefenauflösung von $<$50 nm erreicht, die ausreicht, um die Platinkonzentration nur auf der Oberfläche zu quantifizieren. Mit räumlich aufgelösten Messungen konnten Gradienten in der Probe aufgedeckt und der Produktionsprozess optimiert werden.

- **Quantitative Tiefenprofile mit Online-LASIL:** Online-LASIL kann die Verwendung von matrixangepassten Referenzmaterialien umgangen werden. Dies wurde genutzt, um eine quantitative Tiefenprofilierung an siliziumdotierten Chromboridproben durchzuführen, die Korrosionsexperimenten unterzogen wurden. Es war möglich, Einblicke in die Stöchiometrie der Oxidschicht zu gewinnen. Die Ergebnisse wurden mit Daten der materialwissenschaftlichen Charakterisierung bestätigt.

- **Ortsaufgelöste LIBS Analytik von Fluor:** Fluor ist ein Element, das mit LIBS nur schwer zugänglich ist. Molekulare Emission anstelle von atomarer Emission zu verwenden ist eine Möglichkeit die Empfindlichkeit für Fluor zu steigern. Zwei Methoden zum Aufbringen einer dünnen Schicht eines Elements, dass mit Fluor im Plasma ein Molekül bilden kann, wurden untersucht und verglichen, und zum ersten Mal diese Technik für die ortsaufgelöste Analyse von Fluorpolymeren zu verwenden.

Mit den in dieser Arbeit gewonnenen Erkenntnissen ist es möglich, die Anwendbarkeit von auf Laserablation basierenden Methoden auf ein breites Spektrum von materialwissenschaftlichen Fragestellungen zu erweitern. Die vorgestellten Methoden lassen sich flexibel auf andere Materialsysteme anpassen.

3 Acknowledgments

The success of the last three years would have been unthinkable without the support of the people surrounding me. First of all, I have to express my gratitude to my PhD supervisor Andreas Limbeck, who has given me the opportunity to be part of his research group for many years now and has been the best mentor to guide me through my PhD journey. Fruitful collaborations led to an astonishing number of publications. First, I have to acknowledge our partners in the FWF project, Jürgen Fleig and his group, and especially Christoph Riedl, the second PhD student in the project. Second, Paul Mayrhofer and Helmut Riedl-Tragenreif and their group of the Institute of Material Science. Through the years my colleagues from the research group and the 4th floor made the time I spent in the lab very enjoyable and provided inspiration and support, especially the former/fellow PhD Students from my group, as well as the many Master, Bachelor and Internship Students, form the last years. Essential was also the support from the technicians of our institute, especially Johannes Frank, Wolfgang Tomiscko, Elisabeth Eitenberger, and Kurt Piplits. My years at the university were delighted by many people whom some accompanied me since my first day and sometimes also joined me in activities outside of academia. Also, my friends outside of the university should not be forgotten. Last, I must thank my parents and family for their support and for sparking my interest in science and technology since my preschool years.

Contents

1 Introduction

1.1 Outline

The urge to reduce anthropogenic CO_2 emissions has created the need for new technologies to drive the decarbonization. New materials play an essential part in this goal, for example, as functional materials in solar cells, fuel cells, and batteries or as coatings for high-temperature applications to increase fuel efficiency and elongate their lifetime. Novel properties are created by skillful combinations of diverse elements in new, elaborate production techniques. Innovative classes of materials are created, from classical metals to high-performance ceramics. The need to understand the properties of these materials creates the urge for a stringent analytical characterization. Especially when innovative production techniques are applied, for example, the diverse physical and chemical vapor deposition methods, it is well recognized that the link between the precursor substances and the composition of the final products needs to be established. It is, for example, a known problem in physical vapor deposition techniques that the prepared sample can deviate from the precursor composition. In this case, the precursor must be adapted to deposit the stoichiometry that delivers the required performance. The exact stoichiometric composition and the addition of dopants at trace and ultra-trace levels play a crucial role and unwanted impurities that can be incorporated into these materials. However, even when the material shows excellent properties at fabrication, they may change with ongoing use, leading to a degradation of their properties. As contaminants from the environment can diffuse in the material, the surface can undergo an oxidation reaction. At the end of the lifetime, materials are discarded. Here complete recycling of the often valuable and rare elements is required. Therefore, the exact type of material needs to be identified and separated from the rest of the components, which often involves supplementary structures.

For this needs, analytical techniques for comprehensive sample characterization are desired. This includes the stoichiometry of the sample as well as the level of dopants and

impurities. To access the homogeneity and distribution of the elements, sometimes also a spatially resolved analysis is desired. Ideal methods give the desired information with reasonable margins of errors and involve little to no sample handling, are not restricted on the nature or structure of the sample, are non-destructive, and do not require additional materials for calibration and quantification. However, these characteristics are not provided by any single method, and compromises must be made.

The development of an analytical method evolves over distinctive stages.[1, 2] Several steps occur from the evaluation of the physical principle until the implementation of routine protocols. In this work, we explore comparably novel methods, parts of the instrumentation are commercial, like the basis instruments of Inductively Coupled Plasma - Mass Spectrometry and optical emission spetrometry (ICP-MS/OES), but others, like the online-LASIL setup, are made in-house, as the sample and standard preparation methods, which are developed from physicochemical principles to new protocols which are then applied to practical applications, to solve research questions which are not accessible with current techniques. In the following chapters, the physical fundamentals of plasmas are described, then the topic of laser ablation, as these two form the basis for all methods used in this work. The next part is the application of those in the practical methods of (LA-)ICP-MS and LIBS. Laser-based methods are put in the context of the analysis of solid samples and are compared with other methods, and the challenges in the field will then be described. The section after that is devoted to the concrete methods used in this thesis.

1.2 Theoretical Background

1.2.1 Plasma Spectrochemistry

A plasma is a gaseous form of matter that is, at least partly, ionized. Typically, it contains ions, electrons, and neutral gaseous species. A plasma is characterized by its temperature and the number density of the species it contains. For spectrochemical purposes, ambient pressure high-temperature plasmas are of interest. The temperature in those is typically in the range of 5.000 – 20.000 K. In a plasma, an ionization equilibrium between neutral species and ions electrons exists. At those temperatures, plasmas emit several forms of electromagnetic radiation, continuous thermal emission, and characteristic atomic and molecular emission. The latter is of analytical interest, as it allows to interfere quantita-

tively the composition of the material forming the plasma. Characteristic emission stems from the electronic transitions from excited states to lower ones. Thereby the difference in energy is released as a photon. Excited states in the plasma are created by the collision of ground-state atoms and ions with other species. The excitation/deexcitation process is an equilibrium; the Saha-Boltzmann Equation describes the ratio of different states:

$$\frac{n_{i+1}n_e}{n_i} = \frac{2}{\sqrt{\frac{h^2}{2\pi m_e k_B T}}^3} * \frac{g_{i+1}}{g_i} * \exp -\frac{\varepsilon_{i+1}-\varepsilon_i}{k_B T}$$

Whereas N_e is electron density n_{i+1} and n_i are the population of the upper (excited) and the lower state, h is the Planck's constant, m_e is the mass of the electron, k_B is Boltzmann's constant, T is the temperature of the plasma, ε_{i+1} and ε_i are the energy levels of the upper and the lower state, g_{i+1} and g_i are the degeneracies of the upper and the lower state.[3] [4][5]

To create a plasma material needs to be transformed in the gaseous state and ionized. This is accomplished through the introduction of high amounts of energy. The two ways relevant to this work are laser ablation and inductively coupled plasmas.

1.2.2 Laser Ablation

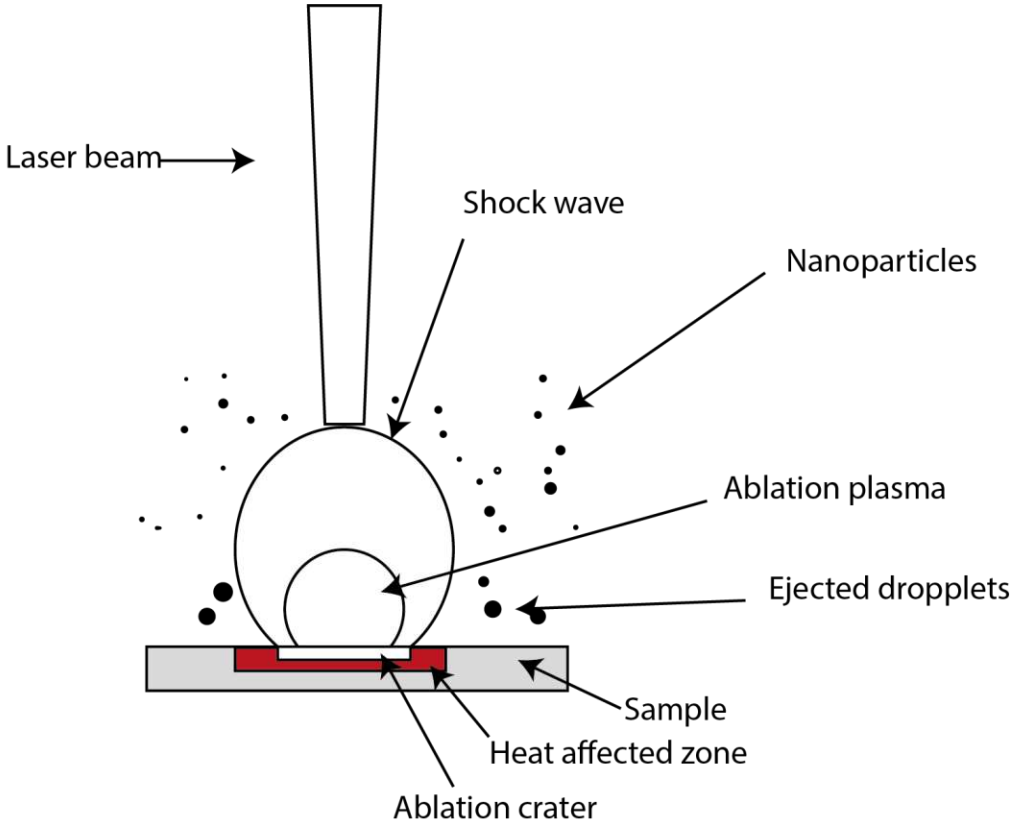

Figure 1: Schematics of the laser ablation process, showing the involved parts.

A small portion of the solid sample can be removed via irradiation with a high-power laser pulse in laser ablation sampling. This effect was discovered shortly after introducing the first lasers in 1962.[6] Laser ablation can not only be used for analytical purposes but is also an established technique for the production of nanoparticles [7] or to produce thin films if the ablated material condenses. Laser ablation is a complex, nonlinear, physical process in which particles, atoms, ions, electrons, and photons are formed from the ablated material and processes over magnitudes of time scales happens, and is in general poorly understood from a fundamental point; [8, 9] in the following the main characteristics and known processes will be described briefly:

A laser is a light source that emits coherent, directional, high-intensity radiation. Lasers can be based on various physical processes, for analytical laser ablation, pulsed solid-state lasers, such as Nd:YAG and Ti:sapphire, or gas lasers, such as excimer lasers,

are used. Laser pulses for ablation are typically in the time range from about 10^{-13} to 10^{-8} s and with irradiances from 10^{6} to 10^{14} W/cm^2.[10] The fluence of a laser is the energy delivered per area (J/cm^2), the irradiance is the power density of the laser beam at the sample (W/cm^2).[5]

In the first step of the laser ablation process, photons of the laser pulse interact with the sample. They are absorbed by linear or nonlinear mechanisms and excite electrons in the sample; if the irradiance is above a certain threshold, a phase transition of the solid in the vapor phase is induced. The ablated plume can then ionize to form a plasma if enough energy is transferred to the sample. The plasma plume forms in a few nanoseconds so that it can absorb incoming laser photons, typical pulse durations of nanosecond lasers are 5-20 ns, through inverse Bremsstrahlung of the free electrons, which shields the sample from the laser radiation, the so-called plasma-shielding, through this process the plasma is further heated.[8] As the material cools down, ions recombine with electrons to neutral atoms and can form molecules until they finally condense into particles, which a gas stream can then transport into an ICP instrument. A schematic of the process is shown in Figure1. The lifetime of the plasma plume is in the order of 10-100 µs, then the plasma extinguishes.[5]

The generated particles generally have a size from low nm to tens of µm. A narrow distribution of small particles is desired for analytical purposes to achieve a high transport efficiency, i.e., the number of generated particles that reach the detection system; This also reduces fractionation effects. The composition of the generated particles can differ from the bulk composition of the investigated material; usually, in the particles, an enrichment of more volatile species can be found; however, this can be corrected with matrix-matched standards for signal quantification. Several parameters are influencing this process, which will be discussed in the following, as their understanding is critical for this work, shortly summarized in Figure 2.

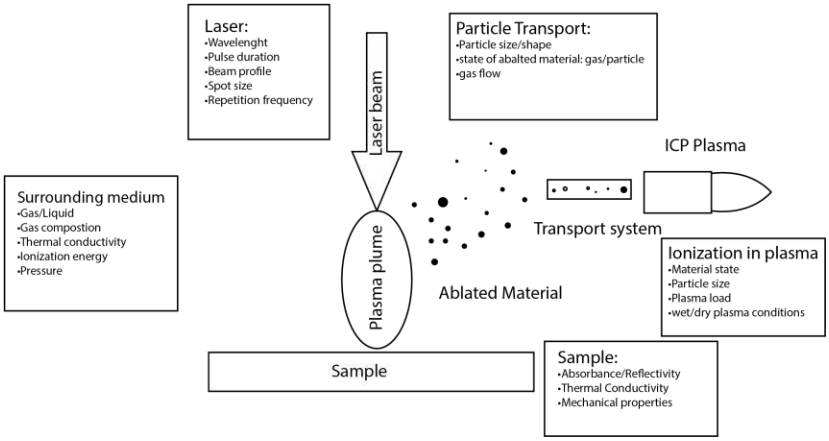

Figure 2: Schematics of the laser ablation process, showing the involved parts.

The duration of the laser pulse determines to a large extent the physical processes of the ablation. For most routine and research applications, nanosecond lasers are used. The short pulse duration is necessary to reach high peak fluences. Shorter pulses in the pico- and femtosecond range have generally been found of superior analytical performance, due to the absence of thermal effects, as the ablation occurs before the absorbed energy can diffuse as heat into the material. Femtosecond laser ablation was found to reduce fractionation and a better crater shape as no melting of the sample surrounding the ablation spot occurs, offering a better depth resolution in depth-profile measurements. However, the required setup is much more complex and expensive, so femtosecond lasers are much rarer than nanosecond lasers in research laboratories.[11, 12]

Laser wavelengths from the deep ultraviolet to the near-infrared are in use. Non-conductive materials generally absorb lower wavelengths better, so UV lasers are beneficial for their ablation. Metallic samples profit more from a shorter pulse duration due to their higher heat conductivity.[6] The surrounding medium has a considerable influence on the plasma and aerosol; for LA-ICP-MS measurements, where a carrier gas is strictly needed, helium is the medium of choice. Compared to argon, used in the early days, it creates a finer aerosol which leads to a better transport efficiency.

Laser-based methods are not limited to gaseous atmospheres, it is also possible to perform laser ablation in a liquid medium, as long as the liquid is transparent to the laser wavelength. On a surface, the technique is then called pulsed laser deposition.[13]

Especially LIBS was also demonstrated with liquids and gases.[14] In liquid media, the ablation generates a shock wave in the liquid. The temperature and pressure in the plasma are higher due to the confinement in the liquid, influencing the condensation of the particles. Further, the liquid is more reactive and can lead to chemical reactions of the formed particles.[15]

There are two principal ways of using laser ablation for analytical chemistry: The removed part can then be analyzed via the characteristic emission of the plasma (as in Laser-induced breakdown spectroscopy) or be transported to a hyphenated instrument for subsequent elemental analysis, in most cases, an ICP-MS or ICP-OES.[16]

1.2.3 LA-ICP-MS (OES)

Inductively coupled plasmas are steady-state plasmas in which energy is introduced continually through a magnetic field created by a radio frequency induction coil. Typical energies in analytical plasmas are up to 2 kW. The magnetic field acts on charged particles which further collide to dissipate their energy. To initially create charged particles for the ignition of the plasma, a spark is used. When new material is introduced in a high-temperature plasma, it undergoes decomposition and can be ionized so that plasmas can also act as an ion source for mass spectrometry.[17] As the high temperatures of up to 12000 K excite higher electronic states of atoms and ions, inductively coupled plasmas are also excellent sources for emission spectroscopy.

The corresponding analytical technique is ICP-OES, whereas in ICP-MS, the ions produced in the plasma were used for analysis. Due to the higher sensitivity and better time resolution, ICP-MS is often preferred over ICP-OES. Within this work, ICP-MS has been used as the primary method, thus principle will be explained in more detail, ICP-OES was employed as an established reference methodology.

In Figure 3 a typical LA-ICP-MS setup with a quadrupole ICP-MS is shown:

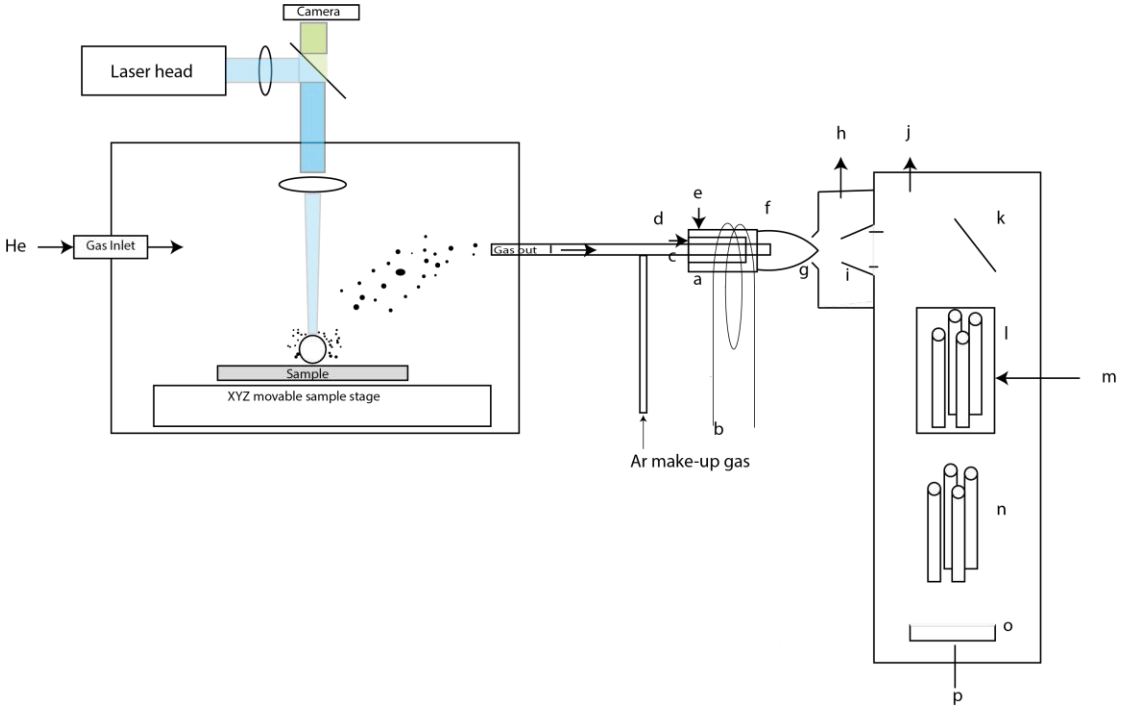

Figure 3: Schematics of a typical LA-ICP-MS system with a quadrupole ICP-MS and a collision reaction cell. The laser ablation system consists of the actual laser head, an optics that guides and focuses the laser on the sample, a microscope to monitor the sample, a movable sample stage, and a chamber with in- and outlets for the carrier gas, usually helium. It is connected to the ICP-MS instrument; argon is mixed with the helium flow before the torch. The parts of the ICP are a: plasma torch consisting of three concentrical tubes, b: the induction coil, c the central carrier gas flow (or the nebulizer gas flow in case of liquid measurements), d: auxiliary argon gas flow, e the cooling gas flow and f: the actual plasma. The interface consists of the sampler cone (h), to an intermediate vacuum, produced by a rotary vane pump (h), after the skimmer cone (i), the high vacuum section of the instrument follows, pumped by a turbomolecular pump (j). A 90° lens deflects the ions from neutral particles and photons. The collision/reaction cell (i) reduces interferences by introducing a gas (m). A quadrupole (n) acts as a mass analyzer. Finally, the detector (o) measures the ins and transmits the data to a PC (p).

An ICP-MS consists of a sample introduction system, a plasma torch with the inductively coupled plasma, a mass separator, and a detector. In the ICP plasma, the analyte decomposes, atomizes, and finally ionizes. The introduction of the sample depends on its physical state; liquid samples are in most cases nebulized, whereas an appropriate

droplet size has to be assured, usually by a spray chamber. With laser ablation, the helium flow, including the suspended particles, is directly introduced in the plasma torch after dilution with an argon stream. As the plasma is under atmospheric pressure and the mass ionizer operates at a high vacuum, a multistage interface consisting of several cones is needed. As mass analyzers, quadrupole is the commercially most abundant, sector fields instruments are used typically for more specialized applications, like isotope analysis in conjunction with multiple detectors. Recently time of flight mass analyzers has gained attention as they are well suited for high-speed imaging and multi-element nanoparticle analysis.

The accuracy and reliability of ICP-MS measurements are affected by matrix effects, which can cause spectral as well as non-spectral interferences. The occurrence of such matrix effects usually results in degraded analytical performance. The atomization and ionization efficiency in the plasma depends on the form in which the sample arrives, on the particle size, and the plasma load, i.e., the total amount of material introduced into the plasma. Ions can interact with each other through space charge effects. Over time deposits can form on the cones and induce a drift of the signal.[18] The degree and extent of these non-spectral interferences are usually determined by the sample matrix. Spectral interferences are caused by ions that cannot be separated from the target ions. These interfering ions exhibit a nominally identical mass to charge ratio as the target ion – are either initially present in the sample or produced by the formation of polyatomic ions.[18] As quadruples do not provide sufficient mass resolution to resolve many relevant mass interferences, these instruments are typically equipped with a collision cell, a reaction cell, or a combination, in which a gas can be introduced, which reacts with the passing analyte ions to reduce interferences.[19, 20] In comparison, sector-field ICP-MS and ToF-ICP-MS offer improved mass resolution, which enables to separate many spectral interferences; however, if this is not sufficient tedious sample pretreatment is required prior to analysis for separation of interfering species.

From early work in LA-ICP-MS, it is known that the generated aerosol is not fully quantitatively transported into the plasma; in the first works, transport efficiencies of 40 % were reported and could, with improved cell design and femtosecond laser systems increased up to 90 %.[21, 22] A particular aspect of the design of LA-ICP-MS equipment is the reduction of the dispersion of the aerosol to achieve a fast washout time.[23] This is of particular interest in high-speed imaging, as the washout time limits the possible scan speed, especially as high repetition rate lasers (up to 1000 Hz) and fast acquisition systems (ICP-TOF-MS) have become commercially available.[23]

1.2.4 Laser Induced breakdown spectroscopy

In laser induced breakdown spectroscopy, the emission from ionic, atomic, and molecular species arising from the laser ablation plasma is observed. In Figure 4, a typical laboratory measurement setup for LIBS is shown. A LIBS system is composed of the laser, the optics transmitting the laser pulse to the sample and forming a focused spot, and optics collecting the emitted light and guiding it to a spectrometer and detector. The measurement can be conducted under ambient conditions or in a designated sample chamber under a controlled gas atmosphere. To increase the signal-to-noise ratio, LIBS measurements are primarily carried out gated. This is explained in Figure5: The spectrometer is synchronized with the laser to start the measurement at a specific time after the laser pulse, the so-called gate delay. The gate width is the time window in which the spectrometer is recording. As seen in Figure 5 in the first nanoseconds, the spectrum is dominated by the continuous emission of free electrons, which gives a background signal. This can be reduced by choosing a longer gate delay. Depending on whether the emission of ions, atoms, or molecules is of interest, the gate delay and width have to be chosen properly so that it covers the temporal window in which the emission of interest is best separated from spectral interferences and background.[5]

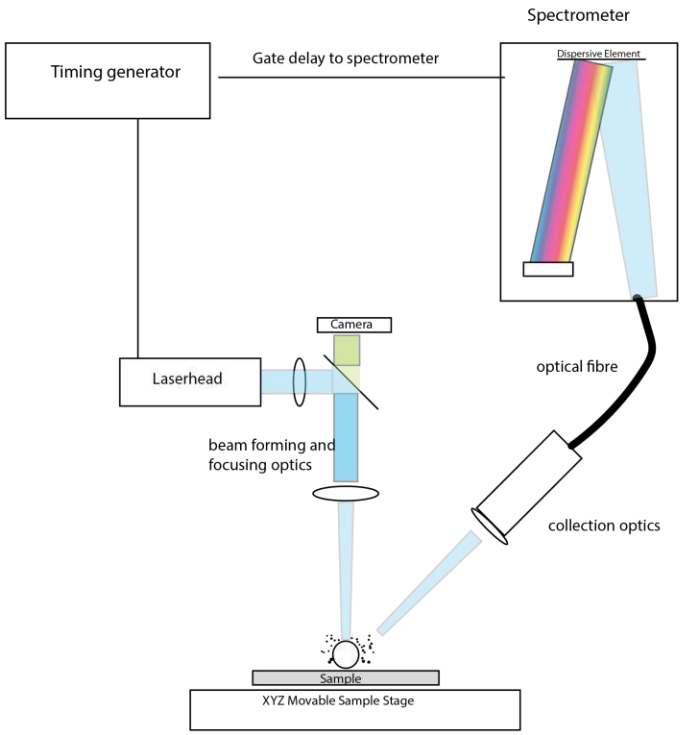

Figure 4: Schematics of a typical LIBS system: consisting of a laser that is focused on the sample. The sample is usually put on a movable stage to allow spatially resolved analysis. As LIBS can be carried out in any atmosphere, the sample can be put in a dedicated sample chamber (not shown) to control the atmosphere or be measured in its native environment, for example, in stand-of measurements. The light emitted from the plasma then needs to be collected and analyzed in a spectrometer. In this example, this is done via an optical fiber, a simple approach used in many instruments. A timing generator synchronizes the laser with the spectrometer to allow a gated exposure for an increased signal-to-noise ratio.

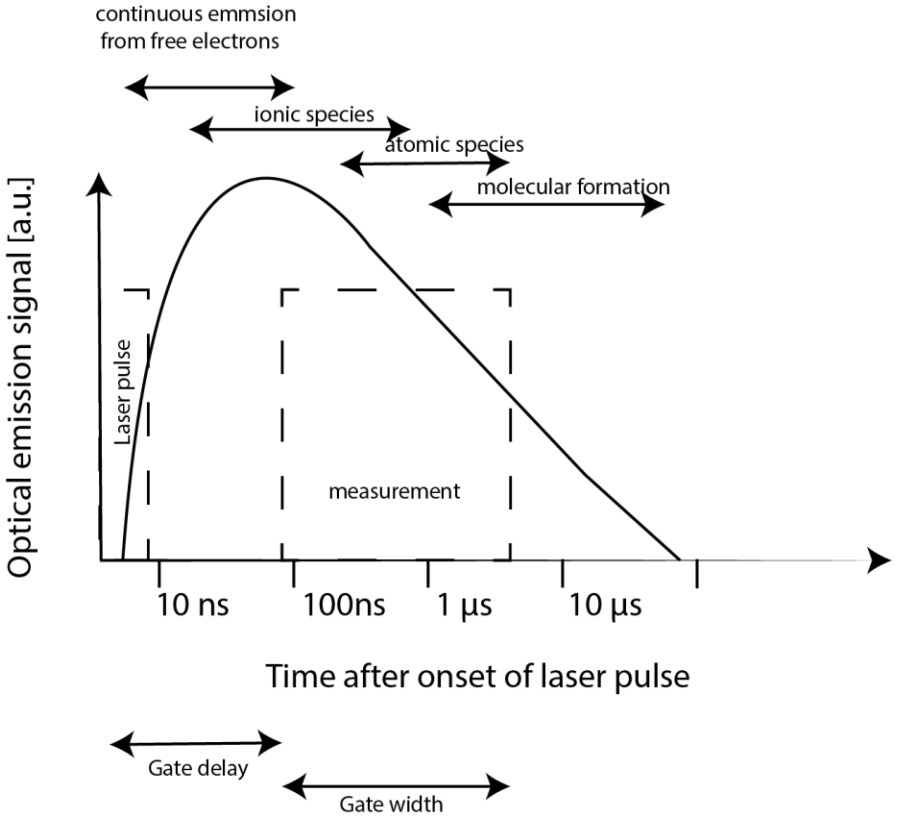

Figure 5: Timescale of the temporal evolution of the LIBS plasma. Different species contribute to the optical emission of the plasma. Initially, in the first stages, when the plasma has its highest temperature, the continuous emission of free electrons dominates. The plasma then cools down, and atoms and later molecules form. LIBS measurements are most often carried out gated, which means the spectrometer starts recording a specific time after the laser pulse, the gate delay, for the gate width time.

LIBS measurements are generally possible under any sounding, which makes stand-off and extraterrestrial analysis feasible. For laboratory use, the atmosphere is in most cases controlled to achieve the best performance. Helium, for example, with its high thermal conductivity, lets the plasma cool down faster, and its highest ionization energy leads to a lower electron density in plasma[14], which is beneficial for the measurement of some elements such as fluorine.[24] For most cases, however, the best results are possible under an argon atmosphere.

1.3 Laser-assisted plasma spectrochemistry techniques in the context of solid-state analysis

The classical way in analytical chemistry is to decompose the solid sample to bring it finally into a diluted acid solution, which is introduced into a nebulizer and then into an ICP-OES/MS or an atomic absorption spectrometer (AAS). The decomposition is carried out by digestion with strong acids, such as HCl, HF, and HNO_3, often under oxidizing conditions, by the use of H_2O_2 and $HClO_4$ at elevated temperatures or by fusing the sample with a suitable flux, like borate, and subsequent dissolution of the obtained fusion disk. These procedures are well established and performed routinely; however, they have several drawbacks: The digestion is labor-intensive and includes dangerous chemicals; during the handling steps, the risk of contamination from the environment or the loss of analyte is created. Further, high-performance materials, especially ceramics, such as SiC, SiN, BN, are chemically very inert, and their decomposition is only possible under extreme conditions, which includes high temperature and pressure.

Apart from laser-based methods, several techniques exist in the field of elemental solid-state analysis. They can broadly be classified in which way the analytical signal is generated: the sample can be interrogated with ions, electrons, or photons, the analytical signal obtained can also be in the form of ions (mass spectrometry), electrons and photons (optical and X-Ray spectroscopy) and will be discussed briefly, as they are often used complementary to LIBS and LA-ICP-MS. In secondary ion mass spectrometry (SIMS) and glow discharged based methods, the material is removed from the sample by sputtering with ions. In SIMS, only the secondary ions generated in the sputtering process are detected in a mass spectrometer. In GD-based methods, the sputtered material collides with argon ions and is electronically excited so that optical emission is measured (GD-OES) or ionized, facilitating the application of mass spectrometry (GD-MS). In X-Ray fluorescence (XRF) and electron microprobe (EMPA) based methods, the characteristic elemental X-Ray emission is detected, which is generated either by interaction with a primary X-Ray (XRF) or a focused electron beam (EMPA). The third way to obtain elemental information is the detection of electrons emitted from the samples, either by producing photoelectrons through X-Rays (XPS) or Auger electrons (AES).

These methods all have their specific advantages, like spatial and depth resolution, and drawbacks compared with laser-assisted methods, so their use is often complementary to get the desired information of the sample. The methods involving ions and electrons

require a high vacuum, as the particles would be scattered by gas. Thus, all these methods require transferring the sample in a dedicated vacuum chamber, which is unnecessary for laser-based methods and XRF. This decreases the throughput of samples and increases the cost of instrumentation.[25]

Besides the determination of bulk composition, these techniques also allow spatially resolved investigations. For this purpose, the primary beam can be scanned over the sample to achieve a laterally resolved image, except for glow discharge which is not suitable for elemental mapping. The accessible resolution is determined by two factors, the sensitivity of the method, as the amount of analyte becomes smaller with a decreased spot size, on the other hand by the focus ability of the primary beam and the interaction of the beam with the sample. The methods are possible based on primary ions and electrons, i.e., SIMS and scanning Auger spectroscopy, with nano-SIMS down to 50 nm. X-ray beams are much harder to focus, typical resolutions are >10 µm, with very sophisticated instrumentation, such as synchrotron light sources, better values are possible. Image resolutions with >1 µm are routinely obtained in laser ablation-based methods. In glow discharge, the sample forms the cathode used for analyses with an aperture in the mm range, so no spatially resolved analysis is usually performed. The depth resolution is determined by the interaction of the primary beam with the sample. In XPS, the short mean free path of electrons in solid materials determines the information depth and is, depending on the energy of the electrons, in the sub-nanometer range. Thus, only information from just the top atomic layers is reachable. To obtain data from deeper layers, usually, the material is sputtered away with an ion beam. In SIMS and GD-OES/MS, the material is also removed by sputtering, which enables depth resolution in the nm range. This excellent depth resolution is beneficial for many applications. However, the sputtering-based methods SIMS and XPS/AES struggle with the analysis of thick layers (>10 µm). In laser ablation, the obtainable depth resolution depends on the laser's interaction with the sample. It is, in general, the best with femtosecond lasers, where little thermal damage on the sample occurs with >10 nm, with standard nanosecond laser usually ablation rates in the order of some hundred nm per shot are possible. The maximum depth is >100 µm and is limited by crater effects. In EMPA, the primary electron beam can be reduced down to single nm; however, due to the scattering of secondary electrons in the sample, the depth and spatial resolution are limited to the micrometer range.[26, 27] In Figure 13, the depth resolutions typically achievable with the mentioned methods are illustrated.

When comparing the sensitivity, it has to be considered that the number of detectable

particles, electrons or photons decreases with increasing depth and spatial resolution. While only the major and minor components are measurable with extremely surface-sensitive methods like XPS, detection limits can go down to the ng/g range with other methods. However, this also depends on the elements to be measured; with mass spectrometry-based methods, the ionization and background limit the detection of some elements. For example, in LA-ICP-MS, elements with higher ionization energy than argon are not detectable, and the gas background makes the observation of nitrogen and oxygen nearly impossible. For comparison with the methods based on the detection on X-Rays are limited to elements with a higher atomic number.

The elegance of the laser-based analytical techniques lies in the fact that there is no physical constraint on which types of solid they can be applied. Neither they have to be conductive nor be stable under vacuum, which makes them especially interesting for the analysis of organic and biological material, and in the field of material science for polymers. As already mentioned before, the two most common methods are LA-ICP-MS and LIBS.[25]

Laser-induced breakdown spectroscopy has some of the most remarkable features of all methods: As only light is involved in the analysis, it has no requirements on the surrounding of the sample as long it is transparent. Measurements in vacuum, under atmospheric conditions, Martian atmosphere, inert gas and under-water are reported, and stand-off measurements with a distance of up to several meters from the setup are well established, which is not possible with other solid sampling methods. This also allows building hand-held instruments for in-field use, which is only possible with LIBS and XRF. One of the main advantages of LIBS is that in comparison to other methods, the whole periodic table of elements is reachable. However, its sensitivity is somewhat limited compared with the mass spectrometry-based methods. Therefore, a leading research focus in recent years has been the enhancement of the LIBS signal [28] through several approaches such as reheating of the ablation plasma through, e.g., a second pulse, electric sparks, or microwave energy, or through a better interaction of the laser with the sample through the application of nanoparticles of the surface (NELIBS – Nanoparticle enhanced LIBS).[29]

1.4 Analytical challenges in solid-state analysis

Analytical methods must be fit for purpose to answer the questions of interest. In classical analytical chemistry, metrics and guidelines have been developed to measure their quality.[30] In the case of material science, in many cases, the stoichiometry or the level of a trace analyte is the property of interest. To make quantitative statements about the composition, it is necessary to quantify the signals, which means to set the signals in a mathematical relationship with the sample composition. In classical liquid analysis, the sample is transformed into dissolved ions so that readily available; universal liquid standards can be used for quantification.[31]

For direct solid sampling methods, the gold standard is the use of certified reference materials (CRM) that match the type of samples exactly. CRMs are issued by large organizations, like the NIST (National Institute for Science and Technology) or BAM (Bundesanstalt für Materialforschung und -prüfung) and undergo an extensive certification process to determine their values. While this ensured the highest possible quality, it is only economically feasible to produce them for questions with high demand. For materials under current research, such CRMs are not to hand and not likely to be produced, as the often-considerable variation on of the sample composition and the elements in the sample are made. The second-best option is using in-house prepared matrix-matched standards, which have identical or at least very similar physical properties as the sample and contain a known amount of analyte. The composition of these matrix-matched standards is either known through the production process, i.e., mixing of a specific amount of analyte, or by the characterization of them with a validated analytical technique, which can, for example, be conventional digestion and liquid analysis.

The requirements for the degree of matrix matching depend on the characteristics of the method. Generally, when analyte removal and excitation/ionization are separated, like in LA-ICP-MS, and GD-MS matrix effects do not play an as prominent role as, for example, in SIMS or LIBS.[11]

The standards should resemble the sample as closely as possible. This task is relatively easy when the sample is pretreated in some way. When only average values of the sample are of interest, the fusion of the sample with borates or the homogenization and milling to a powder and then pressing the sample with a binder can be performed. Other common sample pretreatments include embedding the sample in a polymer resin and cutting a thin section with a microtome.[32, 33] During this sample preparation step, an internal

standard can be added, or standard addition can be performed. As standard material can be treated the same way, making quantification a relatively simple task. However, a primary advantage of laser-based methods is the analysis of samples in their native state. For many applications, such as biological samples, it is widely used to homogenize the sample matrix and spike the elements of interest. The normalization of the signal to a constant matrix or artificially introduced element [34, 35] can help to reduce effects due to different ablation and transport efficiency and makes the analysis of compact samples without prior homogenization feasible. The detection limits for solid-state analysis are usually calculated by three to ten times the standard deviation divided by the slope of the calibration [36] so that the sensitivity and the noise of the method need to be considered. The reduction of noise can, for example, be accomplished with the use of an internal standard as described before. The desired properties depend on the application, whereas for stoichiometry determination, minimizing the error is the objective, while for trace and ultra-trace analysis, optimization of the sensitivity is the primary objective. For bulk analysis, data points from single sample spots can be accumulated to increase the signal-to-noise ratio and, through that, lower the detection limits. This is not possible for imaging, so generally, a higher sensitivity is required than for bulk analysis.

1.5 Methods used in this thesis

In the next part, the basics of the methods used in this thesis will be described in more detail.

1.5.1 Conventional laser ablation using liquid standards

As liquid CRMs are readily available for all elements, several approaches have been employed for direct solid sampling analysis. This includes methods in which the liquid is nebulized and mixed to the gas stream with the ablated aerosol; this is discussed in the next section of online LASIL. The other possibility is to apply the liquid to a surface and ablate the residue remaining after evaporation of the solvent in the same way as the sample. The simplest way is to use dried droplets;[37] however, liquids tend to spread over a large area, leading to a dilution of the analyte and dry inhomogeneously due to the coffee stain effect.[38] To overcome these drawbacks, more sophisticated approaches were developed. One way is to control the liquid-solid interaction to avoid the spread of the

droplet over a wide area. It is also possible to use a specific printer to deposit picoliter volumes of standard in a defined pattern. To avoid separation effects, the liquid can be confined in structures, such as wells and grooves.[39, 40] In Figure 6, the procedure for producing such standards is demonstrated. With these approaches, it is simple to prepare a large number of standard materials for calibration and adapt them flexibly to the elements in the sample. It is also possible to analyze challenging liquid samples with laser ablation.[41]

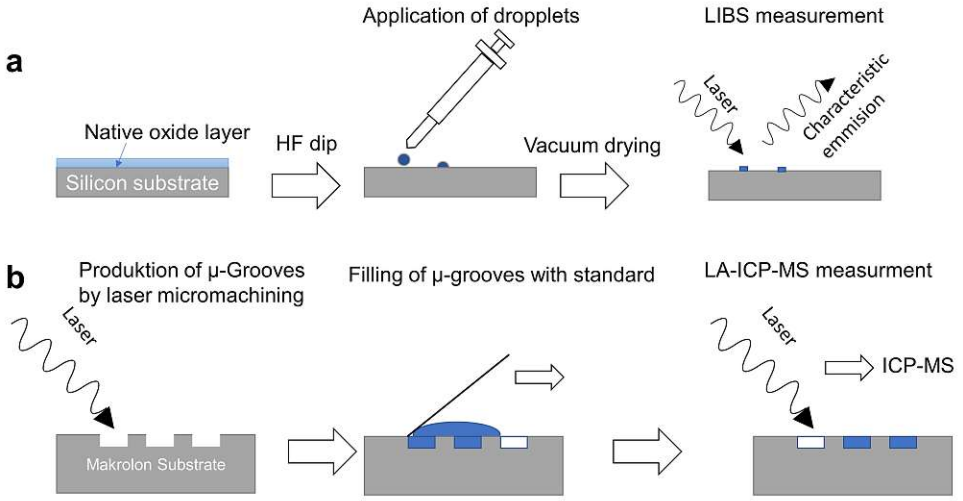

Figure 6: Schematics of the production of dried droplets (upper row) and self-aliquoting microgrooves (lower row).This approach was applied in publication 1.[39]

Another way to use liquid standards for LA-ICP-MS/OES is to nebulize them and mix them with the aerosol gas stream.[42] The droplets of the liquid standard can be further dried [43] with a membrane desolvation to equalize the standard to the ablated aerosol and achieve dry plasma conditions and reduce the load to the plasma. However, in [43], wet plasma conditions were founf to be more robust.

1.5.2 Online LASIL

Laser ablation of solids can also be carried out under a liquid medium, provided that it does not absorb light at the laser wavelength to the degree that the ablation threshold cannot be reached. This process is a well-established route for synthesizing nanoparticles up to the industrial scale. The main advantages compared to other nanomaterial synthesis methods are that a wide variety of materials are accessible as almost all solid targets can be used as a precursor and that fundamentally no chemicals other than the target and the liquid are involved, which makes it a green chemistry technique. Through variation of the laser parameters, the liquid and the use of additives in the solution size, shape, and composition of the nanoparticles can be controlled, as well as the surface can be modified with a variety of ligands.[10, 44] While the ablation of noble metals usually yields the corresponding metallic nanoparticles, more reactive metals react with the medium and form their oxides or hydroxide in aqueous media.[15]

The idea of dispersing solid samples into a colloidal solution by laser ablation in analytical chemistry was first presented by Muravitskaya et al. [45] The ablation was done in a beaker, and the resolution dispersion of the analyte was analyzed offline with an ICP-OES spectrometer. It is well known that particles below a specific size, about 5 µm, fully atomize and ionize in the ICP plasma, which was used in slurry analysis for a long time [21], and allows to use of a liquid calibration standard for quantification, while circumventing conventional sample digestion. This method was taken up by other research groups and was applied to different, mainly refractory materials, like SiC and GaN. This method is of particular interest for these materials, as they oppose many wet chemical digestion processes. The LASIL approach was compared to conventional digestion, was applicable and applied to certified reference material, and its ability to obtain valid results was demonstrated.[46–50] The modal value of the particle size for the ablated material was found to be 150 nm, and no particles greater than 1 µm were found. The ablated particles were further digested with acids before analysis in some works. The quantification was done in all works with external standards or isotope dilution. In Machida et al. [51], the observation was made that there is a particle size-dependent elemental fractionation, where some particles reside in smaller, others more in larger particles. In these works, the ablation step was carried out with commercial laser ablation equipment with 213 nm wavelength in open vessels under deionized water.

The next logical step for LASIL analysis was to switch from an offline approach, where the laser ablation step and the measurement step are separated and require manual

sample handling, to an online measurement, where the laser ablation in liquid is directly connected to the nebulizer of the ICP instrument via a flowing carrier solution.[52] This approach is tempting because it allows automatization of the measurement and direct injection of liquid standards in the carrier solution. Similar approaches were proposed early; for example, Aziz et al. [53] presented a setup where a spark is used to produce a colloid of a solid sample, which is then transferred into an AAS torch and quantified with liquid standards. In analytical chemistry, flow injection has been established to be a routine approach for automated analysis of samples and to minimize sample handling.[54]

The first online-LASIL setup was realized by Bonta et al.(2018)[55], where the stoichiometry of strontium titanate was determined. Liquid standards were directly injected into the setup to achieve quantification with an ICP-OES instrument. During this study, the observation was made that with LASIL, a better depth resolution than with conventional nanosecond laser ablation can be achieved. The setup was further refined, and in Herzig et al. (2019) [56], air bubbles were used to reduce the washout time of the setup, and the high accuracy and sensitivity of this method were demonstrated. As a direct solid sampling approach, with online-LASIL also spatially resolved measurements are possible, as shown in Herzig et al. (2020) [57] were structured gadolinium doped ceria films were imaged with a resolution down to 20 µm, and the use of standard addition in conjunction with ICP-MS was used. Online-LASIL is especially suitable for material science samples. Through the combinatorial combination of elements throughout the composition state new materials with unique properties are created and the fast pace of development does not give enough time for the creation of matrix matched standard materials.

The basic setup of the online-LASIL approach developed at TU Wien is shown In Figure 7. A prerequisite is to confine a liquid flow over the sample. This is achieved by putting the sample in a well-fitting sample holder; for details, see Figure 8. The fluid path is constrained on the side by a PDMS (polydimethylsiloxane) spacer, which also seals the cell and prevents it from leaking, and on the upside by a UV transparent window. A fast, quantitative washout of the ablated material is needed to achieve the required analytical performance. As the design of the LASIL system is crucial for this, the details will be discussed in the following:

The ICP nebulizer sets the boundaries for the flow rate of the carrier solution maximal flow of about 1 mL, lower boundary about 50 µl. These flows are significantly lower than in LA-ICP-MS, where helium carrier flows of up to 1000 mL per minute are used, which

results in a slower velocity in the tubing and, therefore, a longer transport time, leading to broader peaks due to dispersion in the flow compared with classical LA-ICP-MS.

The materials of the ablation cell have to be inert, as acidic media are used, and the ablated material shall not react or get absorbed into it. For the tubing, fluoropolymers like PTFE (Polytetrafluoroethylene) and PFA (Perfluoroalkoxy alkane) are state of the art in trace metal analyses and are used for this application. The ablation cell is machined from PFA, which is, on the one hand, relatively chemically resistant and inert and, on the other, mechanically robust enough to allow a production through milling with tolerances in the lower micrometer range, which is necessary to obtain a liquid-tight fitting. The window must be made of a material transparent in the deep ultraviolet range down to at least 213 nm, the fifth harmonics of an Nd:YAG laser, which limits this in practice to fused silica, CaF_2, and corundum. The cell dimensions were chosen so that samples from the cooperation partners could tightly fit in. Cell designs were first constructed around the 5x5x0.5 mm single crystals used for the fabrication of PLD thin films in electrochemistry. Other samples, such as silicon or alumina wafers used as substrates in thin film deposition, can also be used when cut or broken to an appropriate size.

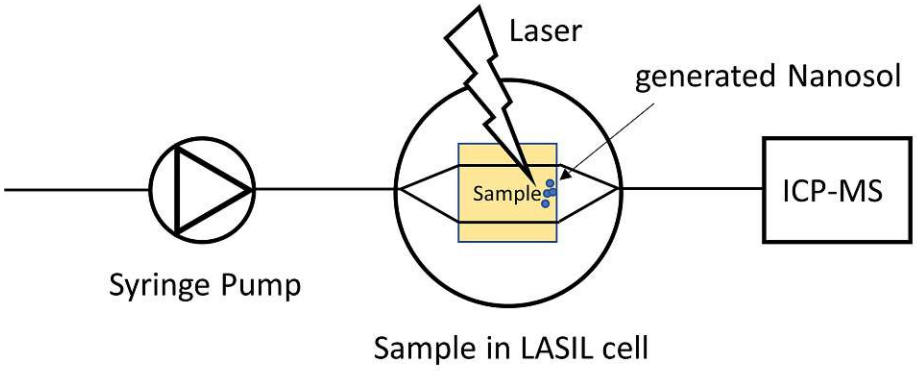

Figure 7: Schematics of the basic online LASIL setup consisting of a pump, a LASIL cell containing the sample, and an ICP instrument, all connected by tubing.

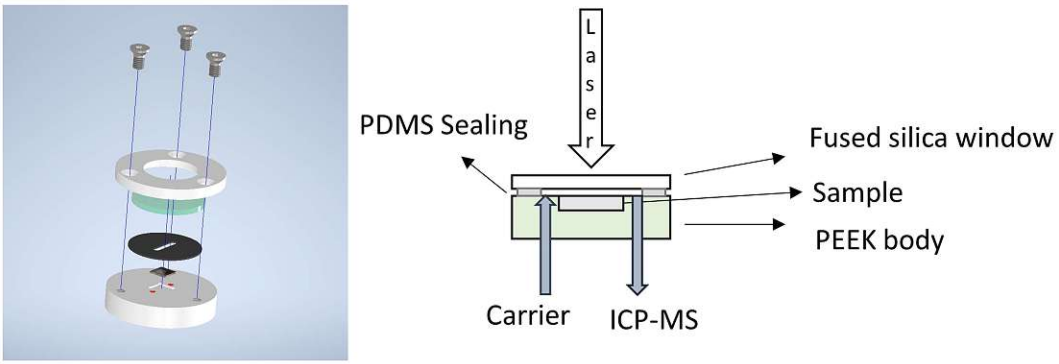

Figure 8: Left: explosive view of the online LASIL cell used in [58], Right: cross-section of the same.

For the design of the ablation cell, it has to be considered that due to expansion of the ablation plasma, a shockwave is formed, which propagates through the liquid.[59] These processes are essential to lead to fundamental considerations in the design of the ablation cell, as for online-LASIL, the fluid path is encapsulated to pump the fluid to the ICP instrument, the cell, especially the glass cover, has to withstand the mechanical stress induced by the shock wave. Further, the cavitation bubble induces discontinuities in the flow, which hardens computational fluid dynamic (CFD) based simulation and makes empirical optimization of the flow conditions and cell design necessary.

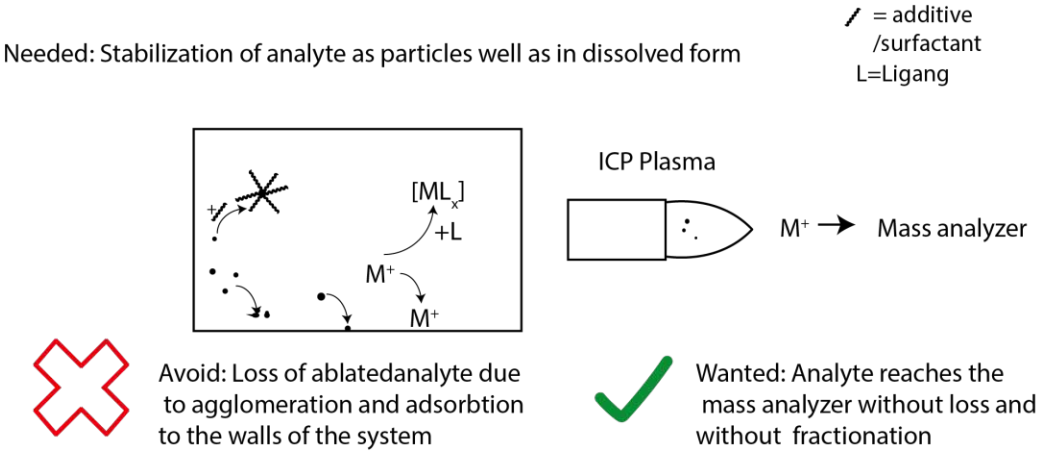

Figure 9: In online-LASIL several processes can lead to loss of analyte, which needs to be avoided through careful optimization of the parameters.

In some of the early offline LASIL works, the ablated particles are further digested with acid before introduction into the ICP plasma. From the classical liquid elemental analysis, it is well known that stabilizing the analyte solution is necessary to prevent precipitation and adsorption to the walls of tubing and vessels. This is usually accomplished by using diluted acids as the matrix or the addition of complex-forming agents, such as chelators. In online-LASIL, the ablated material can be in the form of particles or dissolved. To achieve a reliable quantification, all forms of the ablated analyte have to be protected from getting lost after the ablation till they reach the ICP plasma. In Figure 9, these processes are demonstrated.

For particles, this small particle size is favorable to prevent gravitational settling and prevent agglomeration of smaller particles. From the fundamental works of laser ablation in liquid, it is well known that the particle size depends on the combination of the laser parameters with the material and can be modified by the composition of the liquid medium. The pH of the liquid medium, its ionic strength, and the deliberate use of additives in the solution influences particle growth and modify the surface chemistry of the particles and, therefore, the stability of the generated colloid.

Dissolved species of the analyte materials can be generated directly from the plasma via reaction with the liquid medium or by the dissolution of particles. Losses of these dissolved species, for example, due to adsorption to the walls of the system, must be prevented. To accomplish this, the cell and all tubing are made of inert materials, like PTFE, PFA, PEEK (Polyether ether ketone) and fused silica, and diluted acids and

complex-forming agents are added to the carrier solution.

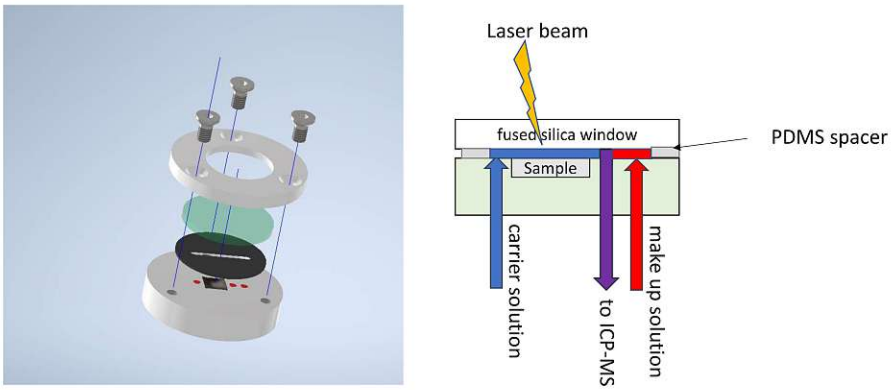

Figure 10: Schematics of the online-LASIL cell with two inlets that allow the addition of a makeup solution, which does not come in contact with the sample.

However, as some samples are not stable in acidic solution and would decompose under acid conditions, a second inlet on the sample cell was added, Figure 10, which allows adding a makeup solution behind the sample in the flow path to modify the liquid properties.

1.5.3 Molecular LIBS

LIBS has the ability to monitor each element in the periodic table. However, this is in practice hindered by the low sensitivity for some elements, especially halogens, oxygen, nitrogen, and sulfur. This is caused by the fact that the main emission lines of these elements are in the vacuum UV spectral range,[60] which would require a dedicated instrument to monitor them. The spectral lines in the visible range have very high excitation energy and so give a low emission intensity. This is especially relevant as these elements are hardly measurable with other methods. A possible circumvention of this limitation is not to measure the atomic or ionic lines of the element itself but the specific emission of a molecule, which contains the element of interest. This effect is,

for example, also used for continuous source atomic absorption spectroscopy (CSAAS) [61] or laser ablation molecular isotopic spectrometry LAMIS.[62] For LIBS this was for the first time demonstrate in 1996 to use the CuCl molecule to monitor chlorine.[63]In the LIBS plasma, molecules form through the recombination of atoms in the late plasma stages when it had cooled down enough.[64] As the molecular emission often has much lower excitation energy compared to the atomic emission of the respective element, the sensitivity can easily be increased. The measrument conditions have to be adapted for the detection of molecules, for example in many cases a longer gate delay is employed. For example, Alvarez-Llamas et al.[65] could increase the detection limit for fluorine by order of magnitude by using the CaF molecule. The element that is the partner for molecule formation can either be intrinsic to the sample or added artificially, for example, through the mixing of powders [66] or by the spraying of a liquid [60].

2 Scientific Publications

This thesis consists of four publications, three of them are already published, the last one has been prepared for submission to Molecules. Two papers make use of online-LASIL, one uses liquid calibration standard for classical LA-ICP-MS, and LIBS, and one molecular-LIBS in conjunction with new sample preparation methods. The works were done in close cooperation with other research groups: Solid oxide fuel cell cathode materials, studied by the research division elcetrochemistry headed by Prof. Fleig, were under investigation in one online-LASIL publication, as a recently introduced approach to boost their performance required a new methodology to quantify the surface concentration of platinum. In cooperation with the research groups of Prof. Mayrhofer and Prof. Riedl-Tragenreif from the Institute of Materials Science and Technology of the TU Wien, boride thin films were studied. One publication employed liquid standards for classical laser ablation to gain insights into their stoichiometry, in another manuscript quantitative depth profiles reveal the composition of oxide layers formed during high temperature corrosion. One further publication using molecular enhanced LIBS for the first times enabled spatially resolved measurements of fluorine in a sample were the molecular forming partner is extrinsically added.

These fruitful collaborations also yielded in several co-authored publications, shortly described at the end of this thesis.

Publication 1 Laser-based analysis of transition metal boride thin films using liquid Standards In this publication, the stoichiometry of ternary transition metal boride thin films deposited by magnetron sputtering is determined with LA-ICP-MS and LIBS using liquid calibration standards. Transition metal borides are an emerging class of materials with exceptional properties, such as high hardness combined with ductility and corrosion resistance at high temperatures. These properties can be tailored to the application. However, for quantitative analysis suitable reference materials are required and the large number of possible combinations of elements makes the production of classical matrix-matched reference materials infeasible. As boron is not accessible with the widely

used X-Ray based analysis techniques, the laser-based methods LA-ICP-MS and LIBS are the ideal candidates for this task. For LA-ICP-MS analysis, self-aliquoting microgrooves were used for quantification. These were fabricated with laser micro-machining in polymer slides. For LIBS, dried droplets were used, as higher surface concentrations are needed due to the lower sensitivity of LIBS. A protocol for the surface pretreatment of silicon wafers was developed to reduce the spreading of the liquid standard. A multivariate data analysis model was used to quantify the LIBS spectra to account for spectral interferences. Laser parameters and the composition of liquid standards were optimized to minimize the matrix effect. The results were benchmarked with data from classical liquid digestion ICP-OES, and a high agreement of the results was found.

Publication 2 Quantitative analysis of the platinum surface decoration on lanthanum strontium iron oxide thin films via online-LASIL-ICP-MS It was recently discovered that platinum nanoparticles on the surface of solid oxide fuels cell cathode materials could drastically increase the oxygen reduction kinetics.[67] The nanoparticles are deposited using sputter coating with very short sputtering times. To understand this effect, the exact surface concentration of platinum needs to be known. Although at first glance this seems to be a simple task, accurate determination of the Pt-surface decoration is much more challenging. For electrochemical measurements, a current collector electrode is needed, consisting of platinum and lies under the 100 nm thick mixed ionic electronic conductor. Thus, the application of conventional wet chemical analysis methods was not possible since sample dissolution with subsequent liquid ICP-MS analysis does not allow a differentiation between Pt from the surface decoration and Pt from the collector electrode. As online-LASIL exhibits a way better depth resolution than conventional nanosecond laser ablation and can deliver quantitative results, this technique was chosen for this challenging application. As lanthanum strontium ferried used as a mixed ionic electronic conductor is chemically sensitive and would dissolve in concentrated acid, and the ablated platinum needs to be stabilized in the solution, a stringent optimization of the carrier solution was necessary. To achieve absolute quantification of the surface concentration, matrix-matched standards were used in this case. It was clearly shown that it is possible to separate the two layers of the platinum and to achieve a depth resolution of better than 50 nm. Further, spatially resolved measurements revealed inhomogeneities in the distribution of the platinum.

Publication 3 Elemental Mapping of Fluorine by Means of Molecular Laser-Induced Breakdown Spectroscopy. Fluoropolymers are gaining importance due to their unique properties, such as chemical and physical inertness. Through this inertness,

on the other hand, they can become a threat to the environment due to their persistence. LIBS is one of the few methods capable of measuring all elements in the periodic system, including fluorine. However, the main emission lines of fluorine are in the vacuum ultraviolet spectral region, which would require dedicated equipment, and those in the visible range suffer from low sensitivity due to their high energy of excitation. To overcome this limitation, it is possible to measure the emission of a fluorine-containing molecule. In this publication, two new methods for applying an element that forms a molecule with fluorine were investigated: sputtering a copper thin-film and spray coating with a calcium acetate solution. It was for the first time possible to map the fluorine distribution using molecular emission enhanced LIBS with both methods. In previous works, only bulk measurements were reported. The obtained elemental maps were in excellent agreement with the fluorine distribution in the sample assessed via conventional LIBS measurement of the Fluorine-containing polymers. With pressed powder standards, the sensitivity and linearity of both methods were shown.

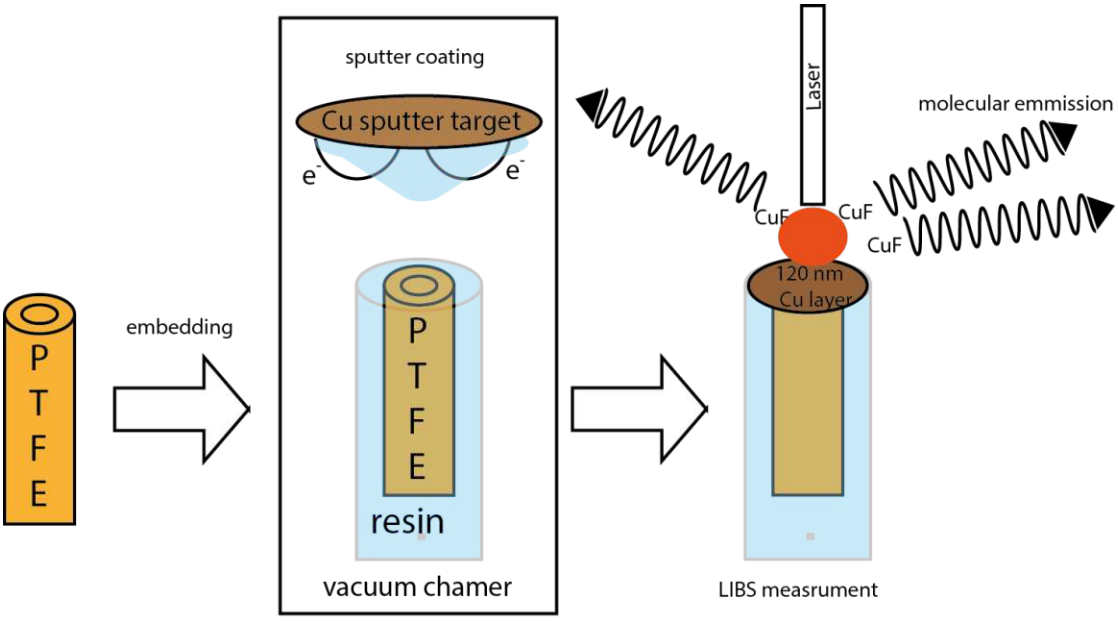

Figure 11: Schematics of one of the protocols for fluorine detection used in Publication 3 by applying a thin copper layer on the surface and monitoring the CuF emission band using molecular LIBS.

Publication 4. At elevated temperatures, oxidation reactions can quickly disintegrate engineering materials. To protect them, special coating materials are used. Transition

metal borides doped with silicon were proven to be suitable candidates for this task.[68] To gain knowledge of the mechanisms of the oxidation, it would be advantageous to know how the stoichiometry of the oxide film is, how it changes in depth and how the bulk material is affected. There exist several depth profiling techniques however, the quantification of the signals is known to be troublesome, as in general, matrix matched standards are needed. If the layers in a depth profile are physically and chemically very different for each layer, a unique reference material would be needed, whereas even one is laborious to produce. To solve this problem, an online-LASIL technique was developed, which allows circumventing this limitation by the use of liquid standards. Parameters were optimized to ensure a transport without fractionation and to maximize the sensitivity for silicon, the least sensitive element in the system. Two silicon doped chromium diboride samples which underwent an oxidation treatment were chosen as samples. They underwent a detailed characterization in previous work, including thermogravimetry (TGA), XRD, TEM cross-sections, and mechanical testing. The obtained online-LASIL depth profiles followed the trend suggested by the TEM cross-sections. The different silicon content of the sample yielded a specific stoichiometry of the oxide phase, suggesting that different processes took place during the oxidation of the samples. The results of the online-LASIL measurement were in accord with the data from the other characterization techniques, underlining the validity of the results.

3 Publication 1

Laser based analysis of transition metal boride thin films using liquid Standards

Maximilian Weiss [a], Helmut Riedl [b] , Vincent Moares [b] , Paul Heinz Mayrhofer [b] , Andreas Limbeck [a]

a Institute of Chemical Technologies and Analytics, TU Wien, Getreidemarkt 9 -1060 Vienna, Austria

b Institute of Materials Science and Technology, TU Wien; Getreidemarkt 9 -1060 Vienna, Austria

Published in:
Microchemical Journal 152 (2020) 104449

Microchemical Journal 152 (2020) 104449

Contents lists available at ScienceDirect

Microchemical Journal

journal homepage: www.elsevier.com/locate/microc

Laser based analysis of transition metal boride thin films using liquid standards

Maximilian Weiss[a], Helmut Riedl[b], Vincent Moares[b], Paul Heinz Mayrhofer[b], Andreas Limbeck[a,*]

[a] Institute of Chemical Technologies and Analytics, TU Wien, Getreidemarkt 9 -1060 Vienna, Austria
[b] Institute of Materials Science and Technology, TU Wien;Getreidemarkt 9 -1060 Vienna, Austria

ARTICLE INFO

Keywords:
Laser-induced breakdown spectroscopy (LIBS)
Laser ablation inductively coupled plasma mass spectrometry (LA-ICP-MS)
Thin films
Borides
Liquid calibration

ABSTRACT

In this work the use of two laser assisted direct solid sampling methods, laser ablation inductively coupled plasma mass spectrometry (LA-ICP-MS), and laser induced breakdown spectroscopy (LIBS) for the determination of the stoichiometry of novel diboride based materials is reported. To overcome the need for certified reference materials or matrix matched standards, which were usually required for quantitative investigations with LA-ICP-MS or LIBS, in this work liquid standards are employed. For LA-ICP-MS the concept of self-aliquoting micro-grooves and for LIBS conventional dried droplets were used. As a model for application of the developed analytical procedures the ternary system $W_{1-x}Ta_xB_{2-z}$ was used. Fabrication of $W_{1-x}Ta_xB_{2-z}$ thin films with varying stoichiometry was performed via magnetron sputtering. Reference compositions were obtained by liquid digestion of the samples and subsequent ICP-OES measurement. Both laser-assisted methods enabled fast and spatially resolved measurements, although the LA-ICP-MS method generally yielded more accurate results. It was shown that the method can easily be adapted for the stoichiometry determination of systems with different elemental composition.

1. Introduction

The surface properties of engineering materials must often be enhanced to protect them from wear, fatigue and failure. A well-established method is the application of hard protective thin films, such as nitrides or carbides. Beside these traditional materials, transition metal diborides are promising candidates for future applications. Tungsten diboride is known for its relatively high fracture resistance combined with high hardness [1], which yields in a high erosion resistance. This is for example needed for high-precision components such as turbine blades, where water turbines suffer from cavitation and jet engine blades are affected by particle erosion at high temperatures. These protective materials are utilized as thin films which can be produced by physical (PVD) or chemical (CVD) vapor deposition, as for borides CVD is difficult to employ [2], PVD is strongly preferred based on the low deposition temperatures. Magnetron sputtering is an important PVD method for industry scale applications of hard protective coatings [3]. With the combination of multiple diborides, for example in the way of co-sputtering, a wide compositional spectrum can be investigated, and related properties fine-tuned for specific applications [4]. As the properties change substantially with the composition [5], an exact knowledge of the stoichiometry is essential to understand these materials and the optimization during the PVD synthesis. In general, deposition parameters such as total pressure, substrate temperature, or bias voltage strongly effects the growth modes and hence the compositions of the films. In addition, scattering effects between light and heavy elements – such as typically for transition metal diborides – as well as diverging work functions between metallic and intermetallic phases cause typically strong deviations with respect to the target compositions [6]. Furthermore, the impact of structural defects such as vacancies needs also to be considered, as physical vapor deposited thin films obtain an extremely high defect density [7,8] For diborides, vacancies are of fundamental importance for the stabilization of metastable structures such as alpha (α-AlB_2-prototype, P6/mmm, SG-191 [9]) structured $W_{1-x}Ta_xB_{2-z}$ [10].

In the past, different approaches for the chemical characterization of diboride thin films were employed. These were investigated with solid sampling techniques such as SIMS (secondary ion mass spectrometry), AES (Auger electron spectrometry), [11], XPS (X-Ray photoelectron spectrometry) [12], ERDA (elastic recoil detection analysis) [10], GD-OES (Glow discharge optical emission [13] and LA-ICP-MS [14] as well with liquid measurement procedures after sample digestion [5]. The in the field of material science commonly used X-ray based methods, like XRF (X-ray fluorescence) and EPMA (electron probe micro analysis) are

* Corresponding author.
E-mail address: andreas.limbeck@tuwien.ac.at (A. Limbeck).

https://doi.org/10.1016/j.microc.2019.104449
Received 4 September 2019; Received in revised form 18 November 2019; Accepted 18 November 2019
Available online 20 November 2019

not able to quantitatively measure boron.

In this work two laser assisted solid samplings methods are employed for the determination of the exact composition of boride thin films: LA-ICP-MS and LIBS. Both enabling spatially resolved analysis of surfaces with information depth in the micrometer range, practically no sample pretreatment and a high throughput in comparison to liquid digestion and to other solid sampling techniques. The instrumentation is fairly simple, and the sample has not to be transferred into vacuum in comparison to SIMS, XPS and ERDA [15]. Application is not limited to electrically conductive samples (like metal and alloys), also ceramics, synthetic polymers and biological materials can be measured without additional pretreatments [16–19]. However, quantification with these methods remains challenging, as non-ideal behavior in all parts of the sampling process, consisting of the laser sample interaction, aerosol generation and transport and the ionization in the plasma, require the use of matrix matched standards [20–22]. As certified reference materials are only sparely available, in-house references have to be produced [16,17,23–25]. In the last years, several approaches have been reported to overcome the need of reference materials, especially the combination of liquid standards with laser ablation is of interest, because it combines the ease of preparation and the flexibility of liquid solutions with those of direct solid sampling.

The easiest way is to produce dried droplets, by the application of the liquid standard to a substrate, the evaporate solvent and subsequently ablate the remaining residue with the laser [26–29]. As the scanning of a large area (usually in the order of several mm^2) consumes a lot of time, an improvement to this method is to confine the liquid into cavities with diameters smaller than the applied laser beam [30,31], which makes the handling more convenient. The use of trenches instead of round cavities [32–34], so called microgrooves is another enhancement of the method. This gives the advantage of longer transient signals, which facilitates data analysis.

The goal of this research is the development of an analytical procedure for the determination of thin film stoichiometry and the application for the analysis of ternary tungsten-tantalum diboride ($W_{1-x}Ta_xB_{2-z}$) films. The quantification was done via liquid standards, which were employed in the form of dried droplets for LIBS and with microgrooves for LA-ICP-MS. Furthermore, to investigate scattering effects during sputter deposition as well as losses in the target production route, the compositions of the coatings have been compared to the used target materials as well as their base powders during manufacturing.

2. Experimental

2.1. Chemicals

Ultrapure water was prepared with a Barnstead EASYPURE II water system (ThermoFisher Scientific, USA), single element ICP standards were purchased from Merck (Germany), as well as hydrochloric acid (HCl), nitric acid (HNO_3) and hydrofluoric acid (HF) and all chemicals not otherwise mentioned in p.a. quality. Tantalum powder as well as sputter targets were provided by Plansee Composite Materials GmbH, Austria. Makrolon® Polycarbonate plates were from Bayer, Germany, Silicon (100) wafers cut into 1 × 1 cm squares were provided by Infineon, Austria.

2.2. Instrumentation

ICP-OES measurements were carried out on an iCAP 6500 RAD (Thermo Fisher Scientific, USA). Samples were introduced with an ASX-520 autosampler (CETAC Technologies, USA) using a HF resistant sample introduction kit, consisting of a Miramist nebulizer (Burger Research, USA), a PTFE spray chamber and a ceramic injector tube. LIBS measurements were conducted using a J200 Tandem system (Applied Spectra Inc., Fremont) with a 266 nm Nd:YAG laser and a six channel Czerny Turner spectrometer, with a spectral range from 187 nm to 1047 nm. The used LA-ICP-MS consists of a quadrupole ICP-MS iCAP Qc (ThermoFisher Scientific, Bremen, Germany) and a NWR213 laser ablation system (ESI, Fremont, USA), connected by PTFE tubing with 2 mm inner diameter.

2.3. Preparation of thin films

The deposition of the ternary $W_{1-x}Ta_xB_{2-z}$ thin films was carried out on an in-house developed magnetron sputtering system equipped with two industrial sized 6-inch cathodes. To gain a strong chemical variation with one deposition run a 4 inch and 0.33 mm thick Si (100) wafer was deposited in a co-sputtering process using a powder-metallurgically (by spark plasma sintering, SPS) prepared WB_2 and TaB_2 target (Plansee Composite Materials GmbH, purity 99.7%), respectively. Each target was driven in a current controlled mode (DC) applying I_{target} = 4.2 A at a total pressure of 0.4 Pa in pure Ar atmosphere. The wafer was heated up to T_{sub} = 400 ± 10 °C and a bias potential of −50 V was applied. Prior to the deposition, the silicon wafer was pre-cleaned in acetone and ethanol for 5 min each. Further details on the deposition and chamber configuration can be found in [1,35].

2.4. Liquid ICP-OES reference measurements

For liquid measurements the fabricated thin film including the silicon substrates were acid digested and measured by liquid ICP-OES. The method is presented and validated in [14]. Thin film samples were broken into pieces of about 3 × 3 mm and the film with the substrate were digested with a mixture of 1 mL HNO_3 and 0.25 mL HF. After a reaction time of about 15 minutes at a temperature of 60 °C the thin films including the substrates were completely mineralized. Derived sample digests were diluted to a final volume of 20 mL with a mixture of 3% HNO_3 0.3% HF. Quantification was done via external calibration with matrix adjusted standards. The parameters of the ICP-OES measurements are listed in Supplementary Table 1.

For analysis of the sputtering targets small samples of about 10–50 mg were broken out of two differing sized WB_2, one TaB_2 and one VB_2 sputtering target, respectively. Also 10 mg aliquots of WB_2 and VB_2 base powder were analyzed. From each sample measurement of triple replicates were performed. Sample processing and measurement were performed the same way as for the thin film samples, but higher amounts of acid mixture (3 mL HNO_3 and 1 mL HF) were used. Samples were centrifuged prior to ICP-OES measurements for 15 min with 4400 rpm to remove insoluble Graphite, which is used as additive in the Targets.

2.5. LIBS measurements and calibration with dried droplet standards

Single element stock standard solutions were prepared by dissolving Sodiumtungate and Boric acid in water. Tantalum powder was dissolved in HF/HNO_3. Standards were prepared by mixing the stock solutions in respective mass ratios, the concentrations were adjusted to match the signal intensities of the investigated thin film samples, the resulting concentrations were in the range of 0.1–10 g/L. The composition of the inhouse prepared standards was controlled by ICP-OES measurements.

For the dried droplet standards 1 × 1 cm silicon wafers were dipped in 2% (v/v) HF for 2 min to remove the native oxide layer. Immediately afterwards a volume of 0.5 µl of the standard solutions were pipetted onto the surface in grids of 3 samples per wafer with 4 replicates each. The wafer with the droplets were dried afterwards in a vacuum desiccator. The resulting dried residues had a diameter of about 2 mm. The conditions used for rastering the entire dried droplet area with LIBS are listed in Table 1, a schematic of the whole dried droplet procedure is depicted in Fig. 1a. In initial experiments gate delay, spot size, energy and atmosphere were optimized for a good signal to background ratio and for an optimal use of the dynamic range of the detector.

Table 1
LIBS Parameters.

	Mapping of dried droplet standards	Measurement of thin film samples
Pulse Energy	3.8 mJ	
Average Fluence	49 J/cm^2	306 J/cm^2
Spot size	100 µm	40 µm
Laser repetition frequency		10 Hz
Argon gas flow	0.5 L/min	
Gate Delay	0.5 µs	
Gate Width	1.05 ms	

In case of ternary tungsten-tantalum diboride thin layer samples line scans with a length of 2 mm were measured with slightly different parameters (for details see Table 1). For the dried droplet standards, the spectra with solely signal from the substrate were excluded. Signals were averaged for each dried droplet and line scan measurement.

2.6. LA-ICP-MS analysis and quantification using microgroove approach

Microgrooves are micrometer sized trenches which are produced by laser micromachining of polymer substrates (Supplementary Figure 1). Microgroove standards [32] were prepared using a NWR213 laser ablation system (ESI, USA), with parameters listed in Table 2, Substrates were Makrolon Polycarbonate slides cut into squares with a side length of approx. 1 cm. The depth of the fabricated microgrooves is about 20 µm, determined with a stylus profilometer (DektakXT, Bruker, USA). For filling the same standard solutions as for LIBS experiments with the dried droplets were used. A volume of 20 µL of standard solution was pipetted on the slide, superfluous liquid was removed with a rubber spatula. Finally, the liquid remaining in the microgrooves was evaporated. The procedure was carried out in the particle free environment of a laminar flow bench (WEISS Technik, Austria). On the microgroove standards three grooves were measured per concentration level with the LA-ICP-MS parameters listed in Table 2, a schematic of the applied microgroove approach is presented in Fig. 1b. The spot diameter was chosen larger (150 µm) than the groove (100 µm) to ensure a quantitative ablation. Transient signals were recorded using the instrument software (Qtegra Version 2.8) in time resolved mode and corrected for gas blank. (Supplementary Figure 1). The ICP-MS system was tuned daily for a maximum ^{115}In signal using SRM NIST612 (National Institute of Standards and Technology, USA), applied measurement Parameters are compiled in Table 2

The much higher mechanical strength of the thin films requires a higher laser fluence than the microgroove standards. On the thin-film samples five ablation lines per sample were measured. The spatial homogeneity as well as the homogeneity in the depth was accessed in preliminary experiments. Because of the much higher density and therefore higher amount of analyte a smaller diameter was chosen for the thin films to keep the signal in the same order of magnitude.

Table 2
Laser Ablation and ICP-MS Parameters.

	Microgroove Preparation	Microgroove Standard measurement	Thin film sample measurement
Average Fluence	1.3 J/cm^2	3.0 J/cm^2	17.6 J/cm^2
Laser Diameter	100 µm	150 µm	13 µm
Scan speed	10 µm/s	100 µm/s	50 µm/s
Carrier gas flow (He)	150 mL/min	650 mL/min	650 mL/min
Repetition rate	20 Hz	20 Hz	20 Hz
RF Power		1400 W	
Auxiliary gas flow (Ar)		0.4 L/min	
Cool gas flow (Ar)		12 L/min	
Make up gas flow (Ar)		0.8 L/min	
Dwell Time		0.01 s	
Measured ions		^{10}B, ^{11}B, ^{27}Al, ^{29}Si, ^{50}V, ^{51}V, ^{181}Ta, ^{180}W, ^{182}W, ^{184}W	

3. Results and discussion

3.1. Analysis of the sputter target composition

The composition of the targets and the base powder materials is shown in Supplementary Table 2.

The analysis of the targets highlighted that there are no significant differences between the used powder materials and the sintered target materials, emphasizing extremely high accuracy with respect to the transformation of the powder chemistry during sintering. All materials exhibit a sub-stoichiometric composition and show a slight boron deficiency (stoichiometric composition WB_2: 89.41 m% W, 10.59 m% B. VB_2: 70.067 m% V, 29.933 m% B, TaB_2: 89.264 m% Ta, 10.736 m% B). This effect is especially high for the WB_2 powders. Nonetheless, all coating samples reflect the composition of the used targets, as can be seen in Supplementary Figure 2. A slight deviation with respect to the Boron content is related to scattering effects during deposition. However, it can be observed that the boron deviancy increases with higher tantalum content, as described in [1] as the formation of o-TaB phases is preferred next to the stoichiometric TaB_2.

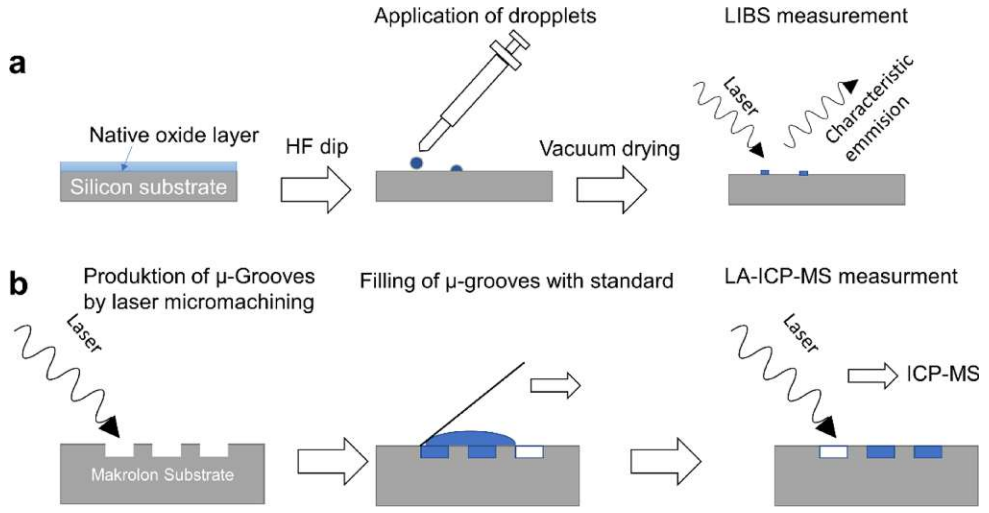

Fig. 1. a: Schematics of the microdroplet procedure with LIBS measurement, b: Schematics of the microgroove approach with LA-ICP-MS detection.

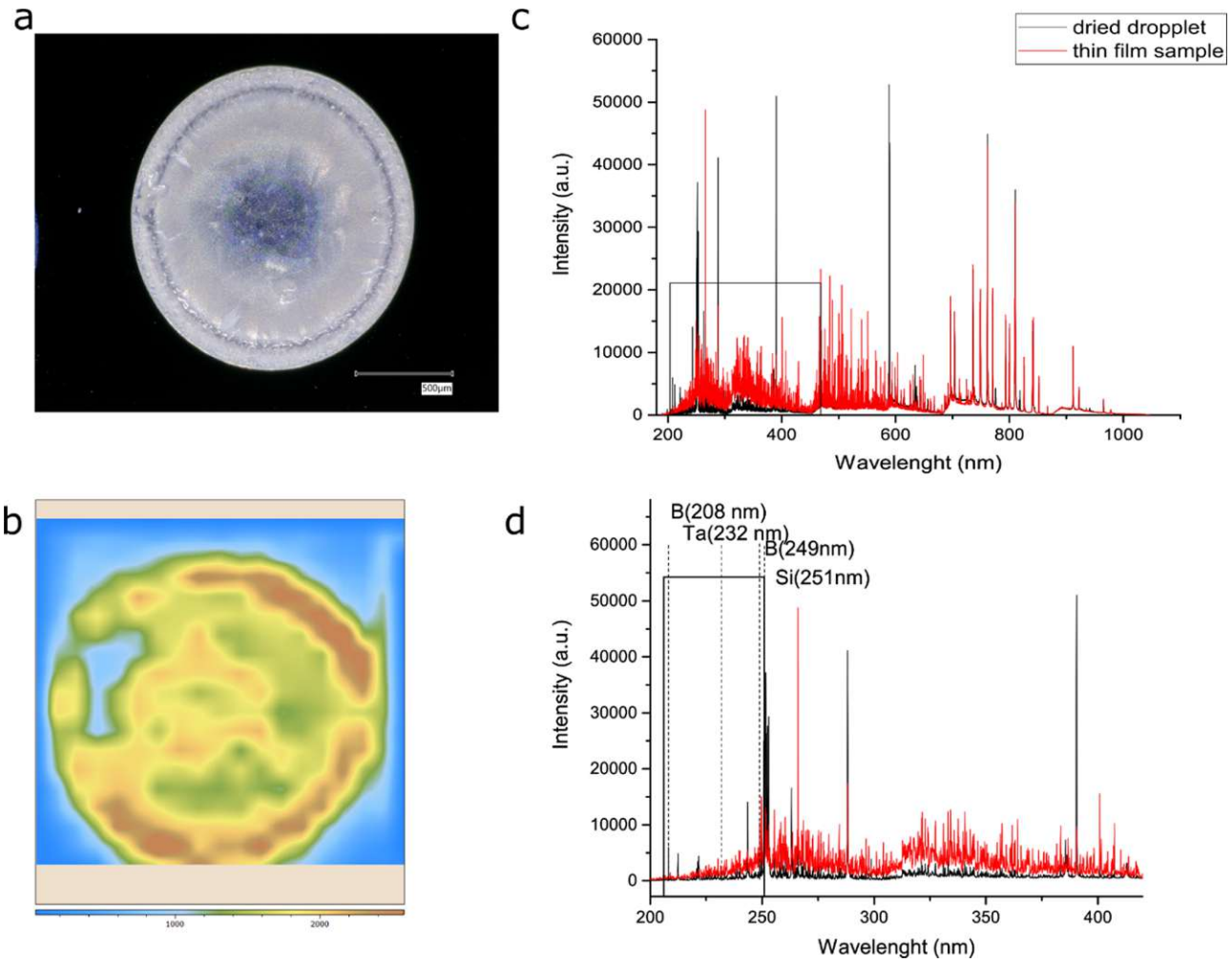

Fig. 2. a: Image of the dried residue of the standard solution after drying. b. Distribution of the Ta 240 nm emission line, indicating a slight coffee stain effect. c: Whole spectrum of a dried droplet standard and a representative sample, box indicates, the part magnified in d. d: Magnified part of the spectra, box indicating the data points used for the limited spectrum PLS.

3.2. Dried droplet calibration model

For the preparation of the dried droplet standards it was important to keep the area of the droplets small, to ensure a high signal to background ratio in the LIBS measurement, as the dried residue would be less concentrated when distributed over a larger area and further to keep the measurement time as short as possible. This was ensured by removing the native silicon dioxide layer to increase the hydrophobicity and therefore increase the surface tension. Vacuum drying prevented reoxidation of the silicon and circumvented a reduction of surface tension by heating. The resulting spots have a near circular shape and a size of about 1 mm (Fig. 2a), which allows fast measurements in about 2 min.

Fig. 2b shows the distribution of the Ta 240 nm signal, showing a higher signal intensity on the edge of the droplet, which indicates a slight coffee stain effect, as expected from literature [36]. This requires the mapping of the whole spot to quantitatively measure the whole amount of applied standard.

Different calibration approaches, such as simple linear regression, multiple regression of integrated lines, Partial Least Square Regression (PLS) of whole and parts of the spectrum [37] as well as of integrated lines were used. For the linear calibration the ratios of the following lines yielded the best results: Boron: 249.77 nm, tungsten: 407.43 nm, tantalum: 240.06 nm. The lines were integrated, and background corrected. The quality of the results was compared by the Root mean square error of prediction (RMSE):

$$RMSE = \sqrt{\frac{\sum_{n=1}^{N} (y_{Ref} - y_{pred})^2}{N}}$$

Where y_{ref} is the reference mass fraction determined by liquid ICP-OES and y_{pred} is the mass fraction of the respective element predicted by the model. For the limited PLS the wavelength range between 200 nm and 250 nm were chosen, because all three major elements have lines in this range and interferences with substrate elements, like silicon, with strong lines between 250 m and 252 nm, and sodium with its duplet at 589 nm are avoided, as can be seen in the overlap of the spectra in Fig. 2c,d. The differences in the absolute intensities are corrected by standardization (Z-core normalization) of the signals. The results of the limited PLS approach with seven components, were slightly better than the PLS using the whole spectrum (RMSE < 11.2, for all elements) and much better than linear calibration, as shown in

Table 3
RMSE of the major components with different data treatment.

	Ta	W	B
PLS with limited range	10.963	10.600	0.842
PLS full spectrum	11.267	10.280	1.486
Linear calibration	16.853	14.956	4.523

Table 3.

3.3. Microgroove calibration model

For the microgrooves only the LA-ICP-MS data is presented, as LIBS is not sensitive enough to give reasonable spectra with the amount of sample in the microgrooves. Different data treatment methods were considered for the evaluation of the LA-ICP-MS signals. Beneath linear regression, the internal standard-independent calibration strategy by [38,39], multiple linear regression [14] and PLS were tried. Best results were obtained by linear regression using ion ratios instead of signal intensities, as used in [34]. However, the model from [34] had to be extended from binary to ternary systems. The mass fractions can be calculated from the mass ratios by the formula:

$$x = \frac{ab}{ab + b + 1} \quad y = \frac{b}{ab + b + 1} \quad z = \frac{1}{ab + b + 1}$$

Where x, y and z are the mass fractions of the elements and $\frac{x}{y} = a$ $\frac{y}{z} = b$ are the elemental ratios, which show a highly linear relationship with the isotope signal ratios, for details see Supplementary Figure 3. The use of ratios compensates variations in signal intensities due to different ablation behavior or different sample thickness.

3.4. Analysis of thin film samples

The stoichiometry of the thin film samples was analyzed with both methods. For estimating content of the single elements, the LA-ICP-MS based approach gives a lower error (RMSEP 2.7) in comparison to the LIBS based (RSMEP 10.9), as seen in the actual vs. predicted graph, Fig. 3a. the LIBS based method tends to overestimate the tungsten content, seen while the tungsten content predicted by the LA-ICP-MS method are in excellent agreement with the ICP-OES reference measurements, Fig. 3b. Reproducibility of measurement given as the relative standard deviation ($n = 3$) is about 3% for the LA-ICP-MS method, and in the order of 5% for the LIBS procedure, which can be considered typical for direct solid sampling methods [40]. It is well regarded in literature, that quantification in LIBS is more challenging than with other solid sampling methods, see e.g. [22,41]. The deviation from the reference values for the LIBS method were in the range of 2–12%, which can be considered acceptable, keeping in mind that no matrix matched standard was used [22]. For the LA-ICP-MS the deviations from the reference method are <6%. However, when the whole film stoichiometry is considered, as shown by the ternary phase diagram in Fig. 3c, both methods show a good agreement to the ICP-OES reference measurements. This outcome indicates that there is no influence from the substrates of the samples, respective other elements present in the standards (e.g. Na). Since the microgroove approach with LA-ICP-MS offered slightly better results this procedure was used for further applications.

3.5. Application example homogeneity assessment of the deposition system

As application example, the ability of the deposition system to produce homogenous samples was investigated. The aim was to determine scattering effects of boron and the transition metals W and Ta during sputtering. Therefore, a silicon wafer was coated using a TaB_2 and WB_2 target. This created a gradient in the tantalum and tungsten composition, while the boron content should ideally stay the same over the whole wafer. The presented method is ideally suited for accessing the homogeneity, as the whole wafer can be loaded into the ablation apparatus and no further sample handling is necessary. The LA-ICP-MS approach was chosen due to its better results as described preliminary. The wafer consists of 52 fields (Fig. 4a), on each three line scans were measured and the data treated as before. As seen in Fig. 4c, the boron content varies from top to bottom, indicating that the boron content rises with the tantalum concentration, which implies scatting effects

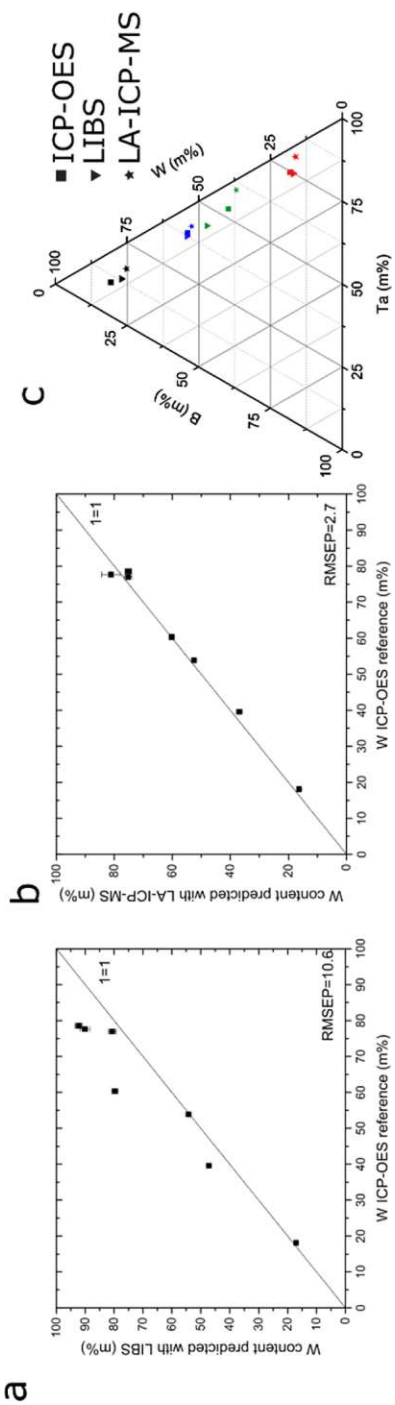

Fig. 3. a: Tungsten content of the samples as predicted by the LIBS with the limited PLS model vs. the ICP-OES reference values. b: Tungsten content of the samples as predicted by the LA-ICP-MS method with microgroove calibration vs. the ICP-OES reference values. c: Ternary phase diagrams showing the agreement of the predicted composition between the LIBS, LA-ICP-MS and the reference ICP-OES values. The error bars represent the standard deviation obtained from three replicate measurements.

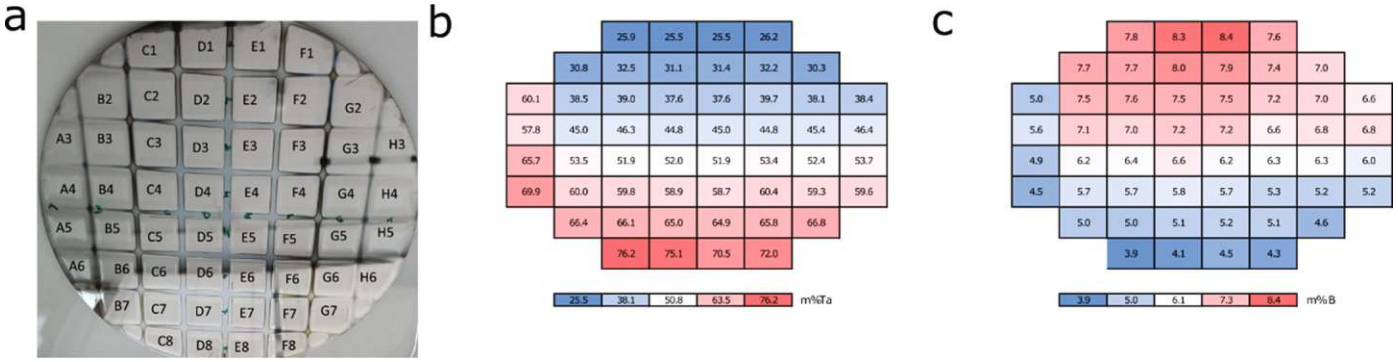

Fig. 4. a: Image of the wafer after deposition, with labels of the fields b: Schematics of the wafer showing the gradient in the tantalum composition, the values in the graphics indicate the tantalum content of the field in m% c: Schematics of the wafer showing the gradient in the boron composition, the values in the graphics indicate the boron content of the field in m%. The boron composition also shows a gradient, which is due to imperfections in the deposition process.

during deposition. Nevertheless, here also the slight increased boron content of TaB_2 target needs to be considered (see also chapter 3.6). This information allows to tune the deposition parameters to obtain thin films with the expected composition.

3.6. Expansion to further systems

The flexibility in the production of dried droplets to produce standards allows to expand this method to different kinds of transition metal boride samples. To demonstrate this ternary tungsten diboride samples alloyed with aluminum, aluminum boride with varying boron content as well as a vanadium alloyed tungsten diboride sample were investigated with the LA-ICP-MS method. [42] Standards were prepared with Aluminum nitrate ($Al(NO_3)_3$) or Vanadium(V)oxide (V_2O_5) dissolved in alkaline solution and processed as described in the experimental section, yielding a highly linear relationship for the calibration ($R^2 > 0.99$). As seen in Supplementary Figure 4, the model yields excellent results (RMSE = 1.87) for predicting the composition of the aluminum-boride as well as the aluminum doped tungsten diboride samples. The approach using the ratios for the model allows to use the same standards for both types of samples. It was also possible to predict the composition of the vanadium tungsten diboride sample with high accuracy, as seen in the ternary phase diagram in Supplementary Figure 4 b.

4. Conclusion

In this work two approaches were presented to combine direct solid sampling with liquid standard quantification. Whereas in previous studies the concept of self-aliquoting micro-grooves was applied in combination with LA-ICP-MS for the quantification of trace elements in challenging liquids [26] or the determination of the Ga content in Ge nanorods [34], we show here that after some improvements this approach can be used for the analysis of protective coating samples consisting of three major constituents. The main advantage of this approach for determination of sample stoichiometry is the fast preparation of standard material and further the flexibility to adopt this method to further elements of interest. In case of LIBS analysis, the use of micro-droplets is an established method for the quantification of trace elements in various sample types [19,27,29,43], here we show that this approach is also applicable for measurement of bulk constituents in protective coating samples.

The determination of the sample stoichiometry was possible with both methods and results were in good agreement with the reference ICP-OES measurements. The LA-ICP-MS based method gave more accurate results than the LIBS based method. This is in accordance with previous studies, as quantitative analysis with LIBS is a more challenging [41,44]. In the concrete application the generally lower linear range in comparison to ICP-MS and the complex spectral overlap between the transition metals is the key factor. However, the simpler instrumentation makes LIBS attractive for quality control, or even in situ applications in vacuum are feasible. The obtained compositions of the samples can be correlated with material properties and used to optimize the deposition parameters.

CRediT authorship contribution statement

Maximilian Weiss: Investigation, Writing - original draft. **Helmut Riedl:** Investigation, Conceptualization, Writing - review & editing. **Vincent Moares:** Investigation. **Paul Heinz Mayrhofer:** Supervision, Resources. **Andreas Limbeck:** Supervision, Conceptualization, Project administration, Resources, Writing - review & editing.

Declaration of Competing interests

The authors declare that they have no known competing financial interests or personal relationships that could have appeared to influence the work reported in this paper.

Acknowledgment

This work was supported by the FWF [grant P31165-N37]. We greatly thank Plansee Composite Materials GmbH, in person Dr. Peter Polcik and Dr. Szilard Kolozsvári, for providing the used target materials.

Supplementary materials

Supplementary material associated with this article can be found, in the online version, at doi:10.1016/j.microc.2019.104449.

References

[1] C Fuger, V. Moraes, R. Hahn, H. Bolvardi, P. Polcik, H. Riedl, P.H. Mayrhofer, Influence of tantalum on phase stability and mechanical properties of WB2, MRS Commun. 9 (2019) 375–380.
[2] C. Mitterer, Borides in thin film technology, J. Solid State Chem. 133 (1997) 279–291.
[3] P.J. Kelly, R.D. Arnell, Magnetron sputtering: a review of recent developments and applications, Vacuum 56 (2000) 159–172.
[4] R. Mertens, Z. Sun, D. Music, J. Schneider, Effect of the composition on the structure of Cr–Al–C investigated by combinatorial thin film synthesis and Ab initio calculations, Adv. Eng. Mater. 6 (2004) 903–907.
[5] H. Euchner, P.H. Mayrhofer, H. Riedl, F.F. Klimashin, A. Limbeck, P. Polcik, S. Kolozsvari, Solid solution hardening of vacancy stabilized TixW1 − xB2, Acta Mater. 101 (2015) 55–61.
[6] E.S.E. Särhammar, N. Martin, T. Nyberg, Sputter rate distribution and compositional variations in films sputtered from elemental and multi-element targets at different pressures, Int. J. Mater. Sci. Appl. 3 (2014) 29–36.
[7] D.M. Mattox, Physical sputtering and sputter deposition, in: D.M. Mattox (Ed.),

Physical sputtering and sputter deposition, Handbook of Physical Vapor Deposition (PVD) Processing (2010).
[8] A.J. Perry, On the existence of point defects in physical vapor deposited films of TiN, ZrN, and HfN, J. Vacuum Sci. Technol.A: Vacuum, Surf. Films 6 (1988) 2140–2148.
[9] A.L. Ivanovskii, Mechanical and electronic properties of diborides of transition 3d-5d metals from first principles: toward search of novel ultra-incompressible and superhard materials, Prog. Mater. Sci. 57 (2012) 184–228.
[10] V. Moraes, C. Fuger, V. Paneta, D. Primetzhofer, P. Polcik, H. Bolvardi, M. Arndt, H. Riedl, P.H. Mayrhofer, Substoichiometry and tantalum dependent thermal stability of α-structured W-Ta-B thin films, Scr. Mater. 155 (2018) 5–10.
[11] A.I. Bazhin, A.A. Goncharov, A.D. Pogrebnyak, V.A. Stupak, S.A. Goncharova, Superhardness effect in transition-metal diborides films, Phys. Met. Metallogr. 117 (2016) 594–601.
[12] C. Jiang, Z. Pei, Y. Liu, J. Xiao, J. Gong, C. Sun, Preparation and characterization of superhard AlB2-type WB2 nanocomposite coatings, Phys. Status Solidi (a) 210 (2013) 1221–1227.
[13] I. Campos-Silva, M. Ortíz-Domínguez, J. Martínez-Trinidad, N. López-Perrusquia, E. Hernández-Sánchez, G. Ramírez-Sandoval, R. Escobar-Galindo, Properties and characterization of hard coatings obtained by boriding: an overview, Defect Diffus. Forum 297-301 (2010) 1284–1289.
[14] A. Cakara, M. Bonta, H. Riedl, P.H. Mayrhofer, A. Limbeck, Development of a multivariate calibration approach for quantitative analysis of oxidation resistant Mo–Si–B coatings using laser ablation inductively coupled plasma mass spectrometry, Spectrochim. Acta Part B: At. Spectrosc. 120 (2016) 57–62.
[15] J. Pisonero, B. Fernández, D. Günther, Critical revision of GD-MS, LA-ICP-MS and SIMS as inorganic mass spectrometric techniques for direct solid analysis, J. Anal. At. Spectrom. 24 (2009) 1145–1160.
[16] A. Limbeck, P. Galler, M. Bonta, G. Bauer, W. Nischkauer, F. Vanhaecke, Recent advances in quantitative LA-ICP-MS analysis: challenges and solutions in the life sciences and environmental chemistry, Anal. Bioanal. Chem. 407 (2015) 6593–6617.
[17] A Limbeck, M. Bonta, W. Nischkauer, Improvements in the direct analysis of advanced materials using ICP-based measurement techniques, J. Anal. At. Spectrom. 32 (2017) 212–232.
[18] Š. Křížová, G. Blažková, R. Skála, Chemical composition of archaeological glasses from prague castle (Czech Republic) from the period 1650–1800 determined by electron probe microanalysis and laser ablation inductively coupled plasma mass spectrometry, Microchem. J. 142 (2018) 236–250.
[19] S.C. Jantzi, V. Motto-Ros, F. Trichard, Y. Markushin, N. Melikechi, A. De Giacomo, Sample treatment and preparation for laser-induced breakdown spectroscopy, Spectrochim. Acta Part B: At. Spectrosc. 115 (2016) 52–63.
[20] V. Lazic, A. Trujillo-Vazquez, H. Sobral, C. Márquez, A. Palucci, M. Ciaffi, M. Pistilli, Corrections for variable plasma parameters in laser induced breakdown spectroscopy: application on archeological samples, Spectrochim. Acta Part B: At. Spectrosc. 122 (2016) 103–113.
[21] Y. Li, D. Tian, Y. Ding, G. Yang, K. Liu, C. Wang, X. Han, A review of laser-induced breakdown spectroscopy signal enhancement, Appl. Spectrosc. Rev. 53 (2017) 1–35.
[22] X.-.L. Yu, Y. He, Challenges and opportunities in quantitative analyses of lead, cadmium, and hexavalent chromium in plant materials by laser-induced breakdown spectroscopy: a review, Appl. Spectrosc. Rev. 52 (2016) 605–622.
[23] Y. Ke, Y. Sun, P. Lin, J. Zhou, Z. Xu, C. Cao, Y. Yang, S. Hu, Quantitative determination of rare earth elements in scheelite via LA-ICP-MS using REE-doped tungstate single crystals as calibration standards, Microchem. J. 145 (2019) 642–647.
[24] A. Hanć, P. Zduniak, K. Erciyas-Yavuz, A. Sajnóg, D. Barałkiewicz, Laser ablation-ICP-MS in search of element pattern in feathers, Microchem. J. 134 (2017) 1–8.
[25] S. Turková, M. Vašinová Galiová, K. Štůlová, Z. Čadková, J. Száková, V. Otruba, V. Kanický, Study of metal accumulation in tapeworm section using laser ablation-inductively coupled plasma-mass spectrometry (LA-ICP-MS), Microchem. J. 133 (2017) 380–390.
[26] W. Nischkauer, F. Vanhaecke, S. Bernacchi, C. Herwig, A. Limbeck, Radial line-scans as representative sampling strategy in dried-droplet laser ablation of liquid samples deposited on pre-cut filter paper disks, Spectrochim. Acta Part B At. Spectrosc. 101 (2014) 123–129.
[27] N. Aras, Ş. Yalçın, Investigating silicon wafer based substrates for dried-droplet analysis by laser-induced breakdown spectroscopy, Spectrochim. Acta Part B: At. Spectrosc. 152 (2019) 84–92.
[28] K. Kysenius, B. Paul, J.B. Hilton, J.R. Liddell, D.J. Hare, P.J. Crouch, A versatile quantitative microdroplet elemental imaging method optimised for integration in biochemical workflows for low-volume samples, Anal. Bioanal. Chem. 411 (2019) 603–616.
[29] N. Aras, S. Yalcin, Development and validation of a laser-induced breakdown spectroscopic method for ultra-trace determination of Cu, Mn, Cd and Pb metals in aqueous droplets after drying, Talanta 149 (2016) 53–61.
[30] S. Rovelli, W. Nischkauer, D.M. Cavallo, A. Limbeck, Multi-element analysis of size-segregated fine and ultrafine particulate via laser ablation-inductively coupled plasma-mass spectrometry, Anal. Chim. Acta 1043 (2018) 11–19.
[31] S.J. Van Malderen, E. Vergucht, M. De Rijcke, C. Janssen, L. Vincze, F. Vanhaecke, Quantitative determination and subcellular imaging of Cu in single cells via laser ablation-ICP-mass spectrometry using high-density microarray gelatin standards, Anal. Chem. 88 (2016) 5783–5789.
[32] W. Nischkauer, F. Vanhaecke, A. Limbeck, Self-aliquoting micro-grooves in combination with laser ablation-ICP-mass spectrometry for the analysis of challenging liquids: quantification of lead in whole blood, Anal. Bioanal. Chem. 408 (2016) 5671–5676.
[33] M. Pabst, S.R. Fagerer, R. Kohling, S.K. Kuster, R. Steinhoff, M. Badertscher, F. Wahl, P.S. Dittrich, K. Jefimovs, R. Zenobi, Self-aliquoting microarray plates for accurate quantitative matrix-assisted laser desorption/ionization mass spectrometry, Anal. Chem. 85 (2013) 9771–9776.
[34] P. Pertl, M.S. Seifner, C. Herzig, A. Limbeck, M. Sistani, A. Lugstein, S. Barth, Solution-based low-temperature synthesis of germanium nanorods and nanowires, Monatsh. Chem. 149 (2018) 1315–1320.
[35] L. Zauner, P. Ertelthaler, T. Wojcik, H. Bolvardi, S. Kolozsvári, P.H. Mayrhofer, H. Riedl, Reactive HiPIMS deposition of Ti-Al-N: influence of the deposition parameters on the cubic to hexagonal phase transition, Surf. Coat. Technol. (2019).
[36] R.D. Deegan, O. Bakajin, T.F. Dupont, G. Huber, S.R. Nagel, T.A. Witten, Capillary flow as the cause of ring stains from dried liquid drops, Nature 389 (1997) 827–829.
[37] R.C. Wiens, S. Maurice, J. Lasue, O. Forni, R.B. Anderson, S. Clegg, S. Bender, D. Blaney, B.L. Barraclough, A. Cousin, L. Deflores, D. Delapp, M.D. Dyar, C. Fabre, O. Gasnault, N. Lanza, J. Mazoyer, N. Melikechi, P.Y. Meslin, H. Newsom, A. Ollila, R. Perez, R.L. Tokar, D. Vaniman, Pre-flight calibration and initial data processing for the Chemcam laser-induced breakdown spectroscopy instrument on the mars science laboratory rover, Spectrochim. Acta Part B: At. Spectrosc. 82 (2013) 1–27.
[38] Y. Liu, Z. Hu, S. Gao, D. Günther, J. Xu, C. Gao, H. Chen, In situ analysis of major and trace elements of anhydrous minerals by LA-ICP-MS without applying an internal standard, Chem. Geol. 257 (2008) 34–43.
[39] T. Vaculovič, K. Breiter, Z. Korbelová, N. Venclová, K. Tomková, Š. Jonášová, V. Kanický, Quantification of elemental mapping of heterogeneous geological sample by laser ablation inductively coupled plasma mass spectrometry, Microchem. J. 133 (2017) 200–207.
[40] A.L. Vieira, T.V. Silva, F.S.I. de Sousa, G.S. Senesi, D.S. Júnior, E.C. Ferreira, J.A.G. Neto, Determinations of phosphorus in fertilizers by spark discharge-assisted laser-induced breakdown spectroscopy, Microchem. J. 139 (2018) 322–326.
[41] F. Ruan, T. Zhang, H. Li, Laser-induced breakdown spectroscopy in archeological science: a review of its application and future perspectives, Appl. Spectrosc. Rev. 54 (2019) 573–601.
[42] R. Hahn, V. Moraes, A. Limbeck, P. Polcik, P.H. Mayrhofer, H. Euchner, Electron-configuration stabilized (W,Al)B2 solid solutions, Acta Mater. 174 (2019) 398–405.
[43] M. Dell'Aglio, Z. Salajková, A. Mallardi, R. Mezzenga, L. van't Hag, N. Cioffi, G. Palazzo, A. De Giacomo, Application of gold nanoparticles embedded in the amyloids fibrils as enhancers in the laser induced breakdown spectroscopy for the metal quantification in microdroplets, Spectrochim. Acta Part B: At. Spectrosc. 155 (2019) 115–122.
[44] M. Rühlmann, D. Büchele, M. Ostermann, I. Bald, T. Schmid, Challenges in the quantification of nutrients in soils using laser-induced breakdown spectroscopy – A case study with calcium, Spectrochim. Acta Part B: At. Spectrosc. 146 (2018) 115–121.

Supplementary Tables

Supplementary Table 1: ICP-OES Parameters

RF-Power	1350 W
Radial observation height	10 mm
Cool gas flow (Ar)	12 L/min
Nebulizer gas flow (Ar)	0.75 L/min
Auxiliary gas flow (Ar)	0.4 L/min
Integration time per replicate	25 s
Replicates per sample	3
Purge pump flow rate	1.6 mL/min
Analysis pump flow rate	0.8 mL/min

Measured Elements	Emission line used for quantification [nm]	Emission line used for quality control [nm]
Al	396.152 (I)	309.271 (I)
B	249.773 (I)	208.893 (I)
Ta	240.063 (II)	268.517 (II)
V	309.311 (II)	286.796 (I)
W	239.709 (II)	224.875 (II)

Supplementary Table 2: Composition of sputtering targets and used powder materials for the spark plasma sintering route (± corresponds to the single standard deviation between three replicate digestions).

	X m%	B m%
WB_2 target 1	90.5 ±0.5	9.5±0.5
WB_2 target 2	91.6±0.1	8.4±0.1
WB_2 powder	91.3±0.6	8.7±0.6
TaB_2 Target	89.7±0.1	10.3±0.1
VB_2 Target	71.1±0.6	28.9±0.6
VB_2 powder	71.4±0.6	28.6±0.6

Supplementary Figures

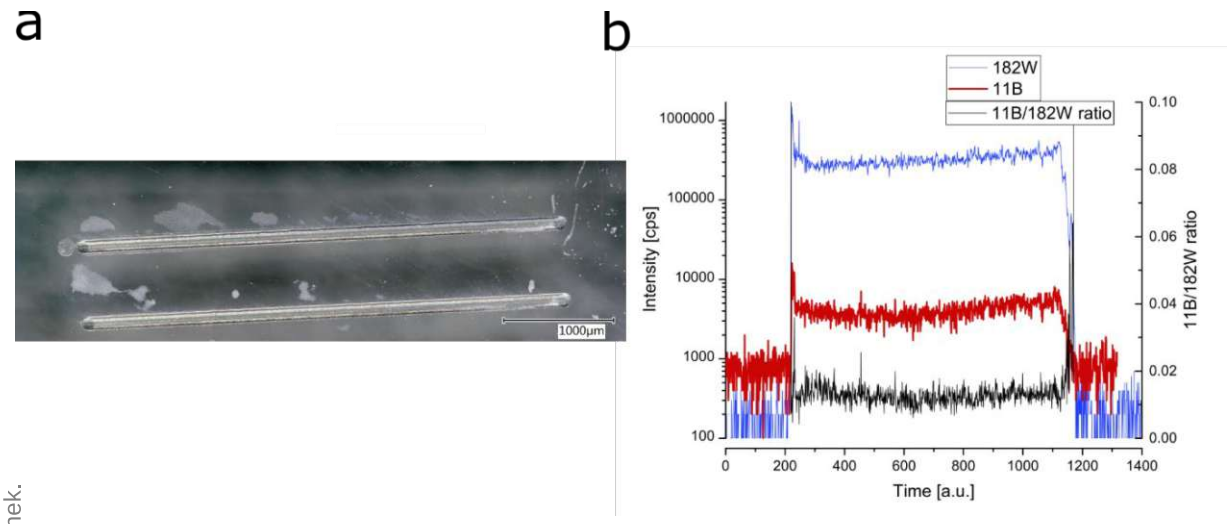

Supplementary Figure 1: a: Microscopic image of the microgrooves filled with standard. b: Transient ICP-MS signals during the ablation of the microgrooves, showing a constant ablation behavior.

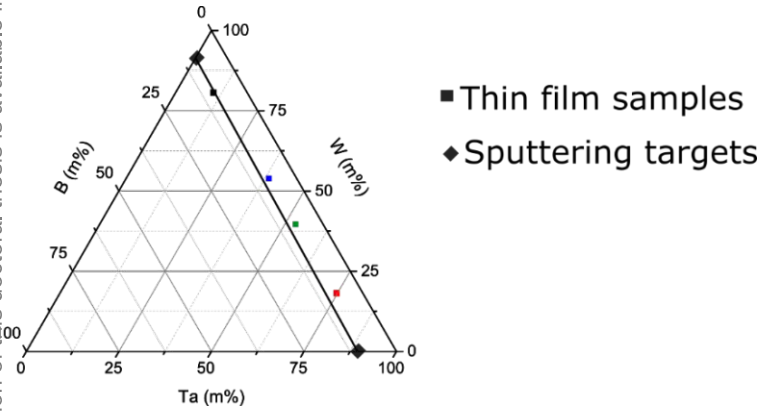

Supplementary Figure 2: Ternary Phase Diagram with the composition of the sputtering targets and the resulting samples. The Full line indicates the composition of ideal mixtures of the two diboride targets

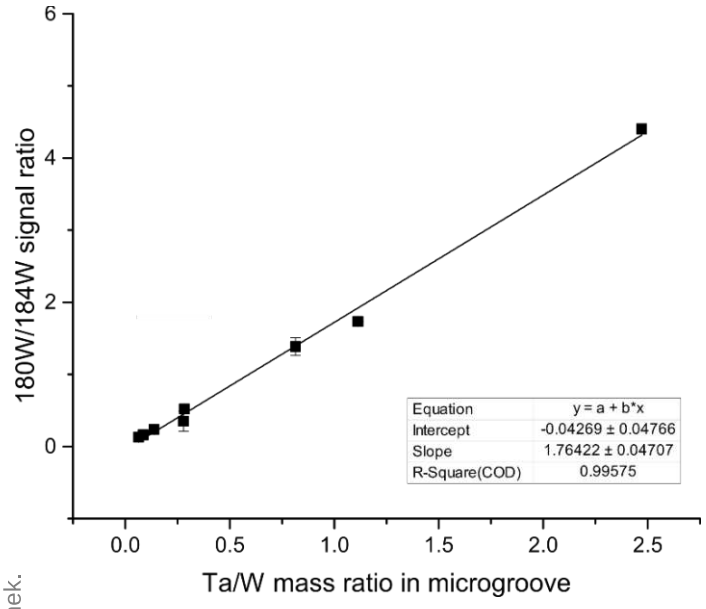

Supplementary Figure 3: Calibration curve for the microgroove calibration using elemental ratios, error bars denoting single standard deviation(n=3), indicating a highly linear behavior(R^2>0.99)

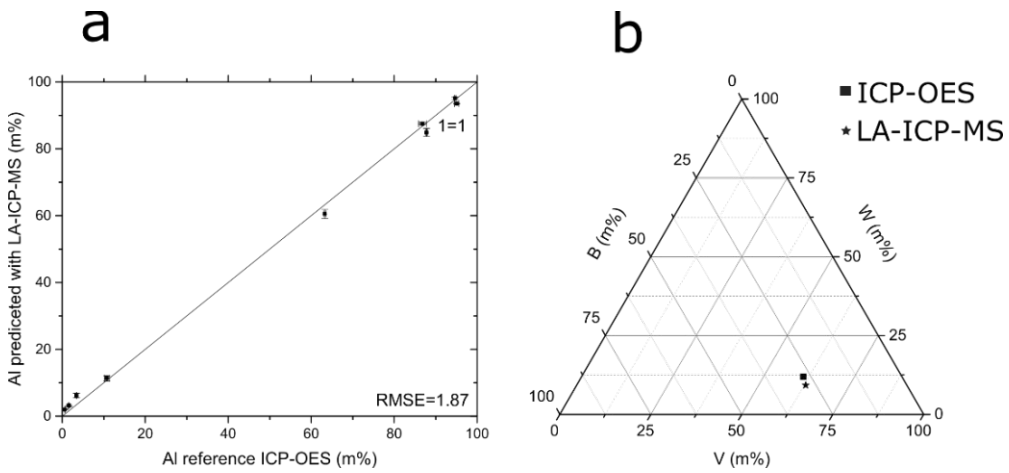

Supplementary Figure 4: Extension of the microgroove method to further systems: a: Aluminum content of the samples as predicted by the LA-ICP-MS method with microgroove calibration vs. the ICP-OES reference values. b: Ternary phase diagram of the Vanadium Tungsten Diboride sample, showing an excellent agreement between the LA-ICP-MS method and the ICP-OES reference values.

4 Publication 2

Quantitative analysis of the platinum surface decoration on lanthanum strontium iron oxide thin films via online-LASIL-ICP-MS

Maximilian Weiss [a], Christoph Riedl [b] , Johannes Frank [c] , Jürgen Fleig [b] and Andreas Limbeck [a]

a Institute of Chemical Technologies and Analytics, TU Wien, Getreidemarkt 9/164-I^2AC -1060 Vienna, Austria

b Institute of Chemical Technologies and Analytics, TU Wien, Getreidemarkt 9/164-EC -1060 Vienna, Austria

c Joint Workshop Technical Chemistry, TU Wien, Getreidemarkt 9, 1060 Vienna, Austria

Published in: Microchemical Journal 166 (2021) 106236

Microchemical Journal 166 (2021) 106236

Contents lists available at ScienceDirect

Microchemical Journal

journal homepage: www.elsevier.com/locate/microc

Quantitative analysis of the platinum surface decoration on lanthanum strontium iron oxide thin films via online-LASIL-ICP-MS

Maximilian Weiss [a,*], Christoph Riedl [b], Johannes Frank [c], Jürgen Fleig [b], Andreas Limbeck [a,*]

[a] TU Wien Institute of Chemical Technologies and Analytics, Getreidemarkt 9/164-I²AC, 1060 Vienna, Austria
[b] TU Wien Institute for Chemical Technologies and Analytics, Getreidemarkt 9/164-EC, 1060 Vienna, Austria
[c] TU Wien Joint Workshop Technical Chemistry, Getreidemarkt 9/164-EC, 1060 Vienna, Austria

ARTICLE INFO

Keywords:
Laser ablation of solids in liquids
ICP-MS
Imaging
Depth profiling
Mixed ionic electronic conductors

ABSTRACT

Solid oxide fuel cells (SOFCs) are one of the key technologies on the way to environmentally friendly power generation. Current research activities aim to reduce their operational temperature to intermediate temperatures (400–600 °C) to make their application more feasible. In a recent approach, lanthanum strontium iron oxide (LSF) thin film electrodes, a mixed ionic electronic conducting (MIEC) material, was decorated with tiny amounts of platinum nanoparticles, which led to a significant improvement of the oxygen reduction kinetics. To understand this material combination a precise characterization is of major interest, especially the exact amount of platinum on the surface. As the studied model-type thin film electrode requires a platinum current collector buried beneath the LSF to improve in-plane electron conductivity, a method providing quantitative information as well as sufficient depth resolution is needed.

In this work, we further improved the recently presented approach of online laser ablation of solids in liquids (LASIL), which enabled in combination with ICP-MS detection a spatially resolved analysis of the sample composition. Careful optimization of laser parameters and carrier solution led to a depth resolution of 30 nm, which allowed a clear separation of the Pt-signals from the surface decoration and the underlying current collector. The amount of platinum on the surface was determined using calibration with a matrix matched standard and validated by another method. Finally, the imaging capabilities of the proposed online-LASIL approach have been employed to assess the homogeneity of the Pt-decoration, indicating significant variations within the investigated area. Thus, further improvements in the electrochemical properties of the investigated LSF electrodes could be anticipated by fabrication of MIECs with a more homogeneous platinum decoration.

1. Introduction

Solid oxide fuel cells (SOFCs) directly convert chemical energy of fuels to electric energy at highly-efficiency and are therefore promising candidates for environmentally friendly power generation [1,2]. One of the main goals of current research activities is lowering the operation temperature of SOFCs from around 800 °C to intermediate temperatures (400 °C – 600 °C) [3,4]. This requires new electrode materials, which should offer sufficiently fast electrode kinetics even at those lower temperatures. Perovskite-type mixed ionic and electronic conductors (MIECs) are among the most promising candidates for future SOFC electrodes. In several studies, the properties of numerous MIEC materials, such as $SrTi_{1-x}Fe_xO_{3-\delta}$ [5–7], $La_xSr_{1-x}MnO_{3-\delta}$, [8] $La_{1-x}Sr_xFeO_{3-\delta}$ [9–12], $La_{1-x}Sr_xCoO_{3-\delta}$, [13–16] $La_{1-x}Sr_xFe_{1-y}Co_yO_{3-\delta}$ [17,18] $Ba_{1-x}Sr_xFe_{1-y}Co_yO_{3-\delta}$ [19,20] were investigated. Apart from faster oxygen reduction kinetics, SOFC electrode materials should exhibit morphological stability, possess high ionic and electronic conductivity, show little degradation and be compatible with other materials of the fuel cell [1].

A recent study [21] revealed lanthanum strontium iron oxide – $La_{0.6}Sr_{0.4}FeO_{3-\delta}$ (LSF64) – thin film electrodes decorated with tiny amounts of platinum show by far lower polarization resistance (e.g., faster oxygen exchange kinetics) than undecorated LSF electrodes. At lower oxygen partial pressures (0.25 mbar O_2) up to 70 times faster oxygen reduction kinetics were measured (e.g., the polarization resistance dropped from 125 Ωcm² to 2 Ωcm², at 600 °C). Moreover, platinum decorated LSF electrodes showed superior properties, such as lower degradation of the electrode and higher reproducibility of

* Corresponding authors.
E-mail addresses: maximilian.weiss@tuwien.ac.at (M. Weiss), andreas.limbeck@tuwien.ac.at (A. Limbeck).

https://doi.org/10.1016/j.microc.2021.106236
Received 2 February 2021; Received in revised form 8 March 2021; Accepted 9 March 2021
Available online 6 April 2021

resistance values.

To understand those promising systems, a precise characterization is desired, to correlate material properties, in particular the deposited amount of platinum, with electrochemical performance. This enables to further boost their performance through optimized material systems and production conditions. Besides the deposited amount of platinum per surface area, also the homogeneity of the Pt-distribution on the LSF surface is of major interest.

At first glance, this seems to be a rather simple task, done by sample digestion and liquid measurement, but for electrochemical impedance measurements of thin film electrodes (~100 nm thickness) current collector grids made out of platinum are used beneath the thin film to improve in-plane conductivity. Thus, an analytical method applicable for analyzing this special kind of samples should have enough surface sensitivity to distinguish between surface decoration and the underlying collector grids. Application of conventional digestion procedures with subsequent analysis is not feasible since a selective digestion of the surface decoration only is not possible, because the platinum originating from the current collector would mask the signal from the surface platinum decoration. Moreover, no information about the platinum distribution is accessible. To circumvent the problems associated with sample digestion, direct analysis of solid materials using solid sampling techniques is recommended [22–24]. Routinely applied direct solid-state methods such as secondary ion mass spectrometry (SIMS), glow discharge optical emission spectroscopy/mass spectroscopy (GD-OES/MS) and X-ray photoelectron spectroscopy (XPS) have their specific advantages but also drawbacks, SIMS is especially prone to matrix effects, GD-OES/MS does not enable spatially resolved measurements, and the application of XPS is limited by the comparatively poor sensitivity [25,26], which limits their applicability for this kind of material.

An alternative solid sampling technique is laser ablation inductively coupled plasma mass spectrometry (LA-ICP-MS). However, the depth resolution of the most frequently applied nanosecond laser-systems is not competitive to the techniques mentioned above, and thus does not allow a differentiation between the platinum surface decoration and the platinum current collector. The use of femtosecond lasers achieves depth resolutions of a few nanometers [27,28], but a much more costly equipment is required which is not accessible to many research groups. Moreover, for quantitative investigations the use of matrix matched reference materials is required, especially for novel classes of materials such standards are usually not available [25,29–32].

A method that fulfills the requirements stated above is laser ablation of solids in liquids (LASIL). Thereby a very fine dispersion of nanoparticulates is produced via laser ablation of a solid sample in a liquid. This method is used extensively in nanomaterial research [33,34] for the production of nanoparticles of different size and composition. The first application for analytical purposes was reported by Muravitskaya et al. [35]. In the studies reported so far [36–38] the produced nanoparticles were analyzed offline using conventional liquid nebulization ICP-OES or ICP-MS. This approach has two distinctive advantages: first it avoids a laborious sample digestion, which might be challenging for some technologically advanced materials, second it enables the use of ready to hand liquid standards, as the nanoparticles are completely ionized in the ICP if they are small enough [39]. To extend the capabilities of this method, recently LASIL was realized in an online approach, [40] which evades all manually performed sample handling steps. Moreover, online analysis of the generated nanoparticle suspension enables spatially resolved investigations, i.e., imaging [41] and depth profiling. Initial experiments performed in the work of Bonta et al. [40] for a material similar to the one used in this study indicated an ablation rate in the order of 35 nm per shot for strontium titanate (STO), which is a considerable improvement when compared to the depth profiling capabilities of conventional LA-ICP-MS with nanosecond laser instrumentation [27,28].

In this work, the applicability of online-LASIL for assessment of the platinum decoration on the surface of LSF electrodes has been investigated. After careful optimization, the procedure enabled the selective analysis of the surface decoration with platinum, moreover, the homogeneity of the platinum distribution could be monitored by spatially resolved measurements of the samples.

Table 1
Instrument operating conditions.

Laser NWR 213		ICP-MS	
Laser Fluence	1.2 J/cm^2	RF Power	1400 W
Spot Size	50 μm	Nebulizer gas flow rate (Ar)	1 L/min
Scanning Speed	50 μm/s	Cool gas flow rate (Ar)	14 L/min
Repetition Frequency	2 Hz	Auxiliary gas flow rate (Ar)	0.65 L/min
Ablated Area	0.35 mm^2	Dwell Time	0.05 s
Liquid carrier solution flow	0.5 mL/min	Monitored isotopes	^{194}Pt, ^{196}Pt, ^{115}In, ^{139}La, ^{90}Zr

2. Experimental

2.1. Reagents

Ultrapure water was prepared with a Barnstead EASYPURE II water system (ThermoFisher Scientific, USA), single element ICP standards were purchased from Merck (Germany), as well as hydrochloric acid (HCl) and nitric acid (HNO_3) and all chemicals not otherwise mentioned at least of analytical grade.

2.2. Instrumentation

For laser ablation, a NWR213 laser ablation system (ESI, USA), operating at a wavelength of 213 nm, was used. A quadrupole ICP-MS iCAP Qc (ThermoFisher Scientific, Germany) instrument with the standard cyclonic spray chamber and PFA nebulizer was used for analyte detection, as well as for liquid reference analysis and operated without collision gas, the applied instrumental settings are listed in Table 1. For the liquid reference analysis, in this case instead of the LASIL cell, an autosampler (SC-2-DX, ESI, USA) combined with an ESI Fast valve (ESI, USA) were connected with the sample introduction system. Data were collected using the instrument software, Qtegra Version 2.8. For imaging experiments, the raw platinum ICP-MS signal was background corrected using OriginPro 2020 (OriginLab Corporation, USA), images were created then with ImageLab Software (version 2.99, Epina GmbH, Austria), normalizing the platinum signal to the indium internal standard for correction of instrumental drift during the data acquisition. One way ANOVA (analysis of variance) was performed in Excel (Microsoft Cooperation, USA), to access the homogeneity of images. Measurement of crater depths was performed using a Dektak XT (Bruker, USA) stylus profilometer. The size distribution of the nanoparticles generated in the LASIL process was determined by particle tracking (ZetaView, Particle Metrix, Germany).

2.3. LASIL setup and measurements

The LASIL setup used in this work is mostly similar to that one described in [42]. In short, the sample is placed in a cavity of the PEEK body, which allows to flush the surface of the investigated 5x5x0.5 mm samples with the carrier solution. The fluid path over the sample is determined by the 2 mm wide channel in the polydimethylsiloxane (PDMS) spacer (thickness 500 μm), which also seals the cell. See Supplementary Fig. 1 and [42] for a more detailed information. On top a UV-transparent fused silica window is placed. The carrier fluid is

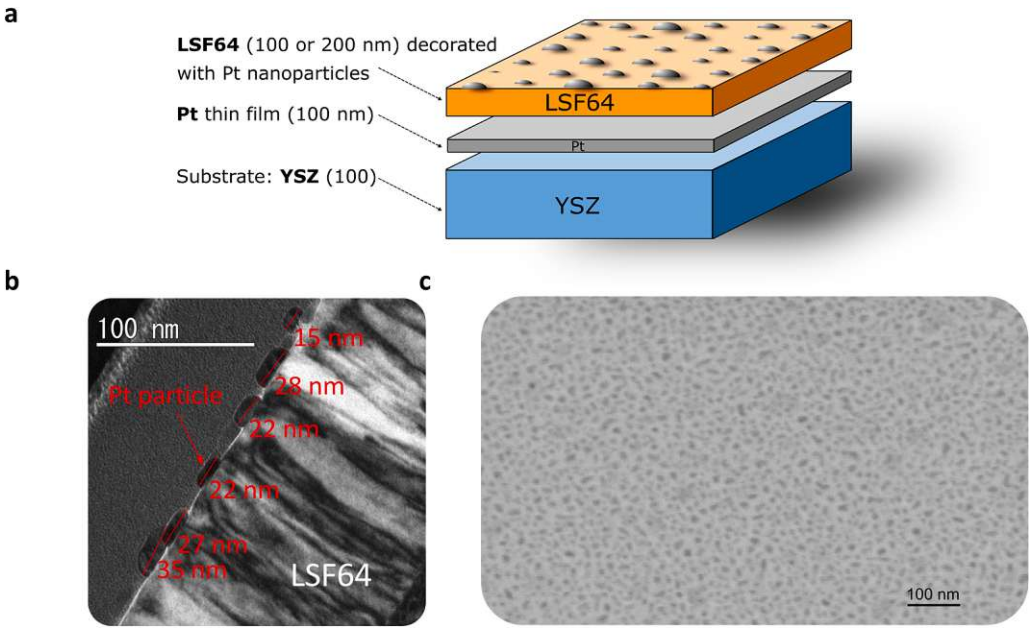

Fig 1. a: Schematic of the samples consisting of a YSZ substrate, a platinum current collector electrode, a LSF thin film and platinum nanoparticles as surface decoration, b: TEM image of cross section showing the platinum nanoparticles on the surface, c: A high resolution SEM image of the surface decoration, showing individual platinum nanoparticles with a size of about 20 nm [21].

pumped by a peristaltic pump (Perimax 12, SPETEC, Germany). All tubing was made of PFA, with an inner diameter of 0.5 mm on the input side to the cell and 0.25 mm between the cell and the ICP-MS instrument, to ensure a fast washout and transport of the analyte particles. The LASIL cell is placed in the ablation chamber of the NWR213 laser. To correct for eventual drifts during the measurement indium as internal standard with a concentration of 1 ng/g was added to all carrier solutions.

Prior to measurement the ICP-MS instrument was tuned for a maximum ^{115}In signal. For sample analysis on each sample 3 patterns using the laser parameters listed in Table 1 were measured. Transient signals were collected and integrated with the Qtegra software and normalized to the signal observed for ^{115}In used as internal standard.

2.4. Production of samples

Dense $La_{0.6}Sr_{0.4}FeO_{3-\delta}$ (LSF) thin films were prepared on one-side polished yttria stabilized zirconia single crystals (100) (YSZ) (Crystec, Germany). LSF powder was synthesized via the Pechini route [43] from Fe, La_2O_3 and $SrCO_3$ and the pulsed laser deposition (PLD) target was then prepared by isostatic pressing (150 MPa) and sintering at 1200 °C for 12 h. Laser deposition was performed at 600 °C substrate temperature (measured with a pyrometer) and 0.04 mbar oxygen partial pressure (Alphagaz, 99.995%) with a KrF excimer laser (Lambda COMPexPro 201F, wavelength 248 nm) at a frequency of 5 Hz, a laser energy of 2 J/cm^2 and a target to substrate distance of 6 cm. The deposition time was 30 min (9000 pulses) leading to a LSF thickness of 100 nm. LSF thin films were then decorated with platinum via magnetron sputter deposition (Baltech MED-020, Liechtenstein) for 2 s at an argon pressure of $2*10^{-2}$ mbar and a sputter current of 100 mA. However, to vary the deposited platinum amount, the sputter current (between 20 mA and 100 mA) and the sputter duration (between 2 and 5 s) were also varied. A cross section of the sample as well as electron microscopic image of the platinum decoration are shown in Fig. 1 The thickness of the LSF thin film was determined by introducing holes in the thin film by applying YSZ paste before the PLD step, which was removed afterwards by rinsing with ethanol. The film thickness was then determined by stylometric measurements with a Dektak XT (Bruker, USA).

2.5. Reference sample analysis

For verification of the online-LASIL measurements, samples without platinum current collector were produced. Those samples were digested with 1 mL aqua regia (3:1 HCl: HNO_3) in 15 mL polypropylene tubes in a water bath at 60 °C for 10 min. The samples were then diluted with ultrapure water to a final mass of 10 g. From this solution three aliquots per sample were further diluted 1:100 with 1% (v/v) HNO_3, and after addition of indium to obtain a concentration of 1 ng/g of this element in the samples, they were analyzed by solution nebulization (NEB) ICP-MS. Calibration solutions (ranging from 0.1 to 10 ng/g prepared in 1% (v/v) HNO_3 were used for calibration.

3. Results and discussion

3.1. Optimization of the carrier solution

Although the production of nanoparticles via laser ablation in liquid is an industrial process, careful optimization of the applied fabrication parameters is necessary to achieve nanoparticle with the desired dimensions. Indeed, particle characteristics such as size, shape and colloidal stability can vary over a wide range and depends on the properties of the used liquid medium. For online LASIL analysis the nanoparticles size must be small enough to prevent deposition in the system, enabling an efficient transport of the particles from the LASIL cell to the ICP-MS. Moreover, smaller particles are also beneficial for the measurement step, since atomization and ionization of larger particles can be incomplete. On top of that, preliminary experiments showed that only a part of the ablated material is transferred into suspended nanoparticles, another part becomes dissolved in the carrier solution. These analyte ions need to be stabilized to prevent unwanted losses due to adsorption of analyte on the walls of the LASIL cell, the applied transport tubing, the nebulizer, or the spray chamber of the sample introduction system.

In more conventional analysis, solutions are usually acidified to prevent analyte loss due to adsorption, or organic additives are used to complex the analyte ion [44]. As LSF would dissolve in concentrated acid [15] and the carrier solutions needs to be transparent in the

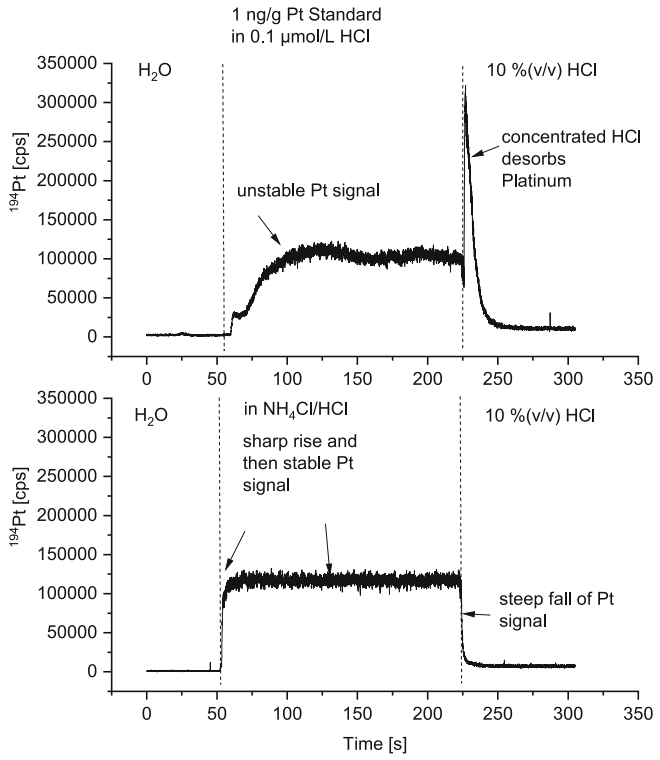

Fig 2. Optimization of carrier solution composition: To optimize the solvent conditions a 1 ng/g platinum standard solution was injected into the LASIL setup. After the signal has stabilized an acid solution (10% (v/v)) HCl was injected to desorb all platinum from the tubing walls. Top: Using only very diluted (1 µmol/L) HCl yields to adsorption of platinum, which gives a slow response in the signal and a large peak of the adsorbed platinum after switching to concentrated HCl. Bottom: Using the optimized NH_4Cl/HCl solution concentration the platinum signal drops fast to the baseline after the switching to concentrated HCl, indicating that no adsorption has occurred. Further the rise of the signal is much faster, and the achieved plateau is much more stable than with diluted acid alone.

ultraviolet region at 213 nm, which rules out many organic compounds, this approach could not be used in the current application. Thus, different combinations of diluted hydrochloric acid and ammonia chloride were investigated. These substances are transparent in the ultraviolet light range and the excess of chloride ions can form stronger complexes with platinum ions to stabilize them. The investigated NH_4Cl/HCl mixing solutions resulted in weak acidic conditions, which did not harm the integrity of the LSF thin film while preventing losses of the ions formed in the LASIL process due to adsorption or precipitation of cations.

Fig. 2 summarizes the optimization of the carrier solution. First, water is pumped through the LASIL cell with a plain YSZ single crystal replacing the actual sample, then the carrier solution is switched to a 1 ng/g platinum standard in the medium of interest – 30 mmol/L HCl in the shown experiment. As can be deduced from Fig. 2 there was no sudden increase in the platinum signal, instead a continuous rise over a period of roughly 50 s was observed until the ICP-MS platinum signal has stabilized. Then, the carrier is switched to a 10% (v/v) HCl, resulting in a sharp increase of the platinum-signal, which decreased quickly to background level. This outcome indicates that a part of platinum in the introduced standard was lost during transport from the LASIL cell to the ICP-MS, since diluted HCl could not prevent the retention of platinum on the surface of LASIL cell or applied transport tubing. Purging of the system with concentrated HCl results in a release of the platinum species which have been adsorbed in the system.

A completely different behavior was observed when using the optimized carrier solution containing NH_4Cl and HCl. Switching from water

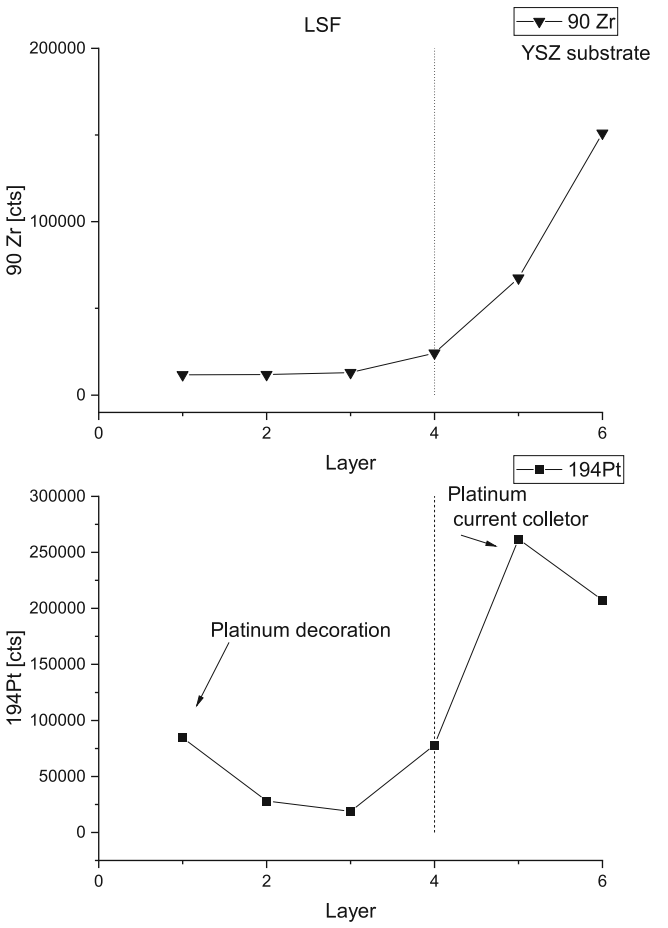

Fig 3. Depth profile of ^{90}Zr (top) and ^{194}Pt (bottom) for sample with a platinum decorated 200 nm thick LSF thin film and a platinum current collector beneath. The depth of one ablation layer is approximately 60 nm. The platinum decoration on top of the LSF can clearly be separated from the platinum current collector beneath, as the platinum signal is high in the first layer, stemming from the surface decoration, then drops, and rises again in the 4th ablation layer, as the platinum current collector is reached. In the 5th ablation layer, the rising zirconium signal indicates that the YSZ substrate has been ablated.

as carrier solution to the NH_4Cl/HCl-solution containing 1 ng/g platinum results in an abrupt rise of the signal, reaching constant level without any further decrease. When switching from this platinum standard to 10% (v/v) HCl as purge solution, no desorption of platinum was observed, but a fast drop of the signal to baseline level occurred. This result indicates that no adsorption and thus no analyte loss has occurred with the use of platinum in NH_4Cl/HCl medium (Fig. 2). The optimized condition was found to be 30 mmol/L hydrochloric acid and 910 mmol/L NH_4Cl, with pH of 5, giving the best stabilization of the platinum ions, while not attacking the LSF.

3.2. Optimization of depth resolution

3.2.1. Single spot measurements

For differentiation of the platinum decoration from the current collector a sufficient depth resolution is required. Therefore, the parameters for sample ablation and transport of the generated nanosol to the detection device have to be carefully optimized, in particular the effect of the carrier solution flow rate and the laser energy. The ablation rate at these optimized conditions (Table 1) was determined by measuring a series of single spots with a profilometer (Dektak XT), which yielded an average ablation of 30 nm per shot. This is in good agreement to previous work [40], where 35 nm per shot were found for strontium

titanate (STO), a similar ceramic material. However, the platinum signals observed for individual spots varied leading to a difficult data interpretation. This can be to one part attributed to the limited signal intensity due to the low coverage of the surface, which therefore yields a poor signal to noise ratio. To the other part, it is not clear if the decoration provides sufficient homogeneity. Therefore, an improved approach is required for the quantitative determination of the platinum decoration.

3.2.2. Measurement of line patterns

To circumvent possible problems with sample inhomogeneity and to give a higher signal for an improved signal to noise ratio, a larger area was ablated with line scans. Repetition rate and scan speed were chosen to allow an overlap between the individual laser spots, resulting in the application of 2 laser spots per position (Table 1). Considering the ablation rate per laser shot of approximately 30 nm this procedure should still provide sufficient depth resolution for differentiation between surface decoration and collector grid. That only the uppermost layer of platinum was ablated was confirmed by measuring two samples with 100 nm thick LSF thin film from the same decoration process, i.e., the same amount of platinum on the top, where one sample was fabricated with and one sample without a current collector. These two samples gave the same platinum signal for the surface decoration ($p = 0.96$). Completeness of platinum removal was controlled by a second measurement of the investigated sample locations using identical LASIL conditions. As expected, the analysis of the sample with no current collector platinum showed signals comparable to the experimental blank, whereas for the samples with current collector a significant increase in the platinum signal was observed.

Using optimized laser conditions, a depth profile was recorded by passing the pattern six times over a sample with a 200 nm thick LSF film (Fig. 3). The platinum signal from the surface decoration is the highest signal in the first ablation layer and drops remarkably in the second and third ablation layer. The fourth ablation layer shows a significant increase in the Pt-signal, indicating that with this ablation layer the current collector has been reached. Contrary results were found for Zr, which is a constituent of the substrate. Signals close to the background level were observed for the first three layers, a slight increase was observed for layer four, and strongly rising signals for the layers five and six. This signal sequence indicates that the first three layers were made only of LSF, the fourth layer partially hit the YSZ substrate, and layers 5 and 6 belong definitively to the YSZ substrate. This outcome is consistent with the findings derived for the ablation rate. As mentioned before the applied LASIL parameters enabled the removal of approximately 30 nm material per laser shot. Thus, with three ablation layers six shots were fired per sample location, resulting in the ablation of around 180 nm deep– up to this sample depth only signals from the surface decoration and the LSF could be expected. With the fourth layer a sample depth of ~240 nm has been reached, hence, there should be signals from the current collector and the YSZ substrate.

For comparison, the same sample was ablated using a conventional 213 nm laser system and single shot ablation mode. Helium was used as carrier gas with a flow of 650 mL/min, argon makeup gas with a flow of 0.8 L/min was added using a concentric mixer.

It was not possible to separate the two layers of platinum, the platinum signal showed a huge intensity for the very first shot, and then decreases approximately to one tenth of the signal with the second shot, whereas the third and all further laser shots revealed signals close to background level. The presence of a high zirconium signal from the YSZ substrate in the first shot, which increased slightly with the second shot and remained constant afterwards, indicated that even with this first shot the substrate has been reached. This result clearly points to a simultaneous ablation of Pt-decoration, LSF thin film and platinum current collector with the employed ns LA-system. Profilometric measurements of the obtained ablation crater revealed an ablation rate of 200 nm per shot, which is clearly not sufficient for the current application.

3.3. Measurements of platinum decoration

From conventional laser ablation ICP-MS it is known that the ablated material is not quantitatively transported to the plasma, due to redeposition of particles. Transport efficiency was about 40% in early studies, with highly optimized cell design and femtosecond lasers up to 80–90% can be achieved. [39,45,46]. In previously reported online-LASIL applications, only elemental ratios were of interest [40–42], where a potential loss of particles is not a problem as long as elemental fractionation is corrected [47]. Even though preliminary experiments with a particle tracking analyzer revealed that the size distribution of the particles produced in LASIL experiments ranges from 20 to 200 nm, the quantitative transport of these particles from the LASIL cell to the ICP-MS is unlikely. This assumption is confirmed by single particle ICP-MS measurements [48], which correct losses of nanoparticles using reference materials for calibration, otherwise a time-consuming determination of transport efficiency and nebulization efficiency is necessary to yield reliable results. Thus, in the current study an absolute quantification of the platinum was not possible and so matrix matched standards have to be used to compensate transport losses of the generated nanosol.

Since for the investigated material no reference material is available, an in-house reference was produced via PLD and sputter coating. For this purpose, four samples with identical platinum surface coverage on LSF thin films were fabricated, three without and one with platinum current collector beneath. The sample with current collector served as one-point calibration standard for quantitative LASIL measurements, the other three samples were used for chemical analysis of the surface decoration using NEB ICP-MS. Therefore, the three samples without current collector were digested and the platinum content determined using NEB ICP-MS. See section 2.5 for details. The mean surface coverage of these samples was 33.3 ± 1.7 ng/mm^2 ($n = 3$).

To check for a complete digestion of platinum surface decoration the substrates were subjected to a second digestion using identical conditions. ICP-MS analysis of the derived sample solutions gave signals comparable to procedural blank solutions, demonstrating that the platinum decoration has been quantitatively dissolved in the first digestion step.

To test the capabilities of the LASIL method a series of four samples was produced with platinum decorations varying over a wider range. For each platinum concentration level, a set of two identical samples was produced, one with current collector for the LASIL measurements and one without current collector, which has been used for validation of the determined surface decoration. This reference sample without current collector was subjected to digestion and platinum determination using NEB ICP-MS.

The samples with platinum current collector were measured by LASIL and quantified using matrix matched standard for calibration as described above. On each sample three patterns were measured, the RSD (relative standard deviation) of the derived results was about 5%, which is consistent with the RSD values using digestion of the samples in combination with subsequent analyte determination by NEB ICP-MS. The limit of detection (LOD) of the LASIL method is 0.02 ng/mm^2 platinum, determined as described in [49], which is more than sufficient for the application of materials like those investigated in this work. The platinum surface coverage varied in the range from 30 to 106 ng/mm^2 platinum, the surface coverage showing the best electrochemical performance is 46 ng/mm^2.

The surface coverage obtained with online-LASIL showed a highly linear correlation ($R^2 = 0.99$) with the reference values obtained by NEB ICP-MS. The root mean square error of prediction (RMSE) for the samples was 5.3 ng/mm^2 platinum, a maximum deviation of 18% between LASIL results and those obtained using NEB ICP-MS was found for the sample with a Pt-decoration of 30 ng/mm^2, the minimum deviation was found to be 4% for a Pt-decoration with 106 ng/mm^2.

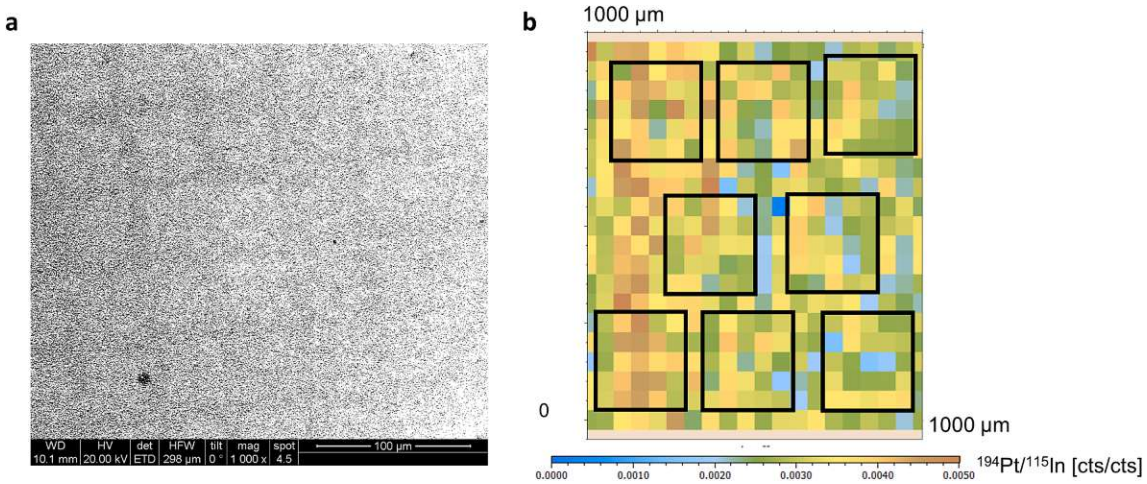

Fig 4. a: SEM image providing information about the homogeneity of the platinum surface coverage, note that the slight grid is an artifact caused from the reuse of YSZ substrates, which have been passed through an ion etching processes prior to the application in this work. For a better contrast, the image is binarized using ImageJ (version 1.52b), b: Mapping of the ^{194}Pt surface signal normalized to ^{115}In over a representative part of a sample, the black frames indicate the sample areas used for ANOVA analysis.

3.4. Homogeneity assessment

In previous work, the electrochemical characterization was performed with macroscopic samples, so only relationships between the mean surface coverage of the whole sample and the electrochemical performance were accessible. However, in future investigations measurements might be scaled down using different methods of sample preparation, thus better information about the uniformity of the distribution of the platinum nanoparticles is of interest. From SEM images (Fig. 4a and Fig. 1c) such distribution cannot be assessed with confidence, if the Pt-decoration of the sample is homogeneous or if there is a gradient present. As online LASIL allows to record spatially resolved, quantitative elemental data [41], it is the ideal method for this task.

To test the uniformity of the platinum decoration, a sample area of 1x1 mm^2 was imaged using the parameters presented in Table 1. Measurement carried out to generate the platinum distribution image (Fig. 4b) with a resolution of 20x20 pixel took 2 h. In the imaged sample area, there are some areas with higher, and others with lower Pt-coverage. The RSD of all pixel intensities is 25%, which can be regarded as the microscopic inhomogeneity due to the stochastic variations resulting from the low surface coverage. To access the overall homogeneity a one-way ANOVA (analysis of variance) was performed. Within the imaged sample area eight 5x5 groups of pixels were chosen (for details see Fig. 4b) and the variability within and between them was evaluated. The ANOVA revealed that there was a significant variation ($F = 6.88$, $p = 2.6*10^{-7}$) of the surface coverage within the investigated area. Having this information in mind is important for future investigations, as with different production processes a higher level of uniformity of the platinum coverage can be achieved, which can be accessed with this method.

4. Conclusion

In this work, we exploited the capabilities of online LASIL for the absolute quantification of the platinum surface decoration of LSF thin films, a promising material for SOFC electrodes. In contrast to previously reported applications focused on the determination of the overall thin film stoichiometry demands this task investigations with sufficient surface sensitivity. Moreover, instead of bulk components the analysis of trace constituents is mandatory. To fulfill these requirements a thorough optimization of the ablation parameters was necessary, resulting in an improved depth resolution for online LASIL when compared to conventional LA-ICP-MS. The ablation per shot for LSF was found to be in the order of 30 nm deep with online-LASIL, compared to approximately 200 nm for LA-ICP-MS. This improved depth resolution was beneficial for the analysis of the surface decoration of platinum on LSF electrodes. It was possible to separate the platinum decoration on top of the electrodes, from the platinum current collector, which lies buried in the depth of 100 nm. However, performed experiments indicated that LASIL generates not only nanoparticles, a fraction of the ablated sample material also becomes dissolved. Thus, a careful optimization of the carrier solution is necessary to avoid losses of the dissolved part of the ablated material, while not harming the integrity of the LSF electrode. Platinum signal could be quantified using a matrix matched standard for calibration. The platinum amount per area determined in the surface coverages showed a good agreement with liquid reference values determined for samples prepared without current collector electrode. A main advantage of online LASIL is the possibility of analyzing spatially resolved element distributions. A sample area of 1x1 mm^2 was imaged with a resolution of 50 µm. This revealed that the samples show some degree of inhomogeneity on the microscopic level, which is an important information for further optimization of the LSF production process.

Funding

This work was supported by the Austrian Science Fund-FWF grant P31165-N37.

CRediT authorship contribution statement

Maximilian Weiss: Investigation, Writing - original draft. **Christoph Riedl:** Investigation, Writing - review & editing. **Johannes Frank:** Investigation, Resources. **Jürgen Fleig:** Supervision, Resources, Writing - review & editing. **Andreas Limbeck:** Supervision, Conceptualization, Project administration, Resources, Writing - review & editing.

Declaration of Competing Interest

The authors declare that they have no known competing financial interests or personal relationships that could have appeared to influence the work reported in this paper.

Acknowledgements

We want to thank Elisabeth Eitenberger for conduction of SEM images and the University Service Centre for Transmission Electron

Microscopy of the TU Wien (USTEM) for providing SEM and TEM measurements.

Appendix A. Supplementary data

Supplementary data to this article can be found online at https://doi.org/10.1016/j.microc.2021.106236.

References

[1] E. Ivers-Tiffée, A. Weber, D. Herbstritt, Materials and technologies for SOFC-components, J. Eur. Ceram. Soc. 21 (2001) 1805–1811.

[2] K.M. El-Khatib, R.M. Abdel Hameed, R.S. Amin, A.E. Fetohi, Core-shell structured Pt-transition metals nanoparticles supported on activated carbon for direct methanol fuel cells, Microchem. J. 145 (2019) 566–577.

[3] E.D. Wachsman, K.T. Lee, Lowering the temperature of solid oxide fuel cells, Science 334 (2011) 935–939.

[4] B.A. Boukamp, Fuel cells: the amazing perovskite anode, Nat. Mater. 2 (5) (2003) 294–296.

[5] A. Nenning, L. Volgger, E. Miller, L.V. Mogni, S. Barnett, J. Fleig, The electrochemical properties of Sr(Ti, Fe)O3-δ for anodes in solid oxide fuel cells, J. Electrochem. Soc. 164 (4) (2017) F364–F371.

[6] W. Jung, H.L. Tuller, Impedance study of SrTi1−xFexO3−δ (x=0.05 to 0.80) mixed ionic-electronic conducting model cathode, Solid State Ionics 180 (11-13) (2009) 843–847.

[7] S.-L. Zhang, D. Cox, H. Yang, B.-K. Park, C.-X. Li, C.-J. Li, S.A. Barnett, High stability SrTi1−xFexO3−δ electrodes for oxygen reduction and oxygen evolution reactions, J. Mater. Chem. A 7 (37) (2019) 21447–21458.

[8] E. Navickas, T.M. Huber, Y. Chen, W. Hetaba, G. Holzlechner, G. Rupp, M. Stöger-Pollach, G. Friedbacher, H. Hutter, B. Yildiz, J. Fleig, Fast oxygen exchange and diffusion kinetics of grain boundaries in Sr-doped LaMnO3 thin films, Phys Chem Chem Phys 17 (12) (2015) 7659–7669.

[9] S. Kogler, A. Nenning, G.M. Rupp, A.K. Opitz, J. Fleig, Comparison of electrochemical properties of La0.6Sr0.4FeO3-δthin film electrodes: oxidizing vs. reducing conditions, J. Electrochem. Soc. 162 (3) (2015) F317–F326.

[10] A. Schmid, G.M. Rupp, J. Fleig, Voltage and partial pressure dependent defect chemistry in (La, Sr)FeO3-delta thin films investigated by chemical capacitance measurements, Phys. Chem. Chem. Phys. 20 (2018) 12016–12026.

[11] R. Küngas, A.S. Yu, J. Levine, J.M. Vohs, R.J. Gorte, An investigation of oxygen reduction kinetics in LSF electrodes, J. Electrochem. Soc. 160 (2) (2013) F205–F211.

[12] M. Kuhn, S. Hashimoto, K. Sato, K. Yashiro, J. Mizusaki, Oxygen nonstoichiometry, thermo-chemical stability and lattice expansion of La0.6Sr0.4FeO3−δ, Solid State Ionics 195 (1) (2011) 7–15.

[13] J. Januschewsky, M. Ahrens, A. Opitz, F. Kubel, J. Fleig, Optimized La0.6Sr0.4CoO3-δ thin-film electrodes with extremely fast oxygen-reduction kinetics, Adv. Funct. Mater. 19 (19) (2009) 3151–3156.

[14] M. Kubicek, A. Limbeck, T. Frömling, H. Hutter, J.r. Fleig, Relationship between cation segregation and the electrochemical oxygen reduction kinetics of La0.6Sr0.4CoO3−δ thin film electrodes, J. Electrochem. Soc. 158 (6) (2011) B727, https://doi.org/10.1149/1.3581114.

[15] G.M. Rupp, H. Téllez, J. Druce, A. Limbeck, T. Ishihara, J. Kilner, J. Fleig, Surface chemistry of La0.6Sr0.4CoO3−δ thin films and its impact on the oxygen surface exchange resistance, J. Mater. Chem. A 3 (45) (2015) 22759–22769.

[16] N. Tsvetkov, Q. Lu, L. Sun, E.J. Crumlin, B. Yildiz, Improved chemical and electrochemical stability of perovskite oxides with less reducible cations at the surface, Nat Mater 15 (2016) 1010–1016.

[17] H.J. Hwang, J.-W. Moon, S. Lee, E.A. Lee, Electrochemical performance of LSCF-based composite cathodes for intermediate temperature SOFCs, J. Power Sources 145 (2005) 243–248.

[18] F. Baumann, J. Fleig, H. Habermeier, J. Maier, Impedance spectroscopic study on well-defined (La, Sr)(Co, Fe)O3−δ model electrodes, Solid State Ionics 177 (2006) 1071–1081.

[19] F. Baumann, J. Fleig, H. Habermeier, J. Maier, Ba0.5Sr0.5Co0.8Fe0.2O3−δ thin film microelectrodes investigated by impedance spectroscopy, Solid State Ionics 177 (2006) 3187–3191.

[20] M. Burriel, C. Niedrig, W. Menesklou, S.F. Wagner, J. Santiso, E. Ivers-Tiffée, BSCF epitaxial thin films: electrical transport and oxygen surface exchange, Solid State Ionics 181 (13-14) (2010) 602–608.

[21] C. Riedl, A. Schmid, A. Nenning, H. Summerer, S. Smetaczek, S. Schwarz, J. Bernardi, A. Optiz, A. Limbeck, J. Fleig, Outstanding oxygen reduction kinetics of La0.6Sr0.4FeO3−δ surfaces decorated with platinum nanoparticles, J. Electrochem. Soc. 167 (2020) 104514, https://doi.org/10.1149/1945-7111/ab9c7f.

[22] A. Limbeck, M. Bonta, W. Nischkauer, Improvements in the direct analysis of advanced materials using ICP-based measurement techniques, J. Anal. At. Spectrom. 32 (2017) 212–232.

[23] S. Turková, M. Vašinová Galiová, K. Štůlová, Z. Čadková, J. Száková, V. Otruba, V. Kanický, Study of metal accumulation in tapeworm section using laser ablation-inductively coupled plasma-mass spectrometry (LA-ICP-MS), Microchem. J. 133 (2017) 380–390.

[24] A. Hanć, A. Małecka, A. Kutrowska, A. Bagniewska-Zadworna, B. Tomaszewska, D. Barałkiewicz, Direct analysis of elemental biodistribution in pea seedlings by LA-ICP-MS, EDX and confocal microscopy: Imaging and quantification, Microchem. J. 128 (2016) 305–311.

[25] J. Pisonero, B. Fernández, D. Günther, Critical revision of GD-MS, LA-ICP-MS and SIMS as inorganic mass spectrometric techniques for direct solid analysis, J. Anal. At. Spectrom. 24 (9) (2009) 1145, https://doi.org/10.1039/b904698d.

[26] G. Friedbacher, H. Bubert, Surface and Thin Film Analysis, Weinheim, Germany, 2011.

[27] J. Pisonero, D. Gunther, Femtosecond laser ablation inductively coupled plasma mass spectrometry: fundamentals and capabilities for depth profiling analysis, Mass Spectrom Rev 27 (2008) 609–623.

[28] D. Käser, L. Hendriks, J. Koch, D. Günther, Depth profile analyses with sub 100-nm depth resolution of a metal thin film by femtosecond – laser ablation – inductively coupled plasma – time-of-flight mass spectrometry, Spectrochim. Acta, Part B 149 (2018) 176–183.

[29] A. Limbeck, P. Galler, M. Bonta, G. Bauer, W. Nischkauer, F. Vanhaecke, Recent advances in quantitative LA-ICP-MS analysis: challenges and solutions in the life sciences and environmental chemistry, Anal. Bioanal. Chem 407 (2015) 6593–6617.

[30] Y. Ke, Y. Sun, P. Lin, J. Zhou, Z. Xu, C. Cao, Y. Yang, S. Hu, Quantitative determination of rare earth elements in scheelite via LA-ICP-MS using REE-doped tungstate single crystals as calibration standards, Microchem. J. 145 (2019) 642–647.

[31] A. Hanć, A. Olszewska, D. Barałkiewicz, Quantitative analysis of elements migration in human teeth with and without filling using LA-ICP-MS, Microchem. J. 110 (2013) 61–69.

[32] A. Hanć, P. Zduniak, K. Erciyas-Yavuz, A. Sajnóg, D. Barałkiewicz, Laser ablation-ICP-MS in search of element pattern in feathers, Microchem. J. 134 (2017) 1–8.

[33] H. Zeng, X.-W. Du, S.C. Singh, S.A. Kulinich, S. Yang, J. He, W. Cai, Nanomaterials via laser ablation/irradiation in liquid: a review, Adv. Funct. Mater. 22 (7) (2012) 1333–1353.

[34] G. Yang, Laser ablation in liquids: applications in the synthesis of nanocrystals, Prog. Mater Sci. 52 (2007) 648–698.

[35] E.V. Muravitskaya, V.A. Rosantsev, M.V. Belkov, E.A. Ershov-Pavlov, E. V. Klyachkovskaya, Laser ablation in liquids as a new technique of sampling in elemental analysis of solid materials, Spectrochim. Acta, Part B 64 (2) (2009) 119–125.

[36] D.N. Douglas, J.L. Crisp, H.J. Reid, B.L. Sharp, Laser ablation of a sample in liquid—LASIL, J. Anal. At. Spectrom. 26 (6) (2011) 1294, https://doi.org/10.1039/c0ja00144a.

[37] S. Okabayashi, T.D. Yokoyama, Y. Kon, S. Yamamoto, T. Yokoyama, T. Hirata, Evaluation of Laser Ablation in Liquid (LAL) technique as a new sampling technique for elemental and isotopic analysis using ICP-mass spectrometry, J. Anal. At. Spectrom. 26 (7) (2011) 1393, https://doi.org/10.1039/c0ja00200c.

[38] R. Machida, T. Nakazawa, Y. Sakuraba, M. Fujiwara, N. Furuta, Particle size-related elemental fractionation in laser ablation in liquid inductively coupled plasma mass spectrometry, J. Anal. At. Spectrom. 30 (2015) 2412–2419.

[39] L. Ebdon, M.E. Foulkes, S. Hill, Direct atomic spectrometric analysis by slurry atomisation. Part 9. Fundamental studies of refractory samples, J. Anal. At. Spectrom. 5 (1) (1990) 67, https://doi.org/10.1039/ja9900500067.

[40] M. Bonta, J. Frank, S. Taibl, J. Fleig, A. Limbeck, Online-LASIL: Laser Ablation of Solid Samples in Liquid with online-coupled ICP-OES detection for direct determination of the stoichiometry of complex metal oxide thin layers, Anal Chim Acta 1000 (2018) 93–99.

[41] C. Herzig, J. Frank, A.K. Opitz, J. Fleig, A. Limbeck, Quantitative imaging of structured complex metal oxide thin films using online-LASIL-ICP-MS, Talanta 217 (2020) 121012, https://doi.org/10.1016/j.talanta.2020.121012.

[42] C. Herzig, J. Frank, A.K. Opitz, J. Fleig, A. Limbeck, Quantitative analysis of gadolinium doped cerium oxide thin films via online-LASIL-ICP-OES, J. Anal. At. Spectrom. 34 (11) (2019) 2333–2339.

[43] M.P. Pechini, Method of Preparing Lead and Alkaline Earth itanates and Niobates and Coating Method Using the Same to Form a Capacitor, US Patent US3330697A, Sprague Electric Co., US Patent US3330697A, 1967.

[44] E. Ivanova, F. Adams, Flow injection on-line sorption preconcentration of platinum in a knotted reactor coupled with electrothermal atomic absorption spectrometry, Fresen. J. Anal. Chem. 361 (1998) 445–450.

[45] C.C. Garcia, H. Lindner, K. Niemax, Transport efficiency in femtosecond laser ablation inductively coupled plasma mass spectrometry applying ablation cells with short and long washout times, Spectrochim. Acta, Part B 62 (1) (2007) 13–19.

[46] S.J.M. Van Malderen, A.J. Managh, B.L. Sharp, F. Vanhaecke, Recent developments in the design of rapid response cells for laser ablation-inductively coupled plasma-mass spectrometry and their impact on bioimaging applications, J. Anal. At. Spectrom. 31 (2016) 423–439.

[47] S. Zhang, M. He, Z. Yin, E. Zhu, W. Hang, B. Huang, Elemental fractionation and matrix effects in laser sampling based spectrometry, J. Anal. At. Spectrom. 31 (2016) 358–382.

[48] M. Tharaud, P. Louvat, M.F. Benedetti, Detection of nanoparticles by single-particle ICP-MS with complete transport efficiency through direct nebulization at few-microlitres-per-minute uptake rates, Anal Bioanal Chem 413 (3) (2021) 923–933.

[49] J.-M. Mermet, Limit of quantitation in atomic spectrometry: An unambiguous concept? Spectrochim. Acta, Part B 63 (2) (2008) 166–182.

Supplementary Information

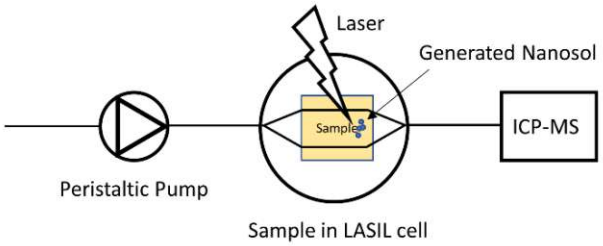

Supplementary Figure 1: Schematics of the LASIL setup, consisting of a pump, the LASIL cell in which the sample is ablated and the detection system, here an ICP-MS, all connected by PFA tubing, see [37] for more details.

5 Publication 3

Elemental mapping of fluorine by means of molecular laser induced breakdown spectroscopy

Maximilian Weiss, Zuzana Gajarska , Hans Lohninger , Martina Marchetti-Deschmann , Georg Ramer , Bernhard Lendl and Andreas Limbeck
Institute of Chemical Technologies and Analytics, TU Wien, Getreidemarkt 9/164 -1060 Vienna, Austria

Published in: Analytica Chimica Acta 1195 (2022) 339422

Analytica Chimica Acta 1195 (2022) 339422

Contents lists available at ScienceDirect

Analytica Chimica Acta

journal homepage: www.elsevier.com/locate/aca

Elemental mapping of fluorine by means of molecular laser induced breakdown spectroscopy

Maximilian Weiss *, Zuzana Gajarska , Hans Lohninger , Martina Marchetti-Deschmann , Georg Ramer , Bernhard Lendl , Andreas Limbeck **

Institute of Chemical Technologies and Analytics, TU Wien, Getreidemarkt 9, 1060, Wien, Austria

HIGHLIGHTS

- Sputtering of Cu and spray coating of Ca-acetate, were tested to deposit a molecular forming element on the surface of a fluoropolymer.
- Reduction of laser energy by a factor of 4 without loss in sensitivity (LOD about 160 μg g^{-1}) compared to atomic emission.
- Spatially resolved measurements of fluorine distribution via molecular LIBS possible.

GRAPHICAL ABSTRACT

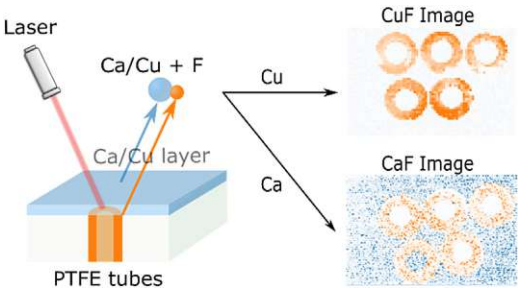

ARTICLE INFO

Article history:
Received 29 October 2021
Received in revised form
21 December 2021
Accepted 30 December 2021
Available online 3 January 2022

Keywords:
Fluorine
Fluoropolymers
Laser induced breakdown spectroscopy
Molecular-LIBS
LIBS imaging

ABSTRACT

The growing importance of fluoropolymers in high-tech applications and green technologies results in the rising need for their characterization. In contrast to conventional methods used for this task, laser-induced breakdown spectroscopy (LIBS) provides the advantage of a spatially resolved analysis. Nevertheless, the high excitation energy of fluorine results in low sensitivity of the atomic F(I) lines, which limits the feasibility of its LIBS-based analysis. This work presents a novel approach for quantitative mapping of fluorine in fluoropolymer samples. It bases on monitoring of molecular emission bands (CuF or CaF) arising from fluorine containing molecules. These species were generated during later stages of the LIBS plasma by a recombination of fluorine atoms originating from fluoropolymer sample with a molecule-forming partner (Cu or Ca) stemming from a surface coating. This approach enables F detection limits in the parts per million (μg g^{-1}) range and elemental imaging using single shot measurements. The elements required for molecular formation are deposited on the sample surface prior to analysis. We evaluate two techniques - spray coating and sputter coating – with regards to their effects on sensitivity and spatial resolution in elemental mapping. Overall, both methods proved to be suitable for a spatially resolved analysis of fluorine: whereas sputter-coating of copper yielded a better sensitivity, spray coating of calcium provided a higher spatial resolution.

1. Introduction

Fluoropolymers are materials with outstanding properties such as mechanical resistance, thermal stability, chemical inertness, and a low dielectric constant [1]. Thus, they have found a myriad of uses

* Corresponding author.
** Corresponding author.
E-mail addresses: maximilian.weiss@tuwien.ac.at (M. Weiss), andreas.limbeck@tuwien.ac.at (A. Limbeck).

https://doi.org/10.1016/j.aca.2021.339422

in different high-tech applications including protective coatings, optical devices, medical implants, insulators and dielectrics or components for automotive industry and aerospace [1–3]. Moreover, fluoropolymers play an important role in the steadily growing field of green technologies [1]. Their annual production reached 320 300 tons in 2018 [4] and is expected to further rise in the future [1].

Nevertheless, the inert nature of these materials results in their low ability to disintegrate over time, which leads to their persistence in the natural environment. Additionally, a recent study suggests possible threat posed by the fluoropolymers related to the release of per- and polyfluoroalkyl substances (PFAS) [4]. Thus, as the production volumes of fluoropolymers rise, the question of their proper disposal becomes of growing concern. Recycling seems to be the best available option, considering the release of hydrogen fluoride and other toxic compounds upon their combustion [5].

As the importance of these materials increases, the need for their characterization steadily grows. The occurrence of fluoropolymers could be assessed with different techniques for analysis of organic macro-molecular compounds or by simple measurement of the element fluorine. State of the art methods for fluorine detection, such as ion chromatography [6], ion sensitive electrodes [7], continuous source atomic absorption spectroscopy (CSAAS) [8] and inductively coupled plasma mass spectrometry (ICP-MS) [9] have in common that they require sample dissolution prior to analysis. For inert materials like fluoropolymers, sample digestion is typically laborious and requires harsh chemicals. Furthermore, it precludes spatially resolved measurements.

We propose to circumvent the dissolution step by using LIBS which has recently gained attention in the field of polymer characterization [10,11]. In contrast to the above-mentioned methods, LIBS is a direct solid sampling technique allowing for a spatially resolved analysis without need for the sample pre-treatment. In LIBS, a short-pulse laser is used to ablate, atomize and excite a small portion of the sample, which results in emission of the characteristic radiation [12]. Its detection results in a complex emission spectrum providing information about the elemental composition of the sample including fluorine.

However, LIBS measurements of fluorine are hindered by the fact that the main emission lines are in the vacuum UV region (below 100 nm) which requires a special instrumental setup. Although additional atomic lines are present in the visible range [13–15], the relatively high excitation energies of the corresponding states [16] require the application of an increased laser energy to achieve a reasonable sensitivity. A possible way to overcome these limitations is the monitoring of molecules containing fluorine. In LIBS, these can arise during later stages of the plasma expansion in which the temperature becomes sufficiently low for the atoms to recombine [17].

The idea of monitoring molecular signals to obtain information about a particular element of interest has been around for a long time [17] and is currently applied in CS-AAS [8] and laser ablation molecular isotopic spectrometry (LAMIS) [18]. In case of LIBS, it was first described for CuCl molecule in 1996 [19] and later applied to the detection of fluorine by means of the CaF emission [20]. Other works dealing with the quantification of fluorine reported an enhancement of the limit of detection (LOD) for fluorine by an order of magnitude when using molecular emissions of CaF [21] and SrF [22] instead of the atomic emission line. Both, the fluorine and the molecular forming elemental partner were either naturally abundant in the sample [14] or the powdered sample was mixed with the element required for molecular formation and pellets were used for measurement [22]. An example of the first approach was the detection of fluorine under Martian conditions [23], the addition of $SrCO_3$ to ore samples to monitor the SrF emission demonstrates applicability of the second methodology [22].

Alvarez-Llamas et al. [16], developed an innovative approach for introducing calcium by liquid nebulization over the sample surface during LIBS analysis. With this approach the analysis of compact samples which do not contain the element required for molecule formation was enabled. In another work, molecular emission was used to quantify fluorine and chlorine in liquid samples by applying them on a calcite substrate [24].

The previously reported methods are well suited for bulk fluorine analysis, nevertheless, they do not allow mapping of the fluorine content. The addition of the molecular forming element as powder is not possible for compact samples and spraying of a liquid is not feasible for water-soluble samples. Moreover, spatially resolved information is so far only reported for samples intrinsically containing both molecular-forming elements [25].

In this work, we present a procedure for the assessment of the fluorine distribution in solid samples using molecular LIBS. Two methods for introducing the molecule-forming partner, enabling the analysis of fluorine in solid materials regardless of their composition, were developed. The first approach is based on sputter deposition of a copper thin film on the sample surface, the second one applies spray deposition of a Ca acetate solution resulting in formation of a thin calcium-acetate layer upon the solvent evaporation. Sputter coating is a widespread method for the deposition of thin films in material sciences [26], however, it has also found application in the field of analytical chemistry. For example prior to SEM-EDX measurements non-conductive samples are coated with a thin layer of elemental carbon [27]. Spray coating is an established method for applying matrices for matrix assisted laser desorption ionization mass spectrometry (MALDI-MS) measurements [28], in particular for imaging applications where a uniform distribution of the MALDI matrix is a prerequisite. The two procedures were employed for the analysis of artificial polymer samples, which enabled identification of their specific benefits and drawbacks.

2. Experimental section

2.1. Preparation of standards

To assess the sensitivity and linearity of the two methods, a series of pressed powder pellets was prepared by combining different amounts of polytetrafluoroethylene (PTFE) powder (particle size 3 μm) from Hagen automation (United Kingdom) with cellulose powder (particle size 20 μm) from Macherey-Nagel (Germany). The weighted powders were premixed with a Vortex Genie 2 shaker (Scientific Industries, USA) and then homogenized in a ball mill (MM 400, Retch Germany) using a shaking frequency of 15 Hz for 2 min. The resulting powder was pressed with a conventional laboratory press (PerkinElmer, Bodenseewerke, Germany). The fluorine content of the prepared standards ranged between 0.6 and 14.5% (w/w). For imaging experiments, five PTFE tubes cut to a length of about 5 mm with an outer diameter of 4 mm and an inner diameter of 2 mm (Bohlender GmbH, Germany) were embedded in a Versocit-2 acrylic resin (Struers, Germany). Prior to analysis, the sample surface was polished using a series of silicon carbide (SiC) grinding papers (Struers, Germany) with grits of 400, 800, 1200, 2000 and 4000. Surface profiles were recorded with a Dektak XT stylus profilometer (Bruker, USA).

2.2. Sputter coating

Copper thin films were deposited via a magnetron sputter coater (Baltech MED-020, Liechtenstein) using a copper target (Micro to Nano, Netherlands) and 150 mA sputter current under

Table 1
Instrumental Parameters used for LIBS measurements.

	Sputtered Cu film	Sprayed Ca layer	F(I) atomic line
Laser energy [mJ]	1.6	1.6	6.5
Spot size [μm]	100	100	100
Frequency [Hz]	10	10	10
Grating grooves [mm^{-1}]	300	300	1800
Stage velocity [mm s^{-1}]	2	1	1
Spot spacing [μm]	200	100	100
Gate delay (ICCD) [μs]	7	2	0.2
Gate width (ICCD) [μs]	10	10	10

0.8 Pa argon atmosphere. After 30 s of pre-sputtering, the actual sputter time was varied between 30 and 200 s.

2.3. Spray coating

Spray coating was performed using a HTX TM Sprayer (HTX Technologies, USA) with a flowrate of 0.03 mL min^{-1}, nozzle temperature of 45 °C, nozzle velocity of 1000 mm s^{-1} and a line spacing of 2 mm. A 37.5 g L^{-1} aqueous solution of calcium acetate, prepared by dissolving calcium acetate (P.A: grade, Merck, Germany) in ultrapure water obtained from a Barnstead EASYPURE II water purification system (Thermo Fisher Scientific, CA, USA), was sprayed onto the sample surface, which resulted in formation of a Ca acetate layer due to the immediate evaporation of the solvent. Multiple application of this spraying procedure on the same sample area enabled optimization of the deposited amount.

2.4. LIBS measurements

LIBS experiments were performed with a J200 Tandem LIBS spectrometer (Applied Spectra Inc., USA), equipped with a 266 nm Nd:YAG laser with 5 ns pulse width and a 6 channel CCD (charge-coupled device) spectrograph covering the spectral range from 188 to 1048 nm. Further an Acton SP2750 spectrometer (Princeton Instruments, USA) with a PIMAX2 1024RB intensified CCD (ICCD) detector (Princeton Instruments, USA) was connected via a fiber bundle to an additional collection optics of the LIBS system. The 6 channel CCD detector was used to monitor broadband emission spectra during imaging experiments, whereas molecular emission and the F(I) atomic emission were recorded with the ICCD system. All measurements were carried out under an argon gas flow of 1 L min^{-1}, except the bulk measurements for atomic emission of fluorine which were performed using a helium flow of 1 L min^{-1} [15]. The parameters used for LIBS measurement are stated in Table 1.

2.5. Data analysis

Raw data was collected with the instrument software (Axiom 2.0 and WinSpec 2.6.24). The data were processed using baseline-corrected integrals [29] The quantitative analysis of the pressed powder standards was performed in OriginPro 2020 (OriginLab Corporation, USA). Graphs were prepared using the python (v 3.7.6, https://www.python.org) programming language and the matplotlib (3.2.3) [30], numpy (1.18.1) [31] and scipy (1.4.1) [32] packages. Images were reconstructed from raw data using Epina ImageLab 3.45 (Epina GmbH, Austria).

3. Results and discussion

3.1. Bulk measurements

In previous molecular LIBS measurements of fluorine [16,22], earth alkali elements were used as molecular forming partners; however, they are too reactive to be sputtered with conventional equipment. Thus, copper was chosen for this work, as it is a rather noble metal frequently applied for magnetron sputtering. Moreover, the CuF molecule emissions in the visible range are free of interference from atomic copper lines [33]. The thickness of the film was optimized in the preliminary experiments to yield the best signal-to-noise ratio. A sputter time of 100 s provided best results and was used for further experiments. This corresponds to a film thickness of 120 nm, measured with a stylus profilometer. Calcium acetate was chosen for spray coating, as calcium was employed in the previous works dealing with the identification of fluorine [16] and acetate as it is a suitable counter-ion introducing no additional elements to polymer samples. Concentration of the calcium acetate and spraying parameters were chosen to provide a nearly continuous layer of calcium acetate, best results were obtained with a mean calcium surface concentration of 0.2 mg cm^{-2}. Details of the molecular bands monitored in the two approaches are described in Table 2.

To assess the sensitivity and linearity of the two methods, pressed powder standards made of cellulose and PTFE were evaluated. PTFE was chosen, as it is the commercially most important fluoropolymer and available in powder as well as in bulk form. These samples were surface treated with both procedures as described before and used for the optimization of LIBS parameters as well as for the assessment of the typical figures of merit. For LIBS analysis, line scans with adjacent single laser shots were performed on an area of 1.2 mm^2 resulting in 60 laser shots for CuF and 120 laser shots for CaF and the measurement of the F(I) atomic line. ICCD gate delays (Table 1) and the wavelength regions (Table 2) used for the analysis were selected in a way to avoid interference from background or prevailing atomic emission lines. To confirm the absence of interfering emissions from trace metals or other constituents of the fluoropolymer LIBS measurements of native PTFE were performed. Using the optimized parameters for gate delay and gate width only weak signals for the C2 swan band were observed, whereas the wavelength regions selected for CuF and CaF

Table 2
Summary of the monitored molecular bands, data from Herzberg. Molecular Spectra and molecular structure-Vol I; [33].

Molecular band	Binding Energy D_0 [eV]	Monitored Transition	v_{00} position [nm]	Spectral region used for integration [nm]
CaF	5.4	$B\ ^2\Sigma^+ \rightarrow X\ ^2\Sigma^+$	530.95	527.13–544.30
CuF	4.4	$C\ ^1\Pi \rightarrow X\ ^1\Sigma^+$	493.36	485.59–498.44

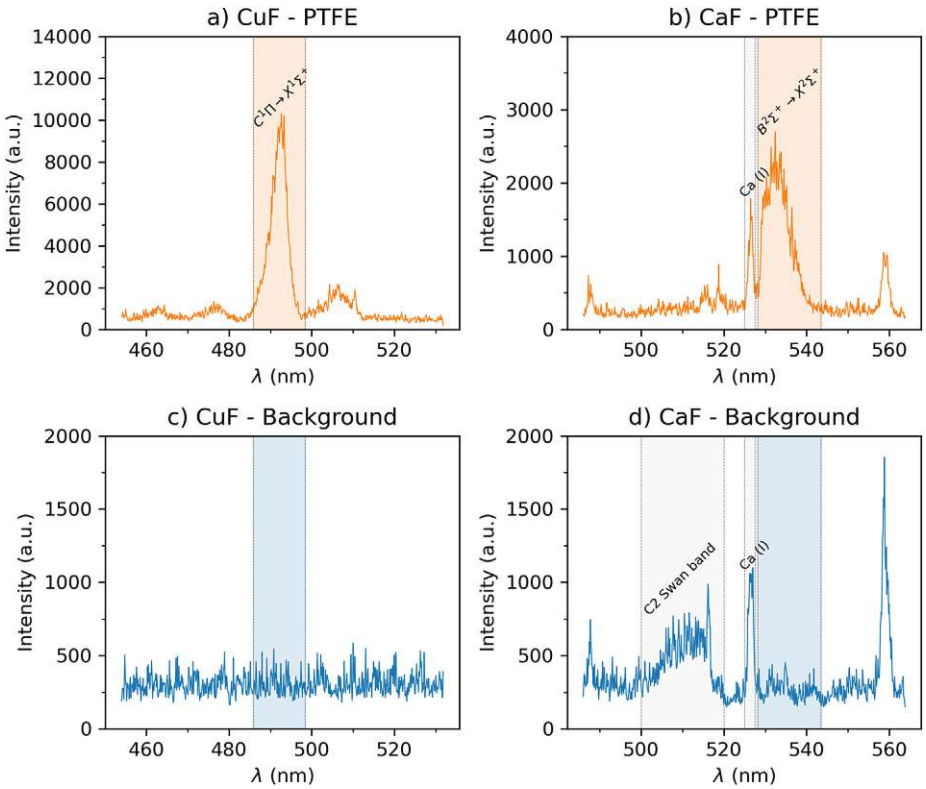

Fig. 1. Single shot spectra of pure PTFE (upper row) and the background acrylic embedding resin (lower row), coated with copper (left) and calcium acetate (right). The areas highlighted in orange/blue indicate the spectral regions integrated and background corrected for image reconstruction, further emission signals from the background acrylic resin are annotated in grey. The exact wavelengths of the used regions are listed in Table 2. (For interpretation of the references to colour in this figure legend, the reader is referred to the Web version of this article.)

measurements showed only signals at the background level. This outcome demonstrates that the molecular emissions obtained in the presence of Cu and Ca are caused exclusively from the generated Fluorine-species (for details see Supplementary Fig. 1). For data evaluation, the spectra were accumulated, and background corrected emission signals were calculated using the spectral regions described in Table 2. For both methods the integrated areas correlated linearly with the fluorine contents of the standards. However, in the case of CaF, the coefficient of determination was not as high ($r^2 = 0.95$) as in the case of CuF ($r^2 = 0.99$). Moreover, the calibration function determined for the CuF approach exhibits a 44 times higher slope, indicating an increased sensitivity for this method. Limits of detection were calculated by dividing three times the standard deviation of the blank by the slope of the calibration curve. This gives fluorine a LOD of 160 μg g^{-1} using CuF and 240 μg g^{-1} using CaF emission, confirming that the CuF approach is more sensitive although less shots were accumulated for CuF than for CaF. A further improvement is possible by increasing the number of shots per measurement, nevertheless achieved findings were in good agreement with literature data, e.g. Alvarez-Llamas et al. [16] report a LOD of 49 μg g^{-1} by averaging the CaF emissions from 140 laser shots for CaF quantification in samples prepared from NaF and Cu powder.

Additionally, the atomic F(I) line at 685.6 nm was investigated to compare the molecule-forming approach to conventional direct detection of atomic lines. For this, a helium atmosphere and the highest possible laser energy of 6.5 mJ was chosen [15]. The standards were analyzed using line scans with adjacent single laser shots with the same 100 μm spacing as used for CaF. As previously, these were accumulated for further analysis. The F(I) atomic line yielded a linear calibration function with an r^2 of 0.94 and an LOD of 160 μg g^{-1}. At first sight, this outcome seems to be comparable with the findings derived for the molecular emissions, however, it must be considered that the applied laser energy was roughly 4 times higher (6.5 mJ for atomic fluorine line vs. 1.6 mJ for the molecular CuF and CaF bands). The substantially higher laser energy necessary for the measurement of atomic lines is a significant drawback. The increased ablation rate reduces the overall in-depth resolution of the method. Additionally, high laser powers restrict the applicability for thermally sensitive samples. On the other hand, measurements with only 1.7 mJ as applied for the CuF and CaF measurements, does not allow for fluorine atomic lines detection.

3.2. Imaging experiments

Bulk measurements normally accumulate multiple measurements taken at different sample locations. For imaging experiments, a so-called continuous scan mode is used [34]. For this, the sample stage moves continuously while the laser is firing repeatedly onto the sample surface. Carefully adjusted repetition rates and scan speeds result in exactly one laser shot per position without overlapping of ablated volumes. Although this measurement mode does not allow signal accumulation, it is the preferred approach for imaging experiments since it enables fast mapping of a rather large area [34]. The suitability of the proposed molecular LIBS procedures for single-shot measurements is very likely but has to be verified. For this purpose, pure PTFE as a representative for a fluorine containing sample and Versocit-2 acrylic resin as an example for a fluorine free sample were analyzed using the conditions reported for bulk measurements, but without the accumulation of individual emission spectra. In Fig. 1, selected regions of single shot spectra acquired from pure PTFE and acrylic resin are

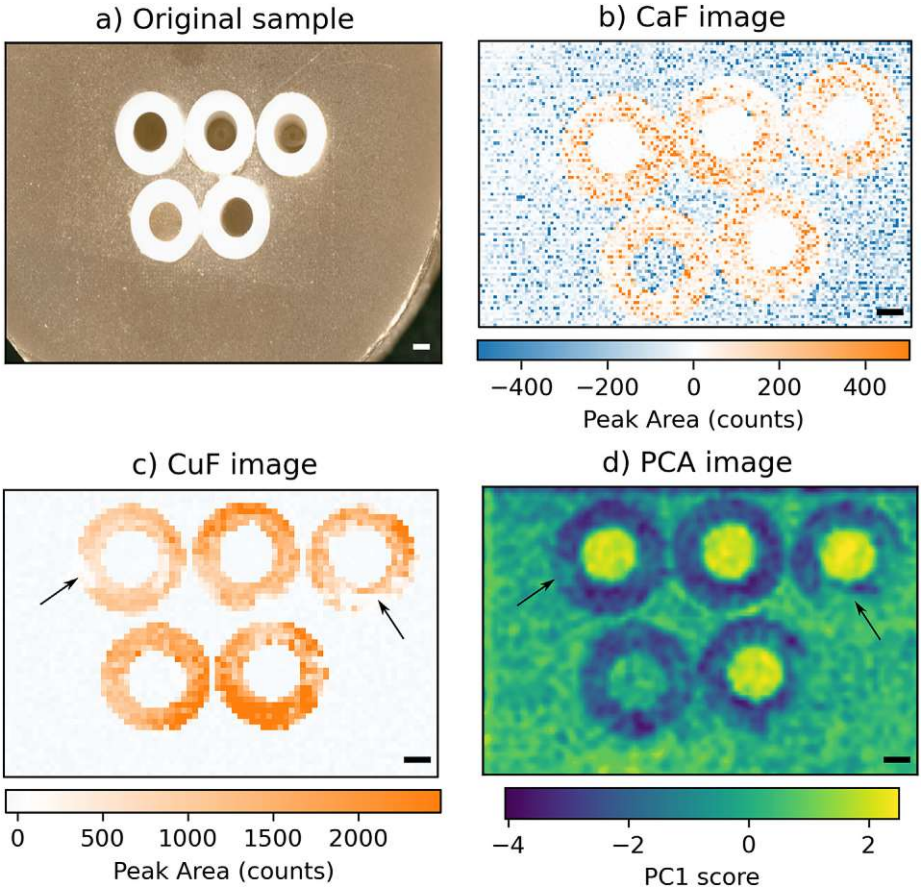

Fig. 2. a: Microscopic image of embedded PTFE tubes used for imaging experiments, b + c: Reconstructed elemental maps from background corrected integrated emission intensities for the (b) CaF, and the (c) CuF molecular band. d: Scores of the first principal component from the broadband six channel detector recorded simultaneously with the molecular CuF band. The scale bar represents 1 mm.

depicted, showing also the areas used for integration of CuF and CaF molecular emissions. It is evident that molecular emissions are measurable even with spectra from single laser shots. Moreover, the significant spectral difference between a blank and the PTFE sample allows simple identification of fluorine containing polymers. This outcome indicates that both coating approaches exhibit sufficient signal intensity allowing ultimately for imaging experiments.

To characterize and compare the mapping capabilities of the two methods, an artificially structured polymer sample consisting of five PTFE tubes embedded in acrylic resin was prepared. The microscopic image of the polished sample is presented in Fig. 2a. Molecular LIBS images of the two samples were acquired by firing single laser shots per sample location using the optimized parameters listed in Table 1. Plotting the intensity of the integrated molecular bands at each acquired position resulted in elemental maps of the CaF (Fig. 2b) and CuF (Fig. 2c) species, which resemble the distribution of fluorine in the sample. Thus, with both techniques, it was possible to reconstruct the PTFE ring structure visible in the microscopic image (Fig. 2a) with a high level of agreement. However, comparing the two coating approaches for the introduction of the molecular-forming partner on the sample surface, distinct differences were observed. At a first glance, the improved sensitivity of the CuF measurement is obvious, which is in agreement with the findings of the bulk investigations reported in the previous section. Besides sufficient sensitivity, spatial resolution is another important parameter for imaging applications. As seen in Fig. 3a, sputter coating results in a continuous film of copper. However, upon laser ablation during the LIBS measurements, the copper layer shows a high tendency to delaminate from the sample. This finding can be attributed to the surface properties of PTFE, which prevent a strong adhesion of the deposited Cu film. Thus, the selected measurement parameters represent a compromise between reasonable signal-to-noise ratio and a fair spatial resolution. In this case, the laser energy of 1.6 mJ per pulse and a laser spot size of 100 μm resulted in the ablation of a circular region of copper exhibiting a diameter of roughly 200 μm. With stylus profilometry it was confirmed that the actual ablation crater still has a size of 100 μm and a depth of about 1 μm. In case of calcium, this behavior was not observed, as the spray coating resulted in separate crystals of calcium acetate on the sample surface (Fig. 3b). However, with LA-ICP-MS measurements it was confirmed that the calcium is present on each part of the sprayed area and not just in the larger crystals (for details see Supplementary Material Fig. 2). Thus, compared to the Cu thin film the sprayed Ca layer is less homogeneous, but offers still a complete surface coverage – a prerequisite for imaging applications. Due to the limitation arising from the delamination of the Cu-film described previously, the CaF image could be acquired with a two times better lateral resolution.

To confirm the applicability of the presented methods for elemental mapping of fluorine, distribution images of PTFE and embedding material were created using the broadband spectra acquired with the 6-channel spectrometer simultaneously to the recording of the molecular bands on the ICCD. To discriminate the PTFE from the embedding materials a set of spectral descriptors representing the baseline-subtracted wavelength ranges of C, H and O atoms, as well as C_2 and CN molecules (see Brunnbauer et al. [35] for a more detailed description of this approach) was

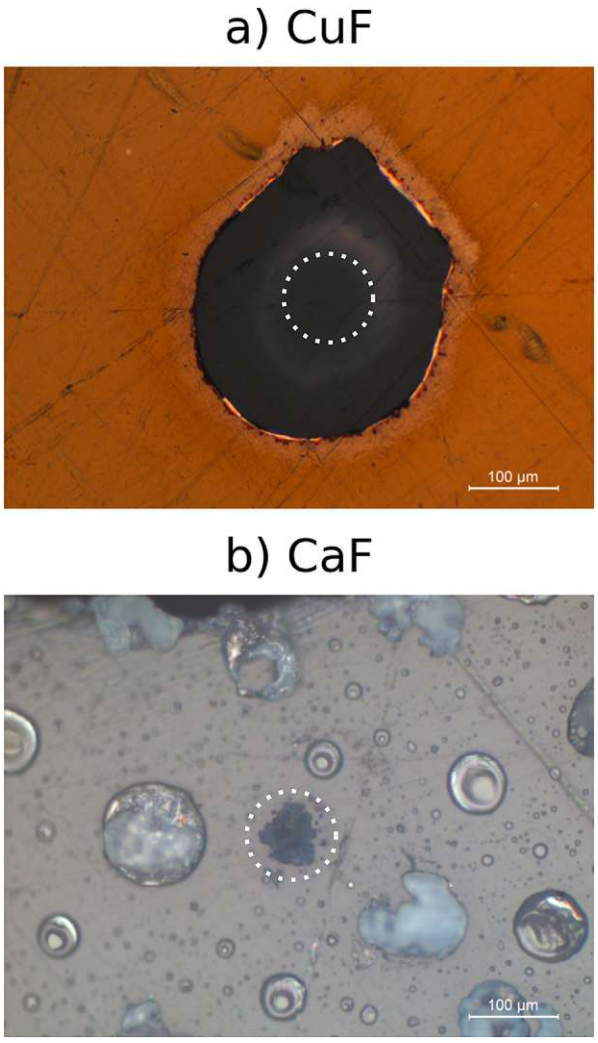

Fig. 3. Detailed view of the crater of one laser shot with 100 µm spot size on (a) copper coated and (b) a calcium acetate sprayed PTFE sample; the marked circle represents the 100 µm laser spot size.

used to extract the polymer-specific information from the raw spectra. An annotated example spectrum with the used spectral descriptors is shown in Fig. 4. The resulting data were subjected to principal component analysis (PCA). Fig. 2d shows the scores of the first principal component, clearly distinguish between PTFE and the embedding material. Compared to the measurement of CuF and CaF molecular emissions this approach offers only limited sensitivity, moreover limited ability to identify and classify fluorine containing polymers in unknown or more complex samples is very likely. Nevertheless, irregularities in the CuF image (Fig. 2c, like in the lower right edge of the third ring - see arrow marks) are also identified by the PCA image (Fig. 2d). As these two images were recorded simultaneously with different collection optics and detection systems, and the failures were observed for the same laser shots (equal to sample positions and thus image-pixels), errors related to signal acquisition are rather unlikely. Instead, sample defects such as artifacts introduced during sample polishing are considered to be responsible for the errors determined in the images.

3.3. Comparison of image quality

To compare the quality of the two fluorine images by advanced data analysis, a mask representing the individual pixels of the PTFE rings and a mask representing the pixels of the background region (acrylic resin) was created for both samples using the microscopic

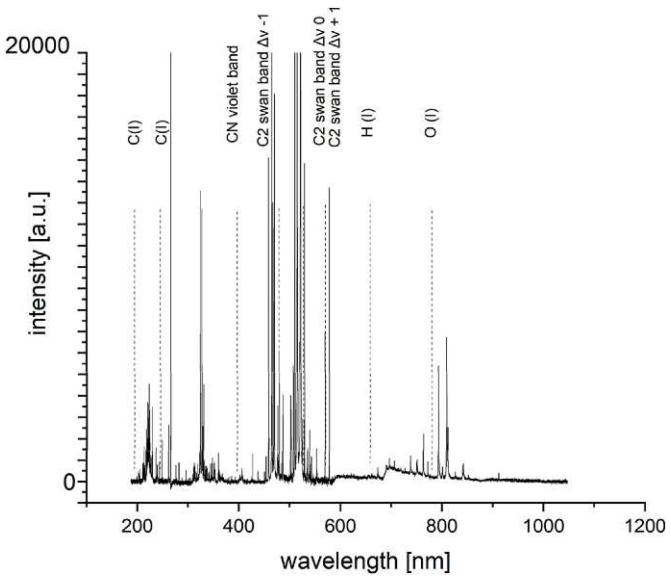

Fig. 4. Exemplary single shot broadband LIBS spectrum recorded with the 6-channel CCD detector during the measurement of the CuF Image in Fig. 2c. The descriptors used to create the PCA image in Fig. 2d are annotated in the spectrum and are taken from Brunnbauer et al., 2020 [35].

image and ImageLab. Using spectral descriptors, the baseline-subtracted molecular bands of CuF and CaF (Table 2) were defined and extracted from the raw spectra. The resulting values were plotted in a histogram representing the distribution of the molecular signal intensities in the region of the PTFE tubes (orange) and the background (blue) for CuF (Fig. 5a) and CaF (Fig. 5b). Furthermore, the means and the variances of the two regions were determined and used for the calculation of Fisher's linear discriminant evaluating the power of discrimination between the two distributions [36,37].

The histograms indicate that using the CuF approach, the signals in the PTFE region can be discriminated from the signals in the background region to a greater extent than in case of the CaF. This observation was confirmed by the Fisher's discriminant values of 2.45 for CuF vs. 0.31 for CaF, whereas a higher value indicates a better discrimination function. Furthermore, a Mann–Whitney *U* test was performed using 300 randomly selected data points (to keep the sample size equal for CuF and CaF) from the ring-PTFE and the acrylic resin, yielding a test statistic of 1687 ($p = 3*10^{-136}$) for CuF and 10 069 ($p = 2*10^{-72}$) for CaF, indicating a highly significant separation of the PTFE from the background for both systems. Thus, the spatial mapping of fluorine in fluoropolymers by means of molecular LIBS proved to be feasible, with sputter coating of copper providing a better discrimination of the fluoropolymer from the background. These numbers confirm the impressions of the elemental maps from Fig. 2, in particular the fluorine mapping obtained using the sputter coating approach seems to offer more homogeneous signal intensities, whereas the spray coating technique delivers signals with higher fluctuations.

To combine the spatially resolved with the statistical information, threshold images of CaF and CuF signal were created (Fig. 5). The threshold was determined with Youden's J statistic [38] and is marked in the associated histograms. With both approaches a classification of the image into fluorine containing and not fluorine containing pixels can be made with a high level of accuracy. However, with CaF the number of misclassified pixels is higher. This outcome could be attributed to the quality of the applied coatings. Copper forms a continuous film on the surface (Fig. 3a), which

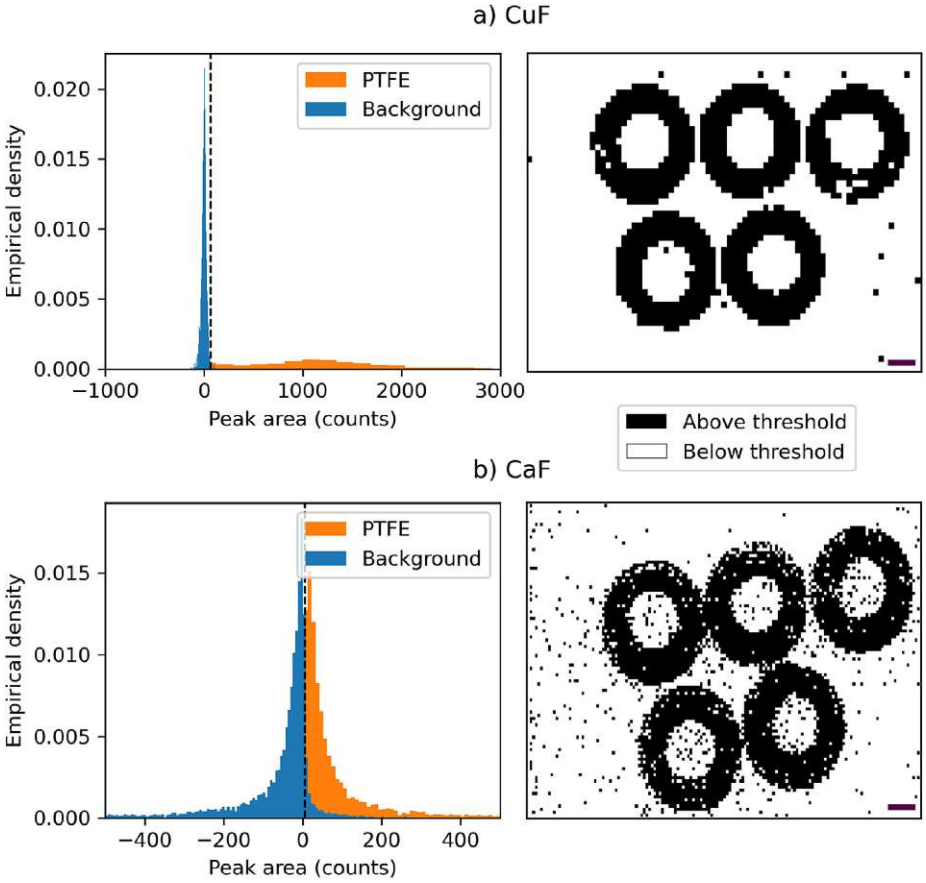

Fig. 5. Left: Histograms representing the distribution of the integrated CuF (a) and CuF (b) molecular band intensities in the region of the PTFE ring (orange) and the acrylic resin (blue). The masks representing the two areas were created using the corresponding optical images. The dotted line represents the PTFE-background threshold determined with Youden's J. Right: Sample images based on the Youden's J threshold. The threshold images of both signals resemble the fluorine distribution present in the optical images. (For interpretation of the references to colour in this figure legend, the reader is referred to the Web version of this article.)

provides constant conditions for the formation of molecules, while the calcium acetate forms stochastically distributed single crystals on the surface of the sample (Fig. 3b), causing distinct point-to-point variations in the emission-intensity of the CaF band.

4. Conclusion

We demonstrated two procedures of applying the element required for molecule formation on a fluorine -containing sample (magnetron sputtering and spray coating), which enabled spatially resolved analysis of fluorine using molecular emission LIBS. Using conventional bulk measurements, the linearity of the analyte content and the measured molecular emission was established and quantitative determination of fluorine in compact solid samples with detection limits in the parts per million ($\mu g\ g^{-1}$) region was shown. Moreover, both methods are sensitive enough to detect fluorine containing molecular emission bands at the single shot level, enabling single shot imaging. Fluorine mappings obtained via measurement of CuF and CaF emission bands were found to be in excellent agreement with the PTFE distribution of the investigated synthetic material, confirming that the proposed molecular LIBS method is able to resemble the fluorine distribution in unknown samples. We used Fisher's linear discriminant as statistical approach to compare the separation power of the signal from the background, yielding that measurement of CuF is better in this aspect, mainly due to the continuous nature of the copper thin film compared to the randomly distributed crystals of the calcium acetate layer. The approach based on magnetron sputtering of a thin Cu film onto the sample surface exhibits further a better linearity in the calibration series and a slightly improved sensitivity. Spray coating of a thin Ca-layer, however, has the advantage of allowing a higher resolution in imaging experiments, as compared to the Cu thin film it does not tend to delaminate during laser irradiation.

To conclude, both methods are feasible for imaging the fluorine distribution in solid samples. Although the present work was focused on measurements of PTFE only, the sensitivity of the two proposed approaches enables also the investigation of other Fluoropolymers with lower fluorine contents. Nevertheless, for a particular application, one must decide whether a higher spatial resolution or a better sensitivity and homogeneity are needed.

Ongoing research will be devoted to improving the adhesion of the Cu thin film and the homogeneity of the Ca layer, enabling further advancements in the spatially resolved analysis of fluorine. Moreover, the proposed coating procedures offer exciting opportunities in combination with molecular LIBS. After appropriate adjustments, analysis of other challenging elements should be possible.

CRediT authorship contribution statement

Maximilian Weiss: Conceptualization, Methodology, Investigation, Formal analysis, Writing – original draft. **Zuzana Gajarska:** Software, Formal analysis, Visualization, Writing – review & editing. **Hans Lohninger:** Software, Resources, Writing – review &

editing. **Martina Marchetti-Deschmann:** Resources, Writing – review & editing. **Georg Ramer:** Software, Formal analysis, Visualization, Writing – review & editing. **Bernhard Lendl:** Resources, Writing – review & editing. **Andreas Limbeck:** Conceptualization, Resources, Project administration, Funding acquisition, Writing – review & editing.

Declaration of competing interest

The authors declare that they have no known competing financial interests or personal relationships that could have appeared to influence the work reported in this paper.

Acknowledgment

This work was supported by the Austrian Science Fund-FWF [grant number P31165-N37]. We want to thank Jakob Willner and Konrad Bielecki for operating the HTX spray coater.

Supporting information

LIBS spectrum of a native PTFE sample, measurement of the homogeneity of the calcium acetate film with LA-ICP-MS, definition and formula for Fisher's linear discriminant and Youden's J.

Appendix A. Supplementary data

Supplementary data to this article can be found online at https://doi.org/10.1016/j.aca.2021.339422.

References

[1] B. Améduri, The promising future of fluoropolymers, Macromol. Chem. Phys. 221 (2020).
[2] H. Teng, Overview of the development of the fluoropolymer industry, Appl. Sci. 2 (2012) 496–512.
[3] J. Lv, Y. Cheng, Fluoropolymers in biomedical applications: state-of-the-art and future perspectives, Chem. Soc. Rev. 50 (2021) 5435–5467, https://doi.org/10.1039/D0CS00258E.
[4] R. Lohmann, I.T. Cousins, J.C. DeWitt, J. Gluge, G. Goldenman, D. Herzke, A.B. Lindstrom, M.F. Miller, C.A. Ng, S. Patton, M. Scheringer, X. Trier, Z. Wang, Are fluoropolymers really of low concern for human and environmental health and separate from other PFAS? Environ. Sci. Technol. 54 (2020) 12820–12828.
[5] S. Ebnesajjad, 13 - safety, disposal, and recycling of fluoropolymers, in: S. Ebnesajjad (Ed.), Introduction to Fluoropolymers, William Andrew Publishing, Oxford, 2013, pp. 293–309.
[6] Y. Noguchi, L. Zhang, T. Maruta, T. Yamane, N. Kiba, Simultaneous determination of fluorine, chlorine and bromine in cement with ion chromatography after pyrolysis, Anal. Chim. Acta 640 (2009) 106–109.
[7] P.A. Mello, J.S. Barin, F.A. Duarte, C.A. Bizzi, L.O. Diehl, E.I. Muller, E.M.M. Flores, Analytical methods for the determination of halogens in bioanalytical sciences: a review, Anal. Bioanal. Chem. 405 (2013) 7615–7642.
[8] S. Mores, G.C. Monteiro, S. Santos Fda, E. Carasek, B. Welz, Determination of fluorine in tea using high-resolution molecular absorption spectrometry with electrothermal vaporization of the calcium mono-fluoride CaF, Talanta 85 (2011) 2681–2685.
[9] W. Guo, L. Jin, S. Hu, Q. Guo, Method development for the determination of total fluorine in foods by Tandem inductively coupled plasma mass spectrometry with a mass-shift strategy, J. Agric. Food Chem. 65 (2017) 3406–3412.
[10] V.C. Costa, F.W.B. Aquino, C.M. Paranhos, E.R. Pereira-Filho, Identification and classification of polymer e-waste using laser-induced breakdown spectroscopy (LIBS) and chemometric tools, Polym. Test. 59 (2017) 390–395.
[11] K. Liu, D. Tian, C. Li, Y. Li, G. Yang, Y. Ding, A review of laser-induced breakdown spectroscopy for plastic analysis, TrAC Trends Anal. Chem. (Reference Ed.) 110 (2019) 327–334.
[12] R.E. Russo, X. Mao, J.J. Gonzalez, V. Zorba, J. Yoo, Laser ablation in analytical chemistry, Anal. Chem. 85 (2013) 6162–6177.
[13] M.A. Gondal, Y.W. Maganda, M.A. Dastageer, F.F. Al Adel, A.A. Naqvi, T.F. Qahtan, Detection of the level of fluoride in the commercially available toothpaste using laser induced breakdown spectroscopy with the marker atomic transition line of neutral fluorine at 731, 1nm, Opt. Laser Technol. 57 (2014) 32–38.
[14] P. Pořízka, S. Kaski, A. Hrdlička, P. Modlitbová, L. Sládková, H. Häkkänen, D. Prochazka, J. Novotný, P. Gadas, L. Čelko, K. Novotný, J. Kaiser, Detection of fluorine using laser-induced breakdown spectroscopy and Raman spectroscopy, J. Anal. At. Spectrom. 32 (2017) 1966–1974.
[15] C.D. Quarles, J.J. Gonzalez, L.J. East, J.H. Yoo, M. Morey, R.E. Russo, Fluorine analysis using laser induced breakdown spectroscopy (LIBS), J. Anal. At. Spectrom. (2014) 29.
[16] C. Alvarez-Llamas, J. Pisonero, N. Bordel, A novel approach for quantitative LIBS fluorine analysis using CaF emission in calcium-free samples, J. Anal. At. Spectrom. 32 (2017) 162–166.
[17] A. De Giacomo, J. Hermann, Laser-induced plasma emission: from atomic to molecular spectra, J. Phys. D Appl. Phys. 50 (2017) 183002.
[18] R.E. Russo, A.A. Bol'shakov, X. Mao, C.P. McKay, D.L. Perry, O. Sorkhabi, Laser ablation molecular isotopic spectrometry, Spectrochim. Acta, Part B 66 (2011) 99–104.
[19] C. Haisch, R. Niessner, O.I. Matveev, U. Panne, N. Omenetto, Element-specific determination of chlorine in gases by Laser-Induced-Breakdown-Spectroscopy (LIBS), Anal. Bioanal. Chem. 356 (1996) 21–26.
[20] M. Gaft, L. Nagli, N. Eliezer, Y. Groisman, O. Forni, Elemental analysis of halogens using molecular emission by laser-induced breakdown spectroscopy in air, Spectrochim. Acta, Part B 98 (2014) 39–47.
[21] C. Alvarez-Llamas, J. Pisonero, N. Bordel, Quantification of fluorine traces in solid samples using CaF molecular emission bands in atmospheric air Laser-Induced Breakdown Spectroscopy, Spectrochim. Acta, Part B 123 (2016) 157–162.
[22] Z. Tang, R. Zhou, Z. Hao, W. Zhang, Q. Li, Q. Zeng, X. Li, X. Zeng, Y. Lu, Determination of fluorine in copper ore using laser-induced breakdown spectroscopy assisted by the SrF molecular emission band, J. Anal. At. Spectrom. 35 (2020) 754–761.
[23] D.S. Vogt, S. Schröder, K. Rammelkamp, P.B. Hansen, S. Kubitza, H.W. Hübers, CaCl and CaF emission in LIBS under simulated martian conditions, Icarus 335 (2020).
[24] Z. Tang, Z. Hao, R. Zhou, Q. Li, K. Liu, W. Zhang, J. Yan, K. Wei, X. Li, Sensitive analysis of fluorine and chlorine elements in water solution using laser-induced breakdown spectroscopy assisted with molecular synthesis, Talanta 224 (2021) 121784.
[25] M. Gaft, Y. Raichlin, F. Pelascini, G. Panzer, V. Motto Ros, Imaging rare-earth elements in minerals by laser-induced plasma spectroscopy: molecular emission and plasma-induced luminescence, Spectrochim. Acta, Part B 151 (2019) 12–19.
[26] D.M. Mattox, Physical sputtering and sputter deposition, in: D.M. Mattox (Ed.), Handbook of Physical Vapor Deposition (PVD) Processing, Elsevier, 2010.
[27] S.J.B. Reed, Sample Preparation, Electron Microprobe Analysis and Scanning Electron Microscopy in Geology, Cambridge University Press, 2005, pp. 149–161.
[28] Y. Dong, B. Li, S. Malitsky, I. Rogachev, A. Aharoni, F. Kaftan, A. Svatos, P. Franceschi, Sample preparation for mass spectrometry imaging of plant tissues: a review, Front. Plant Sci. 7 (2016) 60.
[29] Z. Gajarska, L. Brunnbauer, H. Lohninger, A. Limbeck, Identification of 20 polymer types by means of laser-induced breakdown spectroscopy (LIBS) and chemometrics, Anal. Bioanal. Chem. 413 (2021) 6581–6594.
[30] J.D. Hunter, Matplotlib: a 2D graphics environment, Comput. Sci. Eng. 9 (2007) 90–95.
[31] C.R. Harris, K.J. Millman, S.J. van der Walt, R. Gommers, P. Virtanen, D. Cournapeau, E. Wieser, J. Taylor, S. Berg, N.J. Smith, R. Kern, M. Picus, S. Hoyer, M.H. van Kerkwijk, M. Brett, A. Haldane, J.F. Del Rio, M. Wiebe, P. Peterson, P. Gerard-Marchant, K. Sheppard, T. Reddy, W. Weckesser, H. Abbasi, C. Gohlke, T.E. Oliphant, Array programming with NumPy, Nature 585 (2020) 357–362.
[32] P. Virtanen, R. Gommers, T.E. Oliphant, M. Haberland, T. Reddy, D. Cournapeau, E. Burovski, P. Peterson, W. Weckesser, J. Bright, S.J. van der Walt, M. Brett, J. Wilson, K.J. Millman, N. Mayorov, A.R.J. Nelson, E. Jones, R. Kern, E. Larson, C.J. Carey, I. Polat, Y. Feng, E.W. Moore, J. VanderPlas, D. Laxalde, J. Perktold, R. Cimrman, I. Henriksen, E.A. Quintero, C.R. Harris, A.M. Archibald, A.H. Ribeiro, F. Pedregosa, P. van Mulbregt, C. SciPy, SciPy 1.0: fundamental algorithms for scientific computing in Python, Nat. Methods 17 (2020) 261–272.
[33] G. Herzberg, Molecular Spectra and Molecular Structure-Vol I, Read Books Ltd, 2013.
[34] A. Limbeck, L. Brunnbauer, H. Lohninger, P. Porizka, P. Modlitbova, J. Kaiser, P. Janovszky, A. Keri, G. Galbacs, Methodology and applications of elemental mapping by laser induced breakdown spectroscopy, Anal. Chim. Acta 1147 (2021) 72–98.
[35] L. Brunnbauer, S. Larisegger, H. Lohninger, M. Nelhiebel, A. Limbeck, Spatially resolved polymer classification using laser induced breakdown spectroscopy (LIBS) and multivariate statistics, Talanta 209 (2020) 120572.
[36] R.A. Fisher, The use OF multiple measurements IN taxonomic problems, Annals of Eugenics 7 (1936) 179–188.
[37] K. Fukunaga, Introduction to Statistical Pattern Recognition, Elsevier, 2013.
[38] W.J. Youden, Index for rating diagnostic tests, Cancer 3 (1950) 32–35.

Supplementary Information

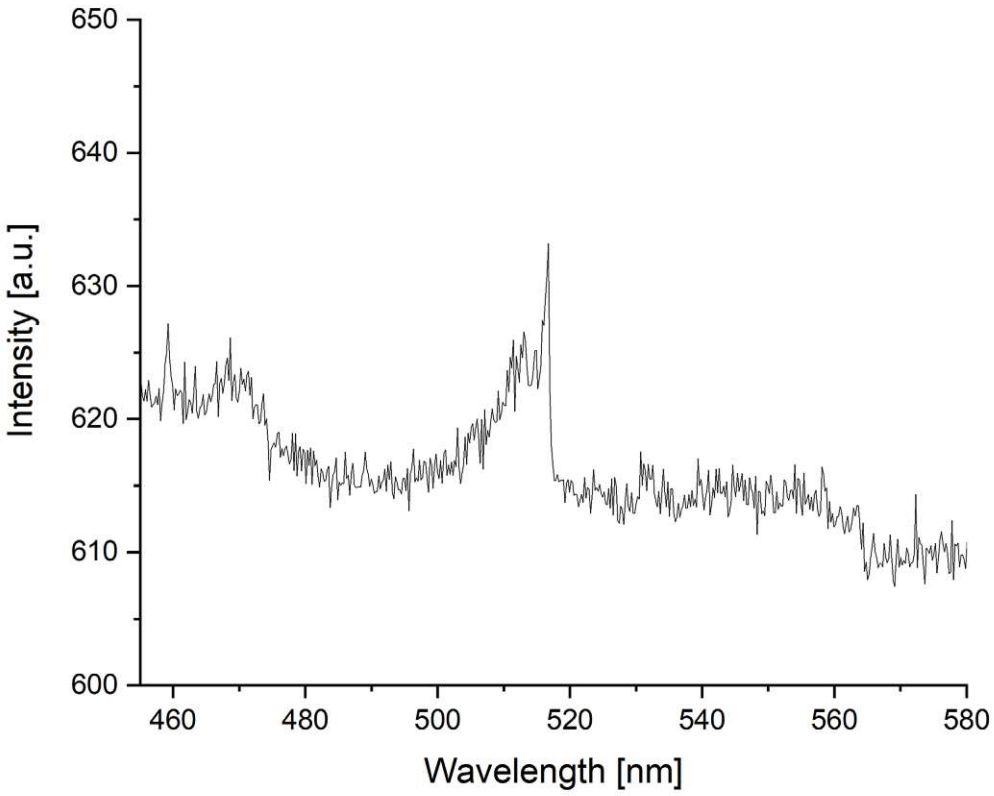

Supplementary Fig. 1 Spektrum of native PTFE recorded with the ICCD spectrometer with a 150 grooves mm^{-1} grating the settings for CaF (2µs Gate delay). Only the strong C2 molecular bands are observable in the respective spectral region on native PTFE. So that measurments of CuF and CaF can be carried out without inferference from potential atomic lines.

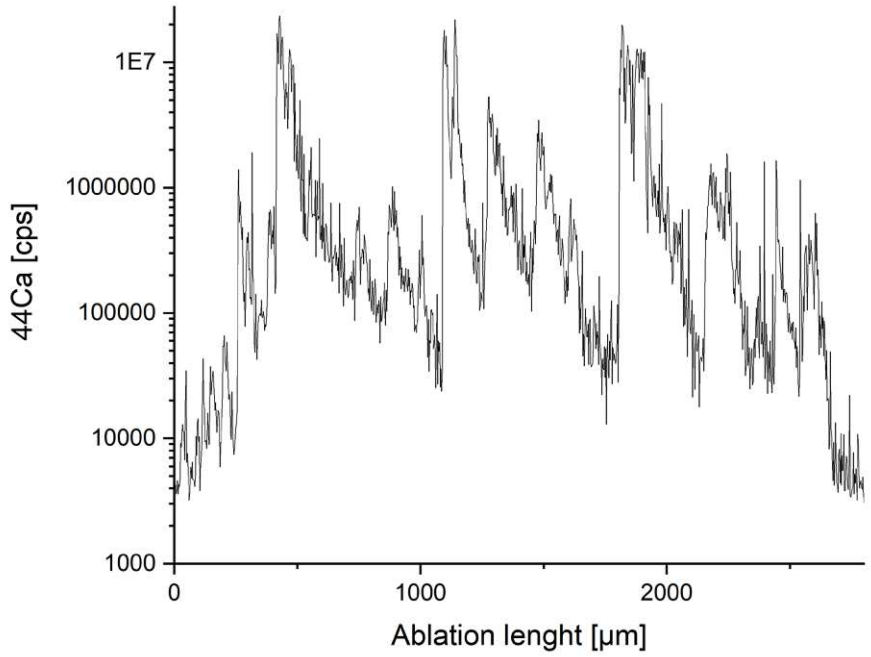

Supplementary Fig. 2: LA-ICP-MS line scan over the calcium acetate sprayed PTFE with a spot size of 25 µm, see supplementary methods for experimental details. The ^{44}Ca ion signal is plotted against the scan length. Calcium signal is present during the entire scan, indicating that even between the observed larger "crystals", which cause the calcium is present.

Supplementary Methods:

To access the distribution of the calcium acetate layer with a higher spatial resolution a LA-ICP-MS lines-scan on the PTFE ring was performed. Laser ablation was done with a NWR213 laser system (ESI, USA) connected via a PTFE tube to a iCAPQ quadrupole ICP-MS (Thermo Fisher Scientific, Germany. A line scan with a length of approximately 3 mm was performed with typical imaging parameters: a spot size of 25 µm, a scan speed of 75 µm/s 20 Hz repetition frequency and 4 J/cm^2 laser fluence. The ^{44}Ca and ^{13}C isotopes were recorded and the ^{44}Ca signal was plotted against the scan length. It can be seen that calcium is present during the entire scan, however the optically visible crystals increase the signal.

Fisher's linear discriminant was calculated using the formula:

$$\boldsymbol{Fisher's\ linear\ discriminant} = \frac{(\boldsymbol{m_1} - \boldsymbol{m_2})^2}{\boldsymbol{v_1} + \boldsymbol{v_2}}$$

with m representing the group means and v the group variances.

Youden's J, used to determine the threshold in signal intensity to best separate the PTFE from the background acrylic resign, by maximizing it, is defined as[1]:

$$\boldsymbol{J} = \frac{TP}{TP + FN} + \frac{TN}{TN + FP}$$

where TP= true positives, FN = false negative, TN = true negative and FP = false positive,

Positive and negative is defined as pixels containing or not fluorine, whereas the optical image (Fig. 2a in the main manuscript) was used to determine the reference values for the pixels.

[1] W.J. Youden, Index for rating diagnostic tests, Cancer, 3 (1950) 32-35.

6 Publication 4

Quantitative depth profiling using online-LASIL to investigate oxidation behavior of transition metal borides

Maximilian Weiss[a], Thomas Glechner[b], Victor Weiss[a], Helmut Riedl[b,c], and Andreas Limbeck[a]

a Institute of Chemical Technologies and Analytics, TU Wien, Getreidemarkt 9/164 - 1060 Vienna, Austria

b Institute of Chemical Technologies and Analytics, TU Wien, Getreidemarkt 9 -1060 Vienna, Austria

c Institute of Materials Science and Technology, TU Wien; Getreidemarkt 9 -1060 Vienna, Austria

Quantitative depth profiling using online-laser ablation of solid samples in liquid (LASIL) to investigate oxidation behavior of transition metal borides

Maximilian Weiss[a], Thomas Glechner[b], Victor U. Weiss[a], Helmut Riedl[b,c] and Andreas Limbeck[a]

A: Institute of Chemical Technologies and Analytics, TU Wien, Getreidemarkt 9, 1060 Wien, Austria
B; Christian Doppler Laboratory for Surface Engineering of High-Performance Components, TU Wien, Getreidemarkt 9, 1060 Wien, Austria
C: Institute of Materials Science and Technology, TU Wien, Getreidemarkt 9, 1060 Wien, Austria

Abstract:

The increased demand for sustainability requires the development of new materials. Transition metal borides are exceptional candidates, as they exhibit fascinating mechanical and thermal properties. However, oxidizing atmospheres at elevated temperatures, their use is limited due to their inadequate oxidation resistance. Recently, it was found that chromium diboride doped with silicon can overcome this limitation. In this work, a method to perform quantitative depth profiles without matrix-matched reference material was developed based on the recently introduced online-LASIL technique. An optimized design of the LASIL system combined with a careful adjustment of the solvent composition and the laser parameter enables the use of liquid standards to quantify the ablated material. It was possible to achieve a depth resolution of 240 nm, only limited by the sensitivity of the system for silicon. The validity of the LASIL results was cross-checked by the comparison with several other analytical techniques. Two samples with different concentrations suffering an oxidation treatment – extensively characterized from morphological and alloying aspects – were used to demonstrate the capabilities of this technique. The concentration profiles of the elements resembled the pathway of the oxidation layers as monitored with TEM. The stoichiometry of the oxidation layers differed strongly between the samples, suggesting different processes are taking place, depending on the silicon doping level of the sample. The online-LASIL depth profiles match the data obtained by XRD and TGA analysis of the samples. The flexibility of the

developed online-LASIL method allows a simple adoption of the technique to a larger number of samples and different materials.

1. Introduction

Corrosion can quickly disintegrate the properties of a material, especially at elevated temperatures, shortening its lifetime and limiting application temperatures. Through the deposition of protective coatings, the properties of the applied engineering materials can be enhanced. In this context, transition metal diborides are among the most promising candidates that have gained attention in recent years.[1-3] The properties of the boron-metal bond allow these materials to combine the favorable properties from metals and ceramics, such as high strength elastic modulus with high thermal and electrical conductivity.[4, 5] Their extremely high melting points (over 3000 °C) makes them suitable for future high-temperature applications. Such environments are, for example, relevant for cutting tools or aerospace industry.[6] However, in practice, this is limited through their poor oxidization resistance.[7, 8] Pure borides tend to form a B_2O_3 layer upon oxidation, which evaporates at elevated temperatures, a process further enhanced by the presence of water vapor by forming the more volatile boric acid, thus limiting the oxidation resistance.[9-11] To enhance the high-temperature performance, the alloying of elements forming highly stable oxides, such as Si and Al, as they are known to yield low parabolic rate constants for the oxidation reaction, was employed.[8, 12] Especially silicon is of interest, as it can form a protective borosilicate glass-like film on borides upon oxidation.[13, 14]

Transition metal borides can exist over a wide stoichiometric range, and systems with a plethora of transition metals are under investigation. Through their synthesis via sputter deposition, the amount of the alloying elements such as silicon can easily be varied over a wide range. [2] To tune the properties of a material, it is of fundamental interest to understand the processes during the oxidation reaction. Hence, a wide range of methods is employed in this field, such as thermogravimetry to measure the reaction kinetics, X-Ray diffraction for the resulting phase composition, and electron microscopy for its microstructure. [15] Of particular interest is the composition of the oxide layer and the change of the underlying thin film. A method to characterize these needs to give quantitative results and sufficient depth resolution to separate the layers. There are several frequently employed methods for the analysis of boride thin films: SIMS (secondary ion mass spectrometry)[16], GD-OES/MS (Glow discharge optical emission/mass spectrometry), [17, 18] XPS (X-Ray photoelectron spectrometry)[19], LA-ICP-MS (Laser ablation inductively coupled plasma mass spectrometry)[20] and X-Ray based methods such as XRF (X-ray fluorescence) and SEM-EDX (Scanning electron microscopy with energy dispersive X-Ray analysis), with their specific strengths and drawbacks, respectively.[18, 21] Of those SIMS, GD-OES/MS and LA-ICP-MS are commonly used for

depth profiling. A general limitation in direct-solid-state analysis, especially for depth profiling, is the availability of suitable reference materials for quantitative analysis. The availability of matrix-matched standards and certified reference materials (CRMs) is limited, especially for novel classes of materials such as borides.[22] A reference material must match the chemical and physical properties of the sample as closely as possible. In the case of the thin films undergoing oxidation, the oxide layer is significantly different in the properties compared to the boride base material, so at least two reference materials are needed to precisely determine the stoichiometry throughout the depth profile.

A promising solution to this limitation is the recently introduced online laser ablation of solids in liquids (online-LASIL) technique, [23] as it can circumvent several limitations of other techniques. In online-LASIL, tiny portions of the samples are removed by laser ablation. The ablation is done in a continuous flow of carrier solution, which transports the removed material into a hyphenated instrument to derive the sample's composition. The main advantage of online-LASIL is that it is possible to use ready-to-hand liquid standards to determine the composition of the particle suspension produced in the LASIL process. It is well known from slurry analysis and single-particle ICP-MS (spICP-MS) that particles below a specific size behave in the ICP plasma like ions and can therefore be quantified with liquid standards. [24, 25] Through this, the use of matrix-matched standards or certified reference materials (CRMs) can be circumvented. The flexible preparation of customized liquid standards allows quantitative investigations of a wide range of materials not accessible with more conventional techniques. The second main advantage of online-LASIL is the improved depth resolution. Whereas with conventional nanosecond laser ablation, usually depth resolutions in the order of some hundred nm are possible [18], previously published online-LASIL applications report values below 50 nm.[23, 26] With these characteristics, online-LASIL is a promising candidate to perform quantitative, depth-resolved analysis to understand the oxidation behavior of transition metal diboride.

In a preceding work [15], the oxidation behavior of several Si alloyed transition metal diborides was investigated. As the systems based on chromium diboride doped with silicon showed an exceptional good oxidation resistance, with only forming oxide scales with an average thickness of 400 nm, they are of particular interest. For this work, two samples with different silicon content were chosen to observe the influence of silicon on the oxide scale formation. A methodology based on online-LASIL was developed to perform quantitative depth profile measurements of these materials, enabling the determination of the oxide scale and changes in the stoichiometry of the underlying thin film. Classical acid digestion with subsequent liquid

ICP-OES was performed to obtain the bulk stoichiometry before the oxidation. With the data from the rigorous characterization of the thin films, including X-Ray diffraction (XRD), thermogravimetry (TGA), and transmission electron microscopy (TEM), the information of the online-LASIL depth profiles could be validated and put into a material science context.

2. Experimental

2.1 Reagents and Instrumentation

High purity (18.2 MΩ resistivity at 25°C) water was obtained from a Barnstead EASYPURE II system (Thermo Fisher Scientific, Waltham, MA, USA). Acids and all other chemicals not otherwise mentioned and certified ICP liquid standards were purchased from Merck (Darmstadt, Germany) in at least analytical quality. Laser ablation was performed with a J200 Tandem (Applied Spectra Inc., Sacramento, CA, USA) equipped with a 266 nm Nd:YAG laser with a pulse duration of 5 ns. For the ICP-MS measurements, an iCAP Qc, (Thermo Fisher Scientific, Bremen, Germany) equipped with an HF (hydrofluoric acid) resistant sample introduction kit (alumina injector tube, a perfluoroalkoxy alkane (PFA) cyclonic spray chamber, and a PFA concentric nebulizer) was used. Liquid ICP-OES measurements were performed on an iCAP 6500 RAD (Thermo Fisher Scientific, USA) coupled to an ASX-520 autosampler (CETAC Technologies, Omaha, NE, USA), equipped with an HF resistant sample introduction kit, which includes a Miramist nebulizer (Burgener Research, Mississauga, Canada), a Teflon spray chamber and an Al_2O_3 injector tube. TEM measurements were performed on an FEI TECNAI F20 (Thermo Fisher Scientific, Bremen, Germany). Depth of ablation craters was recorded on a Dektak XT (Bruker, Billerica, MA, USA) stylus profilometer. Particle size distribution of the ablated material was done on a ZetaView particle tracker (Particle Metrix, Inning am Ammersee, Germany). Data analysis was performed in Excel (Microsoft Cooperation, USA) and OriginPro 2020 (OriginLab Corporation, Northampton, MA, USA).

2.2. Deposition and treatment of samples

The deposition of the coatings, the oxidation treatment, and rigorous characterization of the samples have been described in detail by Glechner et al. [15]. The two samples, designated as A and B in the following, were deposited in-house built magnetron sputter device [27] using a CrB_2 target (Plansee Composite Materials GmbH, Lechbruck am See, Germany) on which Si

wafer plates (CrysTec GmbH, Berlin, Germany) were placed on the racetrack to alloy Si. Through changing the number of silicon plates, the amount of silicon in the samples was varied. Polycrystalline Al_2O_3 (CrysTec GmbH) platelets were used as substrate. The thickness of the deposited films was about 2.4 µm. Oxidation treatment of the samples was performed in a chamber box furnace under ambient air. The temperatures used were 1100 °C for sample A or 1200 °C for ample B, for 3 hours, respectively.

2.3 LASIL setup

For the online-LASIL measurements, specimens are put in a liquid-tight in-house made cell which forms the flow path. The cell design is similar to previous works. [26, 28, 29] The LASIL cell (Figure 1) consists of a PEEK (polyether ether ketone) body with a 5x5x0.5 mm pocket to contain the sample. The employed LASIL cell design contains two inlets and one outlet for fluids. The cell is sealed by a PDMS (polydimethylsiloxane) film (500 µm thick) containing the 500 µm wide flow path to guide the liquid over the sample. A fused silica window, transparent to the UV laser wavelength, is placed on top and aligned to the body by a counterpart made of PEEK. A peristaltic pump (Perimax 12, SPETEC, Germany) is used to transport the required fluid flows through the system. All tubing is made out of PFA with an inner diameter of 0.5 mm on the input side and 0.25 mm between the LASIL cell and the ICP-MS instrument.

The LASIL cell is positioned on the movable XYZ sample stage of the J200 laser ablation platform. To analyze the ablated material, the generated particle suspension was purged with a carrier solution into a quadruple ICP-MS. The instrument was tuned daily for a maximum ^{115}In signal intensity and a minimum $^{140}Ce^{16}O/^{140}Ce$ oxide ratio. The ICP-MS instrument was operated in KED (kinetic energy discrimination) mode using 7 % H_2 in He as collision gas. The ICP-MS measurement parameters are listed in Table 1. The instrument software (Qtegra version 2.10) was used for data collection and evaluation.

For LASIL measurements, substrates were broken into 5x5 mm pieces by scratching with a diamond cutter to fit tightly into the pocket of the LASIL cell. The current LASIL setup allows the use of two fluid flows: a carrier flow and a make-up flow (for details see Figure 1), both contain 10 ng/g of indium as an internal standard to monitor potential signal drifts during measurements. Isotopes selected for ICP-MS analysis, as well as the applied instrumental parameters, are compiled in Table 1. Laser ablation was performed in line scan mode with the parameters stated in Table 2.

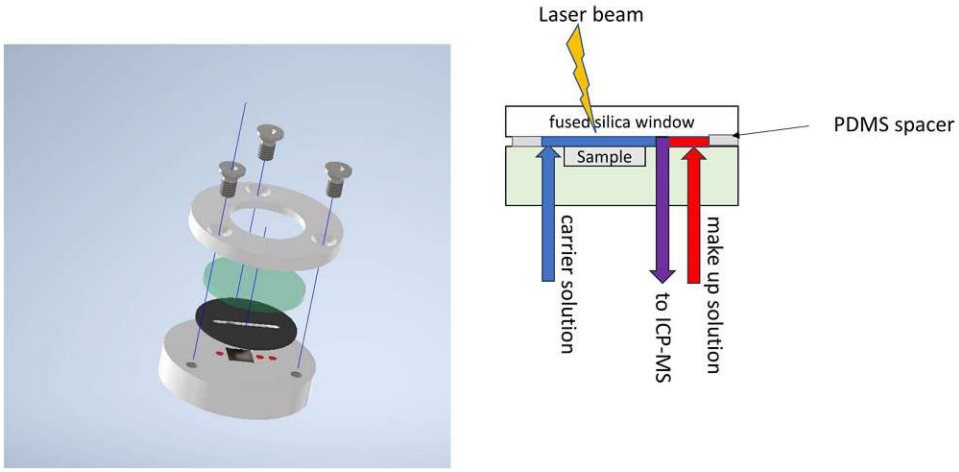

Figure 1: left: CAD explosive drawing of the LASIL cell, the gray parts represent PEEK, the PFA tubing pushed in the PEEK body is depicted in red, the PDMS spacer in black, and the fused silica window in green. Right: cross-section of the LASIL cell showing the fluid path and the flows through the sample cell.

2.4 ICP-OES reference measurements

To obtain reference values for the samples, an aliquot of the native, unoxidized samples was converted into a solution and measured with conventional liquid ICP-OES. For this purpose, samples were broken into pieces of about 5x5 mm and digested in triplicates in metal-free falcon tubes with a mixture of 0.25 mL nitric acid and 0.25 mL hydrofluoric acid at a temperature of 80°C for 10 minutes. Derived solutions were diluted to a final volume of 20 mL with ultrapure water, and europium was added as an internal standard with a final concentration of 1 µg/g. External calibration with matrix-adjusted standards was used for quantification. Two emission lines were observed per element, one used for quantification one for quality control; for further details, see Supplementary Table 1. The applicability of this procedure has been demonstrated recently [6,20,29].

Table 1: ICP-MS measurement parameters for online-LASIL.

RF Power	1550 W
Auxiliary gas flow (Ar)	1.0 L/min
Cooling gas flow (Ar)	14 L/min
Nebulizer gas flow (Ar)	0.8 L/min
CCT Bias	-21 V
Pole Bias	-18 V

KED gas glow (7 % H_2 in He)	5 mL/min
Monitored ions	^{11}B, ^{27}Al, ^{28}Si, ^{52}Cr, ^{53}Cr, ^{115}In,
Dwell Time	0.01 s for ^{27}Al, ^{52}Cr, ^{53}Cr, ^{115}In 0.05s for ^{11}B and ^{28}Si

Table 2: Laser parameters for the online-LASIL measurements.

Laser energy depth profile	0.17 mJ
Laser energy survey run	0.51 mJ
Spot size	100 µm
Scan speed	1000 µm/s
Carrier solution flow	0.53mL/min
Makeup solution flow	0.28 mL/min
Repetition rate	10 Hz
Investigated sample area	0.1 mm^2

3. Results and Discussion

3.1. Optimization of carrier solution

From conventional liquid sample analysis, it is well known that analytes, primarily metal ions, can get lost during sample storage or analysis due to precipitation or adsorption to the walls of the sample container or the analysis system. Therefore, in classical trace elemental analysis, samples and standards are prepared in a diluted acidic solution, usually, 1 % (v/v) HNO_3 or HCl, to stabilize the dissolved ions and prevent possible losses during storage and measurement. When performing laser ablation in liquid, the ablated material can be present in the form of suspended particles but also as dissolved ions. For online-LASIL, this is an especially critical issue as the use of a liquid carrier for the transport of the reaction products from the ablation site to the detection unit might result in fractionation effects preventing an accurate determination of the sample stoichiometry. Possible reasons for the loss of dissolved species have been mentioned above. However, also particles can get lost, for example, through

agglomeration and subsequent sedimentation. Thus, to avoid fractionation effects, a stabilization of both forms, particles, and solvated species, is necessary to prevent losses of these ablation products. For this purpose, The design of the online LASIL cell has been refined [28] to include two inlets for liquid solutions, one for the carrier solution, which flows over the sample surface, and one for the make-up solution, which is mixed with the carrier solution right after the ablation process. As the flow of the carrier solution is chosen to be higher than the make-up solution, it is ensured that the make-up solution cannot be directed into the sample cavity, impeding contact with the sample in the LASIL cell. This concept allows the use of more concentrated acids to prevent a loss of analytes, as the concentrated acid solution does not come in contact with the sample, which is a precondition for the investigation of acid-sensitive samples.

To find an optimal combination for the composition of carrier and make-up solution, the approach presented in Weiss et al. 2021 [26] has been applied as exemplified in Figure 2. A series of standard solutions of the elements of interest were prepared in different candidate make-up solutions. The candidate make-up solution and a candidate carrier solution are flown through the cell until a stable background signal is reached. Then a defined amount of a spiking material has been added to the make-up solution, causing a sudden increase in the respective ICP-MS signals. After the signals in the ICP-MS have reached a plateau for all elements, the spike solution is exchanged to the pure make-up solution again. After the signal has stabilized again, a washing step with 10 % HCl has been performed (flown through both inlets). If the analyte has been adsorbed onto the walls of the system, in this washing step, a strong peak in the signal would appear; if not, the analyte signal would remain at the baseline level. The lowest acid concentration in make-up and carrier solution able to achieve this behavior was considered optimal. Based on the experience from [26], for the carrier solution, an NH_4Cl/HCl buffer with EDTA added was used. A concentration of 910 mmol NH_4Cl and 30 mmol/L HCl resulting in a pH of 5 and an EDTA concentration of 4.17 mg/L for the make-up solution and a mixture of 2 % (v/v) HCl and 0.2 % (v/v) HF for the make-up solution were found to give optimal results, as HF is known to be necessary to stabilize transition elements.[30]

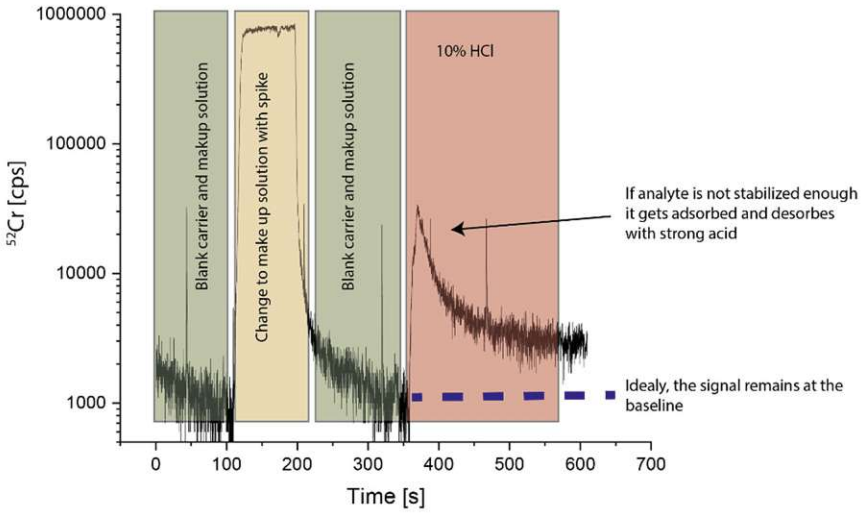

Figure 2: Demonstration of the optimization process for the make-up and carrier solution: If the analyte is not stabilized enough, it gets absorbed to the walls and appears as a peak if it gets desorbed by concentrated acid.

3.2 Quantification of LASIL measurements

In online-LASIL measurements, material is at least partially ablated in the form of particles. To use liquid standards, it is a prerequisite that these particles behave in the plasma the same way as the liquid standards. This assumption is also routinely used in single-particle ICP-MS (spICP-MS), where liquid standards are used to interfere the size of nanoparticles typically below 100 nm and have gained a broad spectrum of applications in the last years.[25, 31]. On the upper end, it was found that particles with a diameter of up to 3 µm can be quantified with liquid standards in slurry analysis. [24] To ensure that the particles generated with online-LASIL are small enough to be fully ionized in the plasma and fulfill the requirements for the application of liquid standard solutions, measurement of the size distribution was necessary. For this purpose, the flow out of the online-LASIL cell was collected in a tube during the ablation. The solution containing the generated nanoparticles was analyzed in a ZetaView particle tracker after dilution with water to give a signal in the working range of the instrument. Particles in the range between 65 and 200 nm were found with a median of 114 nm, which is the size range typically studied in spICP-MS and one order of magnitude below the size limit reported for slurry samples. In supplementary Figure 1, the size distribution graph is shown. Thus, the use of liquid standards is a valid approach for quantification of the particle suspensions produced with online-LASIL.

Online-LASIL measurements were quantified using the standard addition approach [29] by adding defined amounts of the investigated analytes to the make-up solution. In Figure 3, a typical time-resolved signal for ^{52}Cr of a depth profile measurement is demonstrated.

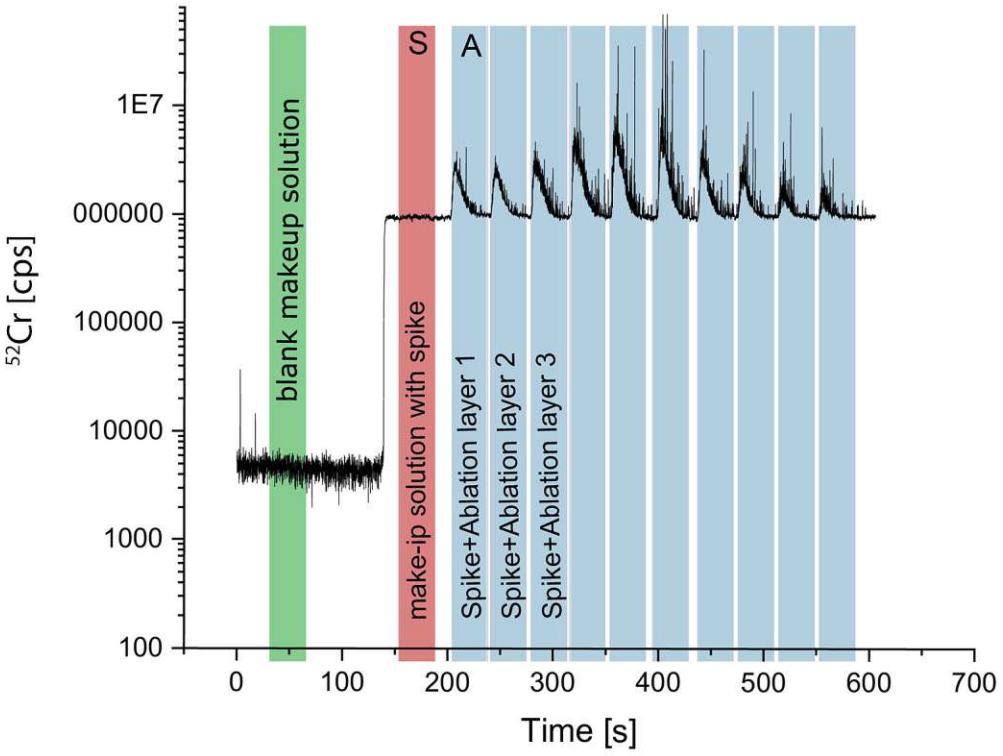

Figure 3: Illustration of the signal during a depth profile measurement with standard addition.

The concentration of the elements in the ablated material can be calculated by the following formula:

$$c_{abl} = \frac{c_s}{S}(A - S)$$

Whereas c_{abl} is the concentration of the respective element in the flow from ablation, c_S is the concentration of the spike, A is the integrated area of the ablation peak, and S is the integrated area from the spike. Note that the integration regions A and S have the same duration.

To exclude that material is removed from the fused silica window of the LASIL cell during ablation, which would contribute to the silicon signal detected with ICP-MS, measurements with pure Al_2O_3 substrates were performed. In these experiments, no increase in the silicon signal was observed during sample ablation, indicating that the use of a silicon window did not influence the analysis of Si.

3.3 Optimization of Depth profile measurements

Measurement of silicon with ICP-MS is challenging due to the high ionization energy of 8.151 eV. Moreover, the main Isotopes ^{28}Si and ^{29}Si are interfered by several polyatomic ions arising from the ICP plasma [32]. Therefore, the detection limit for silicon with ICP-MS is orders of magnitude worse than for most other elements. [33] With the advent of collision-reaction cell technology, the intensities of interfering polyatomic ions could be significantly reduced; thus, the signal ratio of analyte to the background can be improved. [34] However, the sensitivity achieved for silicon is still lower compared to the other elements examined in this study. With the use of Calibration standards which were introduced via the make-up solution, detection limits (LOD) were determined. Silicon has, as expected, the highest LOD of 69 ng/g, compared to 2 ng/g for B 0.08 ng/g for Cr and is, therefore, the limiting factor in the analysis of the samples.

In the used setup, the main parameter influencing the ablation, and therefore the depth resolution, is the laser energy. [35, 36] The ablation energy cannot be arbitrarily reduced, as the ablation process only onsets over a certain energy threshold.[37] The lowest laser energy to achieve a measurable ^{28}Si signal was 0.17 mJ. At this energy, the boride film could be fully ablated with ten layers, indicated by a sudden drop of the total signal observed for the measured elements when the Al_2O_3 substrate has been reached. With further ablation passes at this energy, it was impossible to observe a ^{27}Al signal, indicating that the energy is below the ablation threshold for Al_2O_3. These findings were confirmed by a profilometric scan of the ablation crater, which suggests that in total, roughly 2.4 µm sample has been ablated, resulting in a depth resolution of ~ 240 nm per layer at this laser energy.

In this case, the sensitivity of silicon is the limiting factor, as the amount of ablated material decreases concomitantly with the reduction of the thickness of an ablation layer. Generally, the depth resolution of online-LASIL is limited by the laser-material interaction. To investigate the best possible depth resolution, the samples were also ablated with the conditions used in Weiss et al. [26] with a 213 nm laser ablation system. The crater depth determined with profilometry indicated 50 nm per ablation layer under these conditions; however, no silicon signal could be detected on the ICP-MS, only chromium could be measured clearly, and the boron signal was rather noisy at this level. This is in accordance with previous works [23, 26], where similar depth resolution could be achieved.

On the upper bound, the laser energy is limited by the mechanical strength of the fused silica window, which can burst through the generated cavitation bubble in the carrier solution at about 1 mJ laser energy. Further, it was observed that the boride thin films delaminate from the substrate if the laser energy is too high.

Other factors influencing the ablation are the spot size and the number of shots per sample location. To reduce cratering effects due to the Gaussian profile of the laser beam, overlapping spots were chosen where the Laser hits each ablation spot two times by a stage-velocity of 1 mm/s and a laser frequency of 10 Hz.

3.4. Measurement of oxidized samples

Two silicon-alloyed chromium diboride samples, as stated before, designated as A and B, with different silicon doping levels were investigated within this study and used for the depth profile measurements. Of the as-deposited samples, the bulk stoichiometry was determined with liquid ICP-OES; values are listed in Table 3, the standard deviation was derived from three replicates of the digestion. The obtained bulk stoichiometry agrees with the composition expected from the thin-film production.

In the first step, to validate that online-LASIL yields accurate values for the stoichiometry of the samples, measurements with enhanced laser energy of 0.51 mJ were performed. This high laser energy is not suitable for the depth profile analysis, but the increased ablation rate results in higher analyte concentrations in the carrier solution and thus improved signal-to-noise ratios for subsequent ICP-MS analysis. As can be seen in Table 3 the findings derived for native, non-oxidized samples are in good agreement with the values obtained from ICP-OES measurements, in particular when considering that in the case of online-LASIL only tiny sample areas of around 0.1 mm² were used for analysis whereas for ICP-OES measurements 5x5 mm large pieces were used. The presented averages and standard deviations are determined from tree ablation passes at different sample positions. This outcome demonstrates the applicability of the proposed online-LASIL procedure, but it also confirms that the optimized composition of the carrier solution prevents the fractionation effects of the analyte.

Table 3: Comparison of the results of the stoichiometry determination between the liquid ICP-OES (n=3) and the online-LASIL analysis perfumed on the native samples with high laser energy (0.51 mJ).

Sample	***Measurement***	***Cr at%***	***Si at%***	***B at%***
Sample A	ICP-OES	27.09±0.05	8.92±0.27	63.99±0.32
	LASIL bulk analysis	25.01±1.8	7.65±3.24	67.34±1.45
Sample B	ICP-OES	25.58±0.15	15.81±0.05	58.61±0.13

LASIL bulk analysis	22.79±1.04	18.77±1.53	58.44±0.63

In a second step, depth profile measurements using the optimized laser conditions (laser energy 0.17 mJ) were performed on the two samples after they underwent an oxidation treatment in ambient air for 3 h at 1100 °C (sample A) or 1200 °C (sample B).

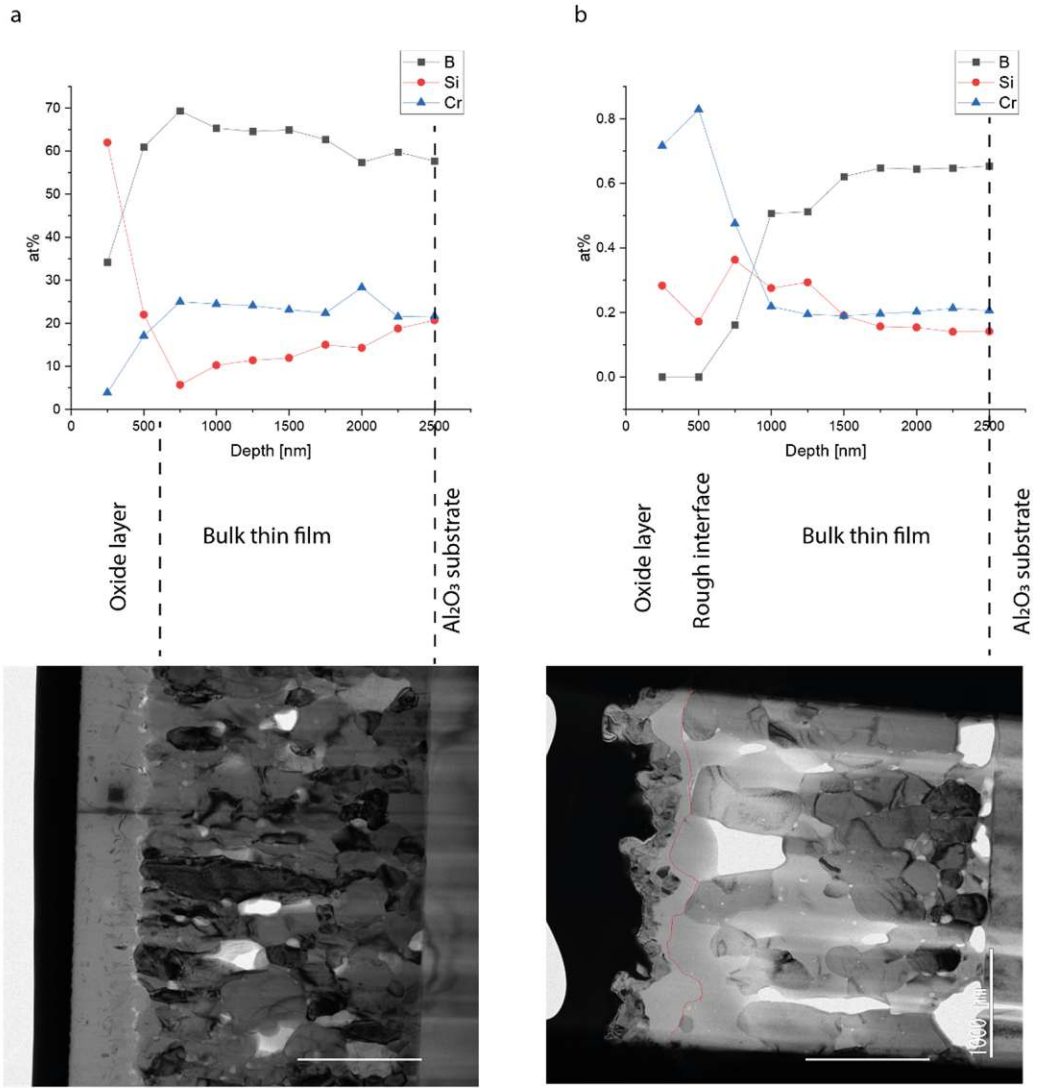

Figure 4: LASIL depth profiles with corresponding bright-field TEM cross-sections of the samples. a: Sample A (native stoichiometry $Cr_{0.27}Si_{0.9}B_{0.64}$) b: Sample B, native stoichiometry $Cr_{0.26}Si_{0.16}B_{0.58}$. The scale bar represents 1000 nm, images have been rotated to correspond to the depth profiles. The thin red line in the TEM image of Sample B indicated the boundary of the oxide and was determined with High-angle annular dark-field imaging (HAAFD) STEM (scanning transition electron microscopy).

In Figure 4, the quantitative online-LASIL depth profiles of the two oxidized samples with BF-TEM cross-sections of the same samples are shown. In the TEM cross-section of Sample A, two layers separated by a sharp interface can be seen; the upper corresponds to the formed oxide scale with a thickness of approximately 500 nm, and the lower is the remaining boride film.

The performed online-LASIL measurement revealed a very similar outcome, showing for the first ~ 500 nm a distinctly different composition when compared to the rest of the sample. The first ablation layer exhibits a stoichiometry of $Cr_{0.04}Si_{0.62}B_{0.34,}$ indicating an enrichment of silicon in the oxide thin film. With the fourth ablation layer, the sample reaches nearly its native bulk composition.

The TEM image of sample B shows a rough interface between the oxide scale and the base boride coating, with a thickness varying between 180 and 750 nm with 400 nm in mean. Further investigations [15] indicate that the oxide film consists of an outer Cr_2O_3 layer and an inner silicon-rich layer. The irregular interface and the large grains stem from recrystallization processes during the heat treatment and are influenced through the higher temperature and the higher silicon content compared to sample A. X-Ray diffractograms [15] obtained from the sample show that Cr_2O_3 and Si are present as phases alongside the base material. This is confirmed through the online-LASIL measurements. The first two ablation layers are highly enriched in chromium, showing no boron signal. In a depth of about 500 nm, the boron signal starts to increase and reaches its bulk value at around 1500 nm. Silicon is enriched in the top layers, which agrees with the large grains of silicon visible in the TEM and reaches the nominal sample concentration at a depth of 1500 nm. Interestingly the composition of the third ablation layer does not match with the top layer nor with the underlying layer and seems to be a mixture of the formed oxide and the bulk material, which agrees with the coarse interface visible in TEM.

Results derived from online-LASIL measurements indicate that no significant change in the overall stoichiometry of the whole film occurred during the oxidation. This finding could be verified with Thermogravimetric measurements (TGA), which showed for both samples no mass losses at high temperatures, confirming that no volatilization of boron species occurred.

3. Conclusion

In this work, the oxidation behavior of two samples of chromium diboride doped with different levels of silicon was investigated. TEM images revealed a clear difference in the oxidation resistance of the two coating materials. Online-LASIL has been applied for the determination of sample stoichiometry but also for the measurement of quantitative depth profiles. Further improvement of the cell design and careful optimization of the measurement conditions enabled reliable analysis of the overall sample composition. Results obtained for the native, unoxidized samples were found to be in good agreement with ICP-OES reference measurements. Derived depth profiles showed a good correlation with TEM images of the samples. Moreover, with

online-LASIL, it was possible to gain insight into the exact stoichiometry of the oxide layer and the change of the bulk sample below. It could be shown that the oxide layers of the two samples had a very different composition. This information is not easily accessible with other techniques capable of depth-resolved measurements, as matrix-matched standards are required for most methods. In this case, where the sample consists of two different materials (the oxide layer and the native boride), at least two CRMs would be needed for quantitative investigations. A difficult task since, for many materials, it remains challenging to find even one suitable CRM.

As the capabilities of online-LASIL for the assessment of depth-resolved changes in the thin-film stoichiometry has been shown in this work, and several reference techniques checked the validity of the results, it is intended in a next step to extend the investigations to a larger number of samples. These should cover a broader range of sample compositions and treatment conditions, providing more insights into the fundamental processes of high-temperature corrosion.

Acknowledgment

This work was supported by the FWF [grant P31165-N37]. The financial support by the Austrian Federal Ministry for Digital and Economic Affairs, the National Foundation for Research, Technology and Development and the Christian Doppler Research Association is gratefully acknowledged (Christian Doppler Laboratory "Surface Engineering of high-performance Components"). We also thank for the financial support of Plansee SE, Plansee Composite Materials GmbH, and Oerlikon Balzers, Oerlikon Surface Solutions AG. We want the University Service Centre for Transmission Electron Microscopy of the TU Wien (USTEM) for providing TEM measurements. The authors acknowledge TU Wien Bibliothek for financial support through its Open Access Funding Programme.

References

1. Euchner, H. and P.H. Mayrhofer, *Designing thin film materials - Ternary borides from first principles.* Thin Solid Films, 2015. **583**: p. 46-49.
2. Mitterer, C., *Borides in Thin Film Technology.* Journal of Solid State Chemistry, 1997. **133**: p. 279-291.
3. Magnuson, M., L. Hultman, and H. Högberg, *Review of transition-metal diboride thin films.* Vacuum, 2022. **196**.
4. Zimmermann, J.W., et al., *Thermophysical Properties of ZrB2and ZrB2–SiC Ceramics.* Journal of the American Ceramic Society, 2008. **91**(5): p. 1405-1411.
5. Gu, Q., G. Krauss, and W. Steurer, *Transition Metal Borides: Superhard versus Ultra-incompressible.* Advanced Materials, 2008. **20**(19): p. 3620-3626.
6. Fahrenholtz, W.G. and G.E. Hilmas, *Ultra-high temperature ceramics: Materials for extreme environments.* Scripta Materialia, 2017. **129**: p. 94-99.
7. Fuger, C., et al., *Influence of Ta on the oxidation resistance of WB2−z coatings.* Journal of Alloys and Compounds, 2020.
8. Bakhit, B., et al., *Improving the high-temperature oxidation resistance of TiB2 thin films by alloying with Al.* Acta Materialia, 2020. **196**: p. 677-689.
9. Fahrenholtz, W.G. and G.E. Hilmas, *Oxidation of ultra-high temperature transition metal diboride ceramics.* International Materials Reviews, 2013. **57**(1): p. 61-72.
10. Parthasarathy, T.A., et al., *A model for the oxidation of ZrB2, HfB2 and TiB2.* Acta Materialia, 2007. **55**(17): p. 5999-6010.
11. Naraparaju, R., et al., *Effect of moisture on the oxidation behavior of ZrB2.* Journal of the American Ceramic Society, 2020. **104**(2): p. 1058-1066.
12. Grančič, B., et al., *Effect of Si addition on mechanical properties and high temperature oxidation resistance of Ti–B–Si hard coatings.* Surface and Coatings Technology, 2014. **240**: p. 48-54.
13. Riedl, H., et al., *Oxidation behavior and tribological properties of multilayered Ti-Al-N/Mo-Si-B thin films.* Journal of Vacuum Science & Technology A: Vacuum, Surfaces, and Films, 2015. **33**(5).
14. Bewlay, B.P., et al., *Ultrahigh-Temperature Nb-Silicide-Based Composites.* MRS Bulletin, 2011. **28**(9): p. 646-653.
15. Glechner, T., et al., *Influence of Si on the oxidation behavior of TM-Si-B2±z coatings (TM = Ti, Cr, Hf, Ta, W).* Surface and Coatings Technology, 2022.
16. Bazhin, A.I., et al., *Superhardness effect in transition-metal diborides films.* The Physics of Metals and Metallography, 2016. **117**(6): p. 594-601.
17. Jiang, C., et al., *Preparation and characterization of superhard AlB2-type WB2 nanocomposite coatings.* physica status solidi (a), 2013. **210**(6): p. 1221-1227.
18. Pisonero, J., B. Fernández, and D. Günther, *Critical revision of GD-MS, LA-ICP-MS and SIMS as inorganic mass spectrometric techniques for direct solid analysis.* Journal of Analytical Atomic Spectrometry, 2009. **24**(9).
19. Campos-Silva, I., et al., *Properties and Characterization of Hard Coatings Obtained by Boriding: An Overview.* Defect and Diffusion Forum, 2010. **297-301**: p. 1284-1289.
20. Cakara, A., et al., *Development of a multi-variate calibration approach for quantitative analysis of oxidation resistant Mo–Si–B coatings using laser ablation inductively coupled plasma mass spectrometry.* Spectrochimica Acta Part B: Atomic Spectroscopy, 2016. **120**: p. 57-62.
21. Friedbacher, G. and H. Bubert, *Surface and Thin Film Analysis*. Wiley-VCH. 2011, Weinheim, Germany.
22. Limbeck, A., M. Bonta, and W. Nischkauer, *Improvements in the direct analysis of advanced materials using ICP-based measurement techniques.* Journal of Analytical Atomic Spectrometry, 2017. **32**(2): p. 212-232.

23. Bonta, M., et al., *Online-LASIL: Laser Ablation of Solid Samples in Liquid with online-coupled ICP-OES detection for direct determination of the stoichiometry of complex metal oxide thin layers.* Anal Chim Acta, 2018. **1000**: p. 93-99.
24. Ebdon, L., M.E. Foulkes, and S. Hill, *Direct atomic spectrometric analysis by slurry atomisation. Part 9. Fundamental studies of refractory samples.* Journal of Analytical Atomic Spectrometry, 1990. **5**(1).
25. Meermann, B. and V. Nischwitz, *ICP-MS for the analysis at the nanoscale – a tutorial review.* Journal of Analytical Atomic Spectrometry, 2018. **33**(9): p. 1432-1468.
26. Weiss, M., et al., *Quantitative analysis of the platinum surface decoration on lanthanum strontium iron oxide thin films via online-LASIL-ICP-MS.* Microchemical Journal, 2021. **166**.
27. Glechner, T., et al., *Structure and mechanical properties of reactive and non-reactive sputter deposited WC based coatings.* Journal of Alloys and Compounds, 2021. **885**.
28. Herzig, C., et al., *Combining electrochemical and quantitative elemental analysis to investigate the sulfur poisoning process of ceria thin film fuel electrodes.* Journal of Materials Chemistry A, 2022. **10**(4): p. 1840-1851.
29. Herzig, C., et al., *Quantitative imaging of structured complex metal oxide thin films using online-LASIL-ICP-MS.* Talanta, 2020. **217**.
30. Makishima, A., R. Tanaka, and E. Nakamura, *Precise elemental and isotopic analyses in silicate samples employing ICP-MS: application of hydrofluoric acid solution and analytical techniques.* Anal Sci, 2009. **25**(10): p. 1181-7.
31. Mozhayeva, D. and C. Engelhard, *A critical review of single particle inductively coupled plasma mass spectrometry – A step towards an ideal method for nanomaterial characterization.* Journal of Analytical Atomic Spectrometry, 2020. **35**(9): p. 1740-1783.
32. Hill, S.J., *Inductively Coupled Plasma Spectrometry and its Applications*. 2007: Wiley.
33. Lee, S., et al., *Nanoparticle size detection limits by single particle ICP-MS for 40 elements.* Environ Sci Technol, 2014. **48**(17): p. 10291-300.
34. Tanner, S.D., V.I. Baranov, and D.R. Bandura, *Reaction cells and collision cells for ICP-MS: a tutorial review.* Spectrochimica Acta Part B: Atomic Spectroscopy, 2002. **57**(9): p. 1361-1452.
35. Koch, J. and D. Gunther, *Review of the state-of-the-art of laser ablation inductively coupled plasma mass spectrometry.* Appl Spectrosc, 2011. **65**(5): p. 155-62.
36. Russo, R.E., et al., *Laser ablation in analytical chemistry.* Analytical Chemistry, 2013. **85**(13): p. 6162-77.
37. Russo, R.E., X. Mao, and S.S. Mao, *The physics of laser ablation in microchemical analysis.* Anal Chem, 2002. **74**(3): p. 70A-77A.

Supplementary Table 1. ICP-OES parameters for liquid reference measurements.

RF-Power	**1300 W**	
Radial observation height	14 mm	
Cooling gas flow (Ar)	12 L/min	
Nebulizer gas flow (Ar)	0.65 L/min	
Auxiliary gas flow (Ar)	0.4 L/min	
Integration time per replicate	8 s	
Replicates per sample	3	
Purge pump flow rate	1.6 mL/min	
Analysis pump flow rate	0.8 mL/min	
Measured Elements	**Emission line used for quantification [nm]**	**Emission line used for quality control [nm]**
B	249.773 (I)	208.893 (I)
Si	250.690 (I)	288.158(I)
Cr	283.563(II)	284.325(II)

The liquid LOD was calculated by $\frac{3*\sigma}{k}$

Whereas k is the slope of the regression line, and σ is the standard derivation of the blank.

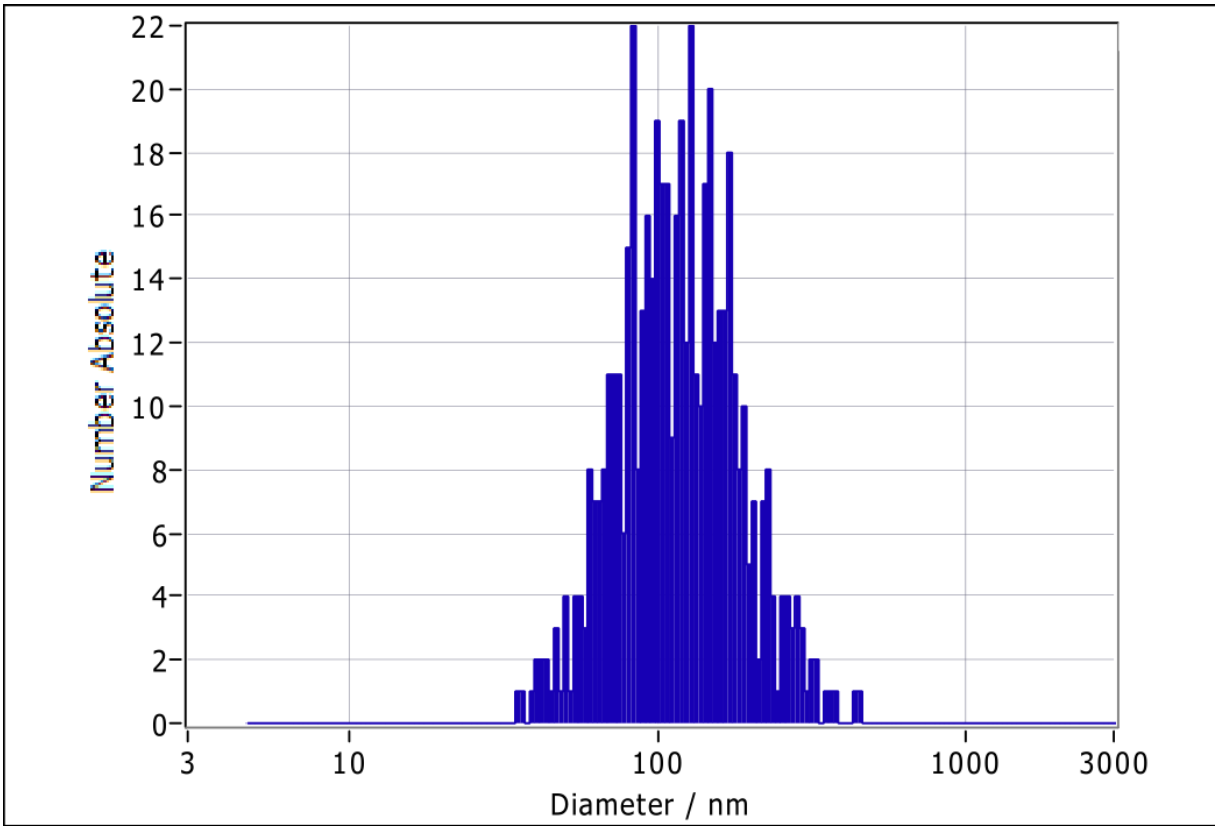

Supplementary Figure 1: Particle size distribution measurement of the particles generated by online-LASIL

7 Coauthored publications

During this research, questions in other groups popped up which could be solved using the methods presented in this thesis and led to the publication of several co-authored papers: The cooperation with the material scientists of the group of Prof. Mayrhofer and Prof. Riedl-Tragenreif not only resulted in two publications presented in this thesis focusing on the development of analytical methods, also papers on the material science site were published where the stoichiometry of several materials was determined. In ***"Influence of Ta on the oxidation resistance of WB 2-z coatings"*** by Fuger et al.[69], ***"Anisotropic super-hardness of hexagonal WB2-z thin films"*** by Fuger et al.[70], and ***"Influence of Si on the oxidation resistance of TM-B2±z coatings (TM = Ti, Cr, Hf, Ta, W)"*** [71]the properties of boride based thin films are investigated. In cooperation with the research devision of electrochemistry, in the paper ***"Performance modulation through selective, homogenous surface doping of lanthanum strontium ferrite electrodes revealed by in situ PLD impedance measurements"***[72], the influence of platinum doping on fuel cell membranes was investigated. In ***"Trace impurities as degradation source of highly active pristine SOFC cathode materials (revealed by in-situ impedance spectroscopy during pulsed lased deposition)"***[submitted, under review] it is shown that even traces of sulfur compounds in laboratory gases can diminish the efficiency of fuel cell materials. In ***"Depletion of Boric Acid and Cobalt from Cultivation Media: Impact on Recombinant Protein Production with Komagataella phaffii"*** [73], the influence of boron and cobalt on the growth of microorganisms was explored, and alternatives to the addition of these substances were searched to comply with current regulation.

8 Contributions to scientific conferences

During this thesis I had the opportunity to visit seven international conferences, to which five oral presentations and six posters were contributed. Two posters achieved awards: ***"Characterization of high-tech materials using online-LASIL"*** won the best poster award at the Winter Conference on Plasma Spectrochemistry in Tuscon 2022 and ***"LIBS analysis of fluorine in solid samples via measurement of molecular emission bands"*** won the 2nd best poster award at the AOFKA 2021 in Freiberg. In the following the posters are presented:

LIBS as versatile tool for characterization of LLZO garnets

M. Weiss[1], S.Smetaczek[1], D.Rettenwander[2], J.Fleig[1], A. Limbeck[1]

[1] Institute of Chemical Technologies and Analytics, TU Wien, 1060 Vienna, Austria

[2] Institute for Chemistry and Technology of Materials, TU Graz, 8010 Graz, Austria

Introduction

The need for high energy density storage has increased the demand for Lithium ion batteries. However current technology suffers from safety concerns, because of the commonly used organic electrolytes. A way to overcome this is replacing them with inorganic solid ion conductors. Cubic $Li_7La_3Zr_2O_{12}$ (LLZO) garnets show high conductivity and good electrochemical stability, what makes them interesting candidates for solid state Lithium ion batteries. Former studies [1,2] show that the composition of samples is not homogenous, however, no direct relationship between composition and conductivity could be found [2]. Further it is known that upon exposure to ambient atmosphere a $LiCO_3$ layer forms, which increases the surface resistance. In this work we study the feasibility of LIBS to monitor the change of the concentration profiles of the main elements as well as non-metallic impurities during the exposure of pristine LLZO with atmospheric contaminant gasses (H_2O and CO_2). The degradation occurs according to the following equations:

[1] $Li_7La_3Zr_2O_{12} + CO_2 \rightarrow Li_2CO_3 + Li_5La_3Zr_2O_{11}$

[2] $Li_7La_3Zr_2O_{12} + H_2O \rightarrow 2\,LiOH + Li_5La_3Zr_2O_{11}$

[3] $2\,LiOH + CO_2 \rightarrow Li_2CO_3 + H_2O$

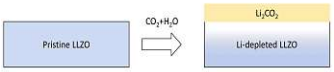

Figure 1: Schematics of the degradation effect

[1] Wachter-Welzl, A., et al., T Solid State Ionics, 2018. 319: p. 203-208.
[2] Smetaczek, S., et al. Journal of Materials Chemistry A, 2019. 7(12): p. 6818-6831.

Experimental

- Samples: Al-stabilized sintered LLZO pellets
- Applied Spectra J200 Tandem LIBS spectrometer with 266 nm Nd:YAG laser
- Sample preablated to create clean surface, heated to remove absorbed water
- Exposure to 3.2 % CO_2 and 890 ppm H_2O
- Heated again to remove physically adsorbed species

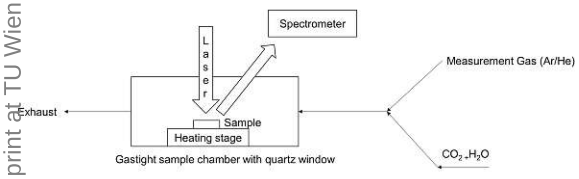

Figure 2: Schematics of the used setup

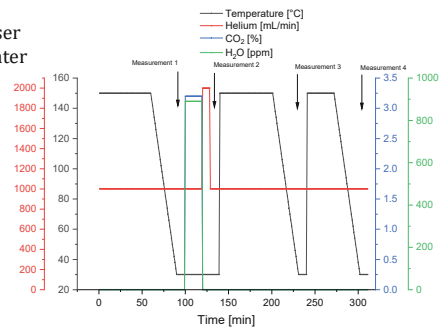

Figure 3: Temperature and gas flow during the experiment

Table 1: LIBS parameters

	Depth profile
Pulse Energy	1.9 mJ
Repetition rate	10 Hz
Gate Delay	0.1 µs
Number of point accumulated	133
Number of Layers measured	10
Laser Diameter	60 µm
Scan speed	600 µm/s
Measurment gas flow (He)	1000 mL/min

Results and Discussion

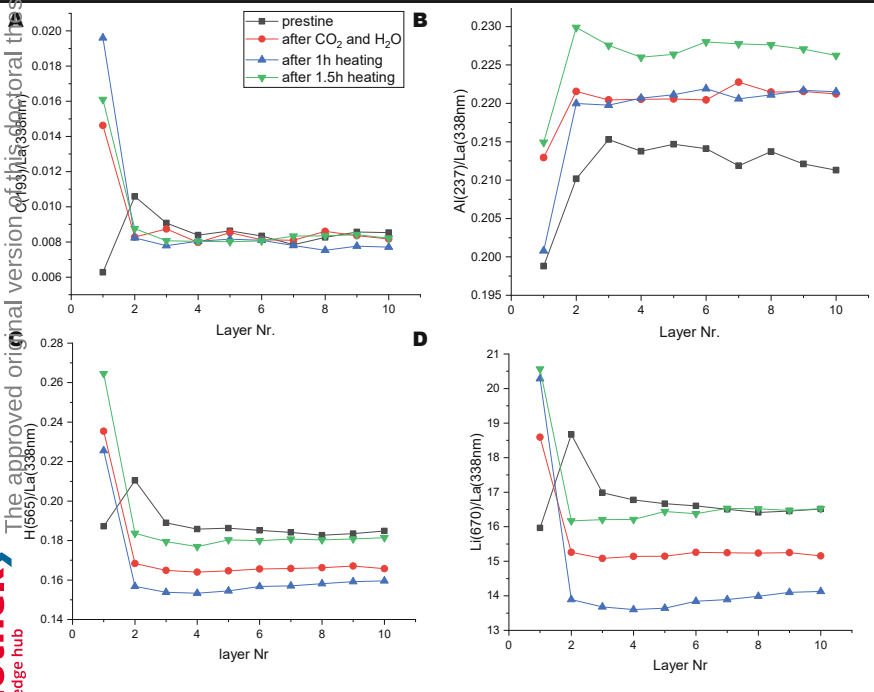

Figure 4: LIBS depth profiles: A: Carbon (normalized to Lanthanum), B: Aluminium (normalized to Lanthanum), C: Hydrogen (normalized to Lanthanum), D: Lithium (normalized to Lanthanum)

- Signals normalized to stable matrix elements to compensate for differences in ablation
- Results comparable for normalization to La and Zirconium
- Parameters compromise between LOD for H and C and saturation and self-absorption for matrix elements (especially Li)
- Preliminary experiments show that water vapor is necessary for the uptake of CO_2
- Carbon and hydrogen signal rise in first layer after contact with H_2O/CO_2
- Does not change after heating --> stable species on surface forms
- Increase of Lithium signal after contact with CO_2/H_2O supports lithium enrichment on surface and formation of $LiCO_3$ as described in equations [1-3]
- CO_2 concentration higher than in ambient atmosphere --> no change of signal after 5 minutes
- Aluminum shows depletion on surface even in pristine state

Acknowledgment

I want to thank the FWF - grant P31165-N37 and W1243 for their financial support

Conclusions and Outlook

- LIBS capable of measuring light elements
- Formation of degradiation product as expected
- Outlook: Correlation of degredation with electrical properties
- Time resolved measurments with lower concentration of gases

Contact

Weiss Maximilian

maximilian.weiss@tuwien.ac.at

LIBS analysis of Fluorine in solid samples via measurement of molecular emission bands

Maximilian Weiss[1], Zuzana Gajarska[1], Hans Lohninger[1], Georg Ramer[1], Bernhard Lendl[1] and Andreas Limbeck[1]

[1] Institute of Chemical Technologies and Analytics, TU Wien, 1060 Vienna, Austria

Introduction

The growing importance of fluoropolymers in high-tech applications and green technologies results in a rising need for their characterization. In contrast to conventional methods, laser-induced breakdown spectroscopy (LIBS) provides the advantage of a spatially resolved analysis. Nevertheless, the high excitation energy of fluorine results in low sensitivity of the atomic F(I) lines, which limits the feasibility of its LIBS-based analysis. We present a novel approach, in which a thin film of copper is deposited on top of the sample via sputter coating. In the late-stage LIBS plasma copper atoms recombine with fluorine to the CuF molecule, which strongly emits in the visible range. We show that this method allows a quantitative, as well as spatial resolved assessment of the fluorine content in the sample.

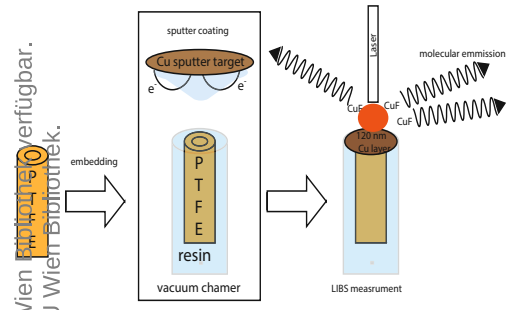

Figure 1: Schematics of the measurement process, from embedding of the PTFE tubes, over sputter depostion of copper to LIBS measurement.

Experimental

To access the applicability of the method, two kinds of samples were produced: For quantitative measurements pressed powder standards were produced from mixtures of PTFE and cellulose powder. To access the imaging capabilities PTFE tubes with an outer diameter of 4 mm and an inner diameter 2 mm were embedded in a Versocit-2 acrylic resin (Struers, Germany). Prior to analysis, the sample surface was polished using a series of silicon carbide (SiC) grinding papers. Copper thin films with a thickness of 120 nm were deposited via a magnetron sputter coater (Baltech MED-020, Liechtenstein) using a copper target. LIBS experiments were performed with a Applied Spectra J200 Tandem LIBS spectrometer equipped with a 266 nm ns Nd:YAG laser and a 6 channel CCD spectrograph covering the spectral range from 188 to 1048 nm. Further an Acton SP2750 spectrometer with a PIMAX2 (ICCD) detector (both Princeton Instruments, USA). All measurements were carried out under an argon gas flow of 1 L/min, the measurement parameters are in Table 1. Surface profiles of craters were recorded with a Dektak XT stylus profilometer (Bruker, USA). Images were reconstructed from raw data using Epina ImageLab 3.45. The data were processed using baseline-corrected integrals. The quantitative analysis of the pressed powder standards was performed in OriginPro 2020, graphs were prepared using the python (v 3.7.6) programming language and the matplotlib (3.2.3), numpy (1.18.1) and scipy (1.4.1) packages.

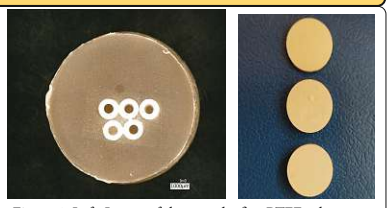

Figure 1: Left: Image of the sample: five PTFE tubes embedded in acrylic resign (Struers Versocit-2), right: Pressed powder standards.

Table 1: LIBS measuring parameters

Parameter	Value
Laser energy [mJ]	1.6
Spot size [µm]	100
Frequency [Hz]	10
Grating grooves/mm	300
Stage velocity [mm/s]	2
Spot spacing [µm]	200
Gate delay (ICCD) [µs]	7
Gate width (ICCD) [µs]	10

Results and Discussion

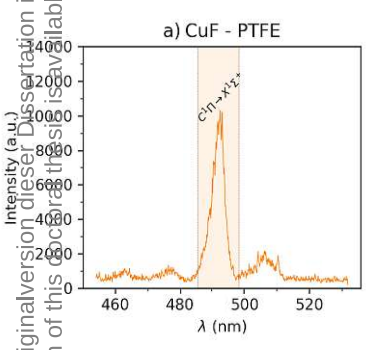

Figure 2: Single shot spectrum of the copper coated PTFE. The highlighted area is the integrated and background corrected region of the CuF C ¹Π -->X ¹Σ⁺ band.

Copper was chosen for this work, as it is a rather noble metal frequently applied for magnetron sputtering. Moreover, the CuF molecule emissions in the visible range are free of interference from atomic copper lines, as can be seen in Fig 1, were the integrated and background corrected area, used for further analysis is highlighted. To assess the sensitivity and linearity of the method, the pressed powder standards made of cellulose and PTFE were evaluated. Here the signal of 60 single shots was accumulated. In Figure 3a, the calibration curve is shown, exhibiting a high linearity (r^2=0.99) and giving a LOD of 160 µg/g fluorine, indication a high enough sensitivity for single shot imaging.

In Figure 3b the crater of a single laser with 100 µm spot size shot on Cu coated PTFE is shown. Due to the bad adhesion of the film a larger area of Cu is removed, limiting the imaging resolution to 200 µm. With profilometry (Fig. 3c) it was confirmed that the actual crater has a diameter of 100 µm, corresponding to the laser spot size.

Using the molecular emission signal a image of the fluorine content could be reconstructed (Fig.4), which resembles the optical image. To access if the defects in the image (marked with arrows) stem from the sample or the measurement, a PCA was performed the co-recorded broadband spectrum (see Brunnbauer et. al. 2020), showing the same artifact. In order to compare separation power of the fluorine from the background, a mask representing the PTFE rings and a mask representing the background region (acrylic resin) was created for both samples using the microscopic image and ImageLab software. The emission signals from Fig. 4 were plotted in a histogram (Fig.5) representing the distribution of the molecular signal intensities in the region of the PTFE tubes (orange) and the background (blue). The dotted line in the histograms represents the PTFE-background threshold determined with Youdens J. To combine the spatially resolved with the statistical information, an image was created (Fig6.). Using this threshold, pixels above the threshold are set to black and below to white.

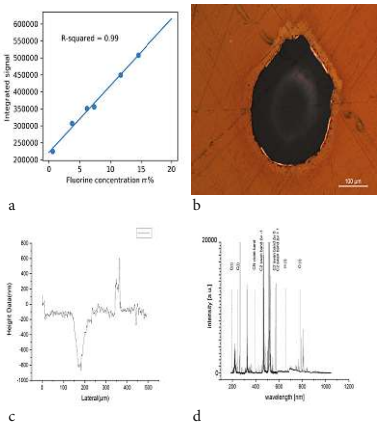

Figure 3: a Calibration graph of the pressed powder standards b: Microscopic image of a laser crater in Cu coated PTFE; c: Surface profile of the crater from b; d: Broadband LIBS spectrum, annotated regions were used for the PCA.

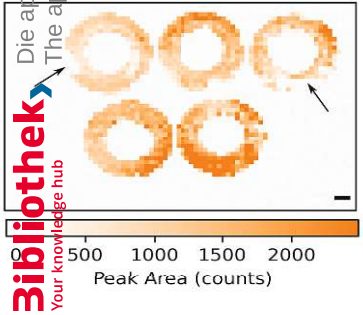

Figure 4: Reconstructed chemical maps from emission intensities of the CuF molecule, scale bar = 1 mm.

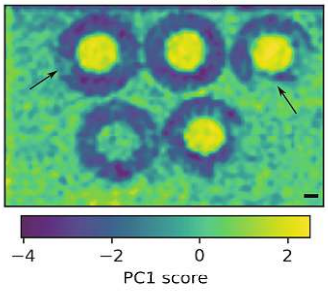

Figure 5: Scores of the first principal component from the broadband six channel detector recorded simultaneously with the molecular CuF band.

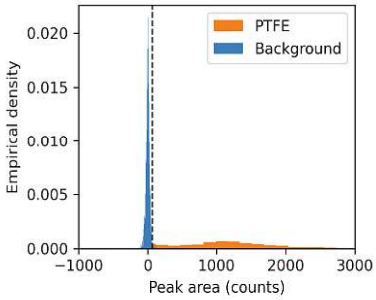

Figure 6: Histograms representing the distribution of the integrated CuF molecular band intensities in the region of PTFE ring (orange) and acrylic resin (blue).

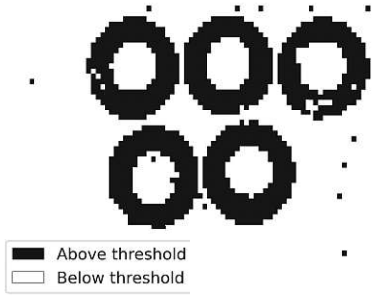

Figure 7: Sample images based on the Youdens J threshold. The threshold images of both signals resemble the fluorine distribution present in the optical images.

Conclusion

- Sputtering is a simple way to apply copper to a sample
- CuF emmsion higly linear corrrelated to fluorine concentration in standards
- Sensitifity high enough for single shot images
- Fluorine mappings in good aggrement with reference values
- The method provides high discrimation power of PTFE from the background

Contact

Maximilian Weiss
maximilian.weiss@tuwien.ac.at
+43 1 58801 15183

CHARACTERIZATION OF SOLID LITHIUM ION CONDUCTORS WITH LIBS

M. Weiss [1] , S. Smetaczek [1] , D. Rettenwander [2] , J. Fleig [1] , A. Limbeck [1]

1 Institute of Chemical Technologies and Analytics, TU Wien, 1060 Vienna, Austria
2 Institute for Chemistry and Technology of Materials, TU Graz, 8010 Graz, Austria

Introduction

The implementation of all solid-state lithium ion batteries promises to solve many security issues associated with conventional lithium ion batteries. However, the used Cubic $Li_7La_3Zr_2O_{12}$ (LLZO) garnets are known to degrade over time when in contact with ambient atmosphere due to the formation of Li_2CO_3 and LiOH corrosion layers with CO_2 and H_2O. In this study we evaluate the use of LIBS for in situ measurements of the formation of these products under controlled atmosphere. LIBS has the unique capability to access all elements of the periodic systems, which enables to see hydrogen, lithium, carbon and oxygen, which would not be possible with other methods. Depth profiles before and after the exposure to CO_2 and H_2O as well as spatial distribution are investigated.

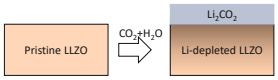

[1] $Li_7La_3Zr_2O_{12}$ +CO_2 --> Li_2CO_3 + $Li_5La_3Zr_2O_{11}$
[2] $Li_7La_3Zr_2O_{12}$ +H_2O --> 2 LiOH+ $Li_5La_3Zr_2O_{11}$
[3] 2 LiOH+CO_2--> Li_2CO_3 + H_2O

Experimental

- Al-stabilized sintered LLZO pellets were used as samples
- Sample on heating stage in gas tight LIBS chamber of Applied Spectra J200 (see right for schematics)
- The flowchart below shows the measurement procedere
- Samples cleaned by preablation and heated to 150°C to remove water
- Exposed first to 3.2 % CO_2 and then additionally to 890 ppm
- Heated again to remove physically adsorbed species
- The process was monitored via depth profiles, recorded as meander pattern with 68 spots per layer and images of the samples

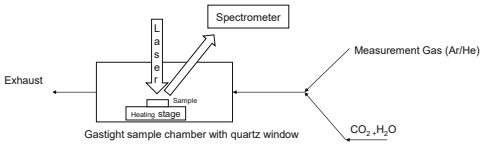

Parameter	Value
Pulse Energy	1.9 mJ
Repetition Frequency	10 Hz
Gate Delay	0.1µs
Spot diameter	100 µm
Scanning speed	100 µm/s
Atmosphere	1 L/min Helium

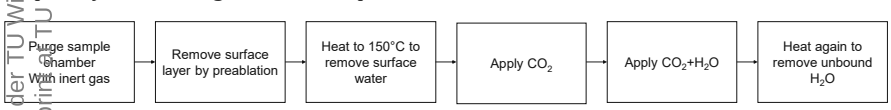

Results and Discussion

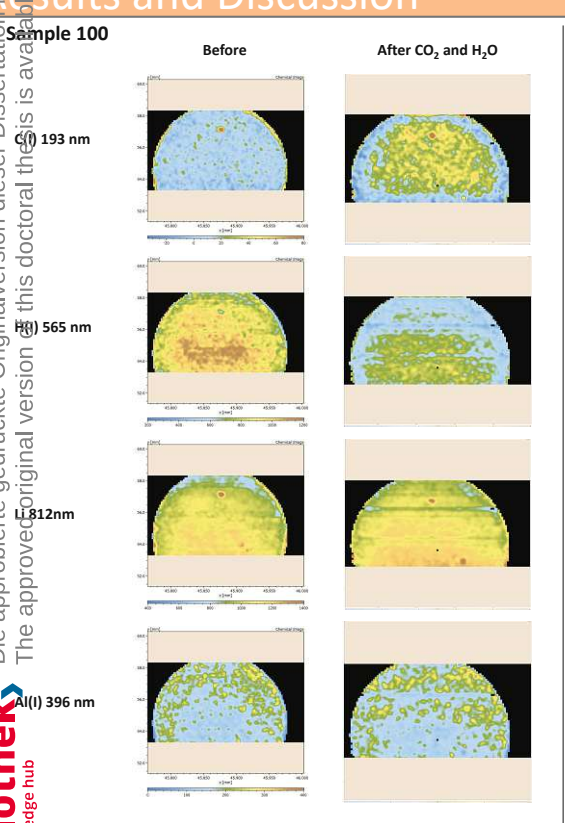

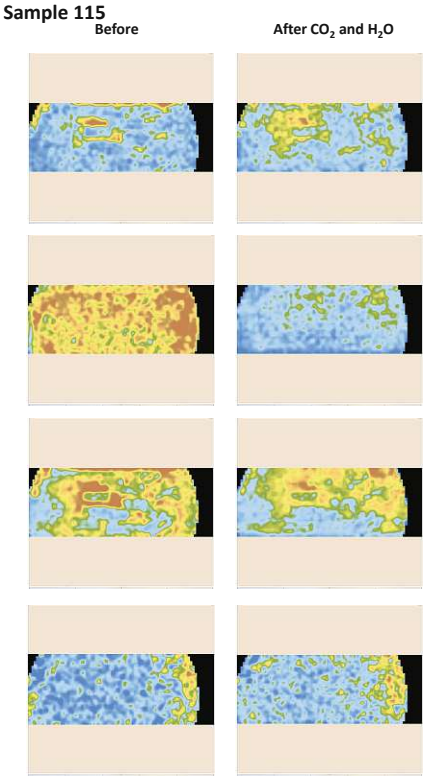

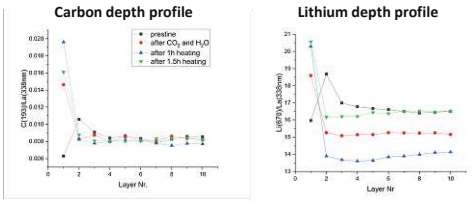

- On the left images of two samples of LLZO before (after cleaning and bake out) and after exposure to CO_2 and H_2O are shown
- As known from literature(1) and preliminary experiments water is necessary for CO_2 uptake
- The Carbon Signal increases, as expected, but Hydrogen decreases as sample exposed to H_2O, probably due to the mechanism in equation[3]
- Al as example for the main elements shows no spatial redistribution, but some inherent inhomogeneity
- The depth profiles show the enrichment of Li on the surface as well as the carbon uptake is limit to the top layer

(1)Xia et al. J Am Ceram Soc. 2017;100:2832–2839
(2) Smetaczek et al. Journal of Materials Chemistry A, 2019. 7(12): p.6818-6831

Acknowledgements

We want to thank the FWF - grant P31165-N37 and W1243 for their financial support and Prof. Rosenberg for providing the gas mixture apparatus.

Conclusion

- As suggested in previous studies(2), the samples show inhomogeneity as in he distribution of the main elements as well as in the formation of corrosion production
- LIBS is a suitable tool as it allows the assessment of all elements of interest
- Future studies will try to connect these findings to the electrochemical properties

Contact

Weiss Maximilian

maximilian.weiss@tuwien.ac.at

LA-ICP-MS depth profiling of micro-alloyed steels

M. Weiss[1], D. Wipp[2], E. Povoden-Karadeniz[2], A. Limbeck[1]

1 Institute of Chemical Technologies and Analytics, TU Wien, A-1060 Vienna, Austria

2 Institute of Materials Science and Technology, TU Wien, A-1060 Vienna, Austria

Introduction

A strong interest in micro-alloyed steel has emerged in the last decades because of increasing cost and scarcity for most alloying elements. Especially, the characterization and control of elemental concentration gradients, segregation to interfaces, and precipitation behavior in micro-alloyed steel is crucial for the improvement of the mechanical properties. However, analysis of light elements, in this case especially boron, in the order of µg/g (ppm) in steel still presents tremendous challenges, as the commonly used SEM-EDX fails for this task. Laser ablation inductively coupled plasma mass spectrometry (LA-ICP-MS), with its high sensitivity, the high linear range covering several orders of magnitude and the ease of measurement, requiring little sample preparation, is the ideal candidate for this task. It is well known, that depth profiling with laser ablation is limited by the crater morphology, especially when the depth of the crater reaches the spot size of the laser beam. Limitations in the diameter of the applied laser beam prevents the analysis of cross-sections with high resolution. Here we present an approach to overcome this drawbacks, by removing material stepwise and sequently measure depth profiles on each step.

Experimental

The used instrumentation consists of a Quadrupole ICP-MS iCAP Qc (ThermoFisher Scientific, Germany) and a NWR213 laser ablation system (ESI, Fremont, USA). Laser ablation is done under helium flow, which is diluted with Ar as make up gas prior to ICP-MS analysis. As samples micro-alloyed steel rods, which underwent a heat treatment were used. The ICP-MS data were quantified by one-point calibration using a certified standard material. Of the cylindrical sample material was removed in 50 µm steps by a workshop lathe (Fig. 1 up). On each resulting terrace a depth profile. For depth profiles a meander pattern was used to limit crater effects and to give a flat crater bottom. The height of each step and the depth of resulting crater was controlled by a stylus profilometer (DektakXT, Bruker,USA)

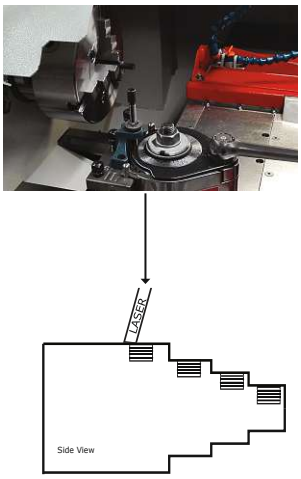

Figure 1: top: image of the lathing process of the sample, right: schematics of the processed sample with the laser ablation process

Table 1: ICP-MS measuring parameters

RF Power	1400 W
Auxiliary/Cool/Make up gas flow (Ar)	1.2 /14/0.85 L/min
Dwell time	0.01s
Measured isotopes	^{10}B, ^{11}B, ^{13}C, ^{27}Al, ^{29}Si, ^{47}Ti, ^{49}Ti, ^{53}Cr, ^{55}Mn, ^{58}Fe, ^{60}Ni, ^{95}Mo, ^{98}Mo

Table 2: Laser ablation sytem parameters

	Depth profile
Average Fluence	18 J/cm^2
Laser Diameter	100 µm
Scan speed	75 µm/s
Carrier gas flow (He)	650 mL/min
Repetition rate	10 Hz

Results and Discussion

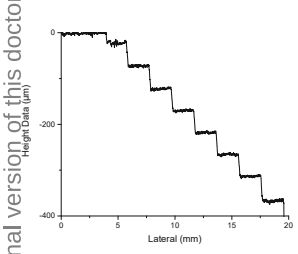

Figure 2: Height profile of the sample after lathing

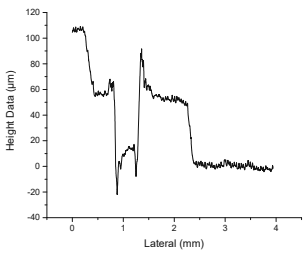

Figure 3: Depth profile of an ablation crater after 70 measured layers

Figure 2 shows the surface profile of the sample after machining. As expected, the steps have a height of a 50 µm and the terraces have a roughness <2 µm, which does not inhibit laser measurements. Figure 3 shows a depth profile crater on a terrace. its depth of 50 µm from 70 laser passes gives a depth resolution <1 µm, which is much higher as can be achieved by classical mapping of cross sections. The limits of the detection of this method is about 1 ppm for boron, which is a difficult element for ICP-MS, as it has a high ionization energy combined with a low atomic mass. A depth profile for the whole sample was created by merging the results for the individual terrraces produced by lathing. (Figure 4) The high-resolution profiles reveal an inhomogeneous distribution of boron. (Figure 4), while other elements, like aluminum, show no variation. The enhanced signal on the surface results from oxide formation. The boron concentration profile shown a minimum in the depth of 10 µm and a maximum in the depth of 20 µm, (Figure 5) which is the result of diffusion during the heat treatment. The concentration then further decreases and reaches a second minima at 120 µm. Afterwards it rises again until it reaches the nominal bulk concentration of 30 ppm. The bulk concentrations measured by LA-ICP-MS agree with the nominal values of the sample.

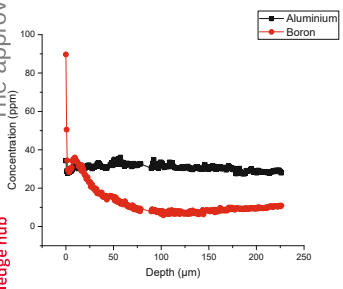

Figure 4: Concentration profile of boron and aluminium, deterimined by depth profiles

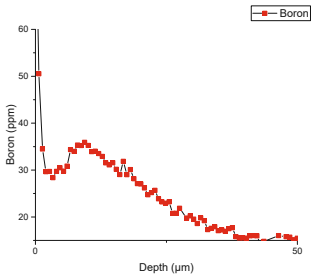

Figure 5: Detail of the boron concentration profile

Acknowledgment

I want to thank the FWF - grant P31165-N37 for their financial support

Conclusions

- Quantitative measurement of trace elements in steel possible
- High limits of detection (<1ppm) even for light elements such as boron
- High depth resolution (~1µm) possible over a wide range, enabled by the combination of depth profiles with lathing
- Measurements reaveal inhomogeneous distribution of boron

Contact

Weiss Maximilian

maximilian.weiss@tuwien.ac.at

Characterization of high-tech materials using online-LASIL.

Maximilian Weiss[1], Maximilian Podsednik [2] , Silvia Larisegger [2] Michael Nelhiebel [2] , Johannes Frank [3] and Andreas Limbeck[1]

1 Institute of Chemical Technologies and Analytics, TU Wien Getreidemarkt 9/164, 1060 Vienna, Austria
2 KAI Kompetenzzentrum Automobil- und Industrieelektronik GmbH, Technologiepark Villach Europastraße 8, 9524, Villach, Austria
3 TU Wien Joint Workshop Technical Chemistry, Getreidemarkt 9, 1060 Vienna, Austria

What is online-LASIL?

In online-LASIL a solid sample is ablated by a Laser into a continuous flow of a carrier solution. The ablated material, which can be in form of (nano-)particles or be dissolved is transported into an ICP-MS/OES instrument. It is possible to inject ready to hand liquid standard solutions into the stream to interfere the composition of the sample without the need of certified reference materials. The flexibility of the method allows the analysis of a wide variety of samples. As online-LASIL is a direct solid sampling technique, mappings with a resolution to in the µm range and depth profiling are possible. In the work (Bonta et. al. 2017) it was found that with online-LASIL a depth resolution compared to conventional nanosecond laser ablation can be achieved.

Challenges

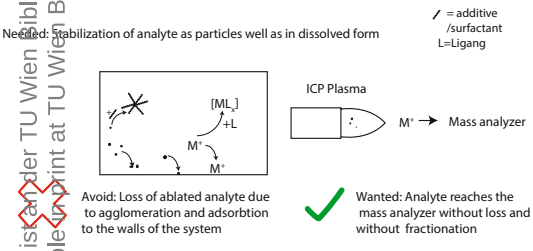

To achieve an optimum performance the LASIL system has to be optimized to yield a high transport efficiency for particles as well as for dissolved species to minimize potential fractionation effects. Therefore, a skillful optimization of the carrier solution is necessary. Further a short washout time is desired to enable fast imaging and a high sensitivity due to high peaks. For stabilization diluted acids or complexing agents are used, however, as the solution comes in direct contact with the sample, it must not dissolve the sample.

Literature:
M. Bonta, O. Hrnjevic, Taibl, J. Fleig, A. Limbeck, Online-LASIL: Laser Ablation of Solid Samples in Liquid with online-coupled ICP-OES detection for direct determination of the stoichiometry of complex metal oxide thin layers, Anal Chim Acta, 1000 (2018) 93-99.
M. Weiss, D. Riedl, C. Moares, P.H. Mayrhofer, A. Limbeck, Laser based analysis of transition metal boride thin films using liquid standards, Microchemical Journal, 152 (2020).

Instrumentation

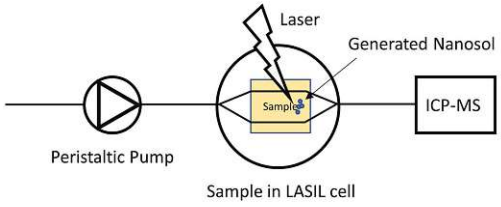

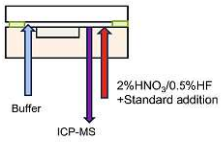

The online-LASIL setup consists of the LASIl cell, in which the sample is placed, a (peristaltic) pump and tubing to connect all parts together. The LASIL cell is constructed from a PEEK baseplate, with a pit for the sample. The fluid flow over the sample is guided by a PDMS spacer of 500 µm thickness, which also seals the sample cell. A UV-transparent fused silica window forms the top of the setup. The LASIL-cell is placed on the XYZ-stage of a commercial laser ablation instrument (Applied Spectra J200 Tandem or ESI NWR213).

The carrier solution needs to stabilize ions, which is usually done with diluted acids. However, some samples are not acid resistance and would decompose under acidic conditions. To allow a stabilization of the ablated material while preserving the sample the LASIL cell has two inlets for liquids. One lies in the fluid path behind the sample, and one after the sample. For sensitive samples and buffer solution is flown over the samples and a more concentrated acid is added afterwards. This also allows to perform standard addition analysis.

To improve the washout, gas bubbles can be introduced as a segmented flow. As the laser ablation process depends on the surrounding medium it is necessary to only ablate into the liquid and not in the gas segments, especially for depth resolved analysis. For this a synchronization of the laser with gas bubble generation is needed. This is done via the setup shown on the right: the gas bubbles are introduced via a 6-channel valve, which is controlled by an Arduino, which also triggers the laser.

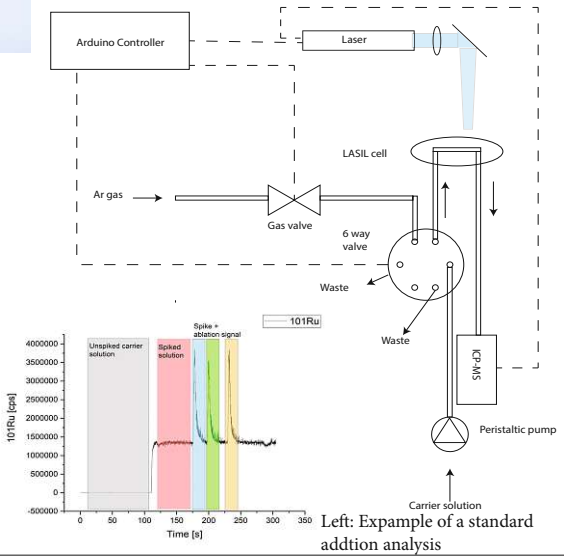

Left: Expample of a standard addtion analysis

Application Examples

Analysis of trace elements

Upper image: online-LASIL was used to quantify trace elements. The NIST612 CRM served as unknown sample. As carrier solution 2% HCl was used, via the makeup solution liquid standards were added, the data was evaluated with standard addition. Signals of the trace elements were normalized to calcium as matrix element with known concentration. Error bars show two standard deviations.

The introduced bubbles ensure a fast washout of the ablated material and lead to a high signal to noise ratio and avoids stickiness of some elements like Th. A good agreement with the certified values was achieved for the investigated elements, showing the capabilities of online-LASIL for quantitative trace element analysis.

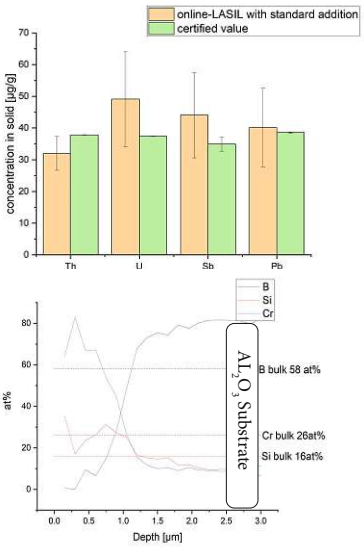

Quantitative depth profile measurement

Lower Image: In this study the high temperature oxidation of transition metal boride thin films alloyed with silicone is investigated. The samples with a thickness of 2.5 µm were deposited on Al_2O_3 substrates using magnetron sputtering. The bulk composition of the thin film was accessed by ICP-OES after digestion. After oxidation at 1200°C depth profiles of the sample were recorded using online-LASIL. To achieve a reasonable sensitivity for silicone more energy was used. 200 nm per ablation layer were found to be a fair compromise between sensitivity and depth resolution. The depth of the craters was determined with a Dektak XT stylus profilometer. It was found that the oxide film is composed of silicone and chromium oxide, after about 600 nm the sample composition converges to the bulk. The thickness of the oxide layer is in good agreement with TEM measurements. The composition of the samples in mean obtained by online-LASIL are in good agreement with the bulk values.

Conclusion

Online-LASIL is a versatile technique allowing bulk, trace, and depth profile analysis. The performance was improved through modifications in the setup via acid addition after the sample and the use of a segmented flow synchronized to the laser.

Contact

Maximilian Weiss
maximilian.weiss@tuwien.ac.at
+43 1 58801 15183

We want tho thank the FWF grant P31165-N37 for their financial support

9 Conclusion

Laser-Assisted Plasma Spectrochemistry methods have proofed to be an essential part of the toolkit of analytical chemistry. During this work LIBS, LA-ICP-MS, ICP-OES and online-LASIL have been used to develop methodologies, which helped to answer questions from material science which were not solvable using other techniques, extending the possibilities of direct solid-state analysis. The developments involve sample preparation, new approaches for quantification, design of measurement systems and finally data evaluation. The main shortcomings in hitherto existing methods that could successfully resolved in this thesis were limited sensitivity for some elements, the limited depth resolution and the lack of suitable standards to quantify measurements.

In Figure 12 the possible spatial resolution of methods used in this work, alongside with other direct solid sampling techniques, are plotted against the sensitivity. The laser-based methods show to be the most versatile as they are a good compromise in both directions. It has to be noted that the spatial resolution is on the one hand limited by the sample-beam interaction, on the other by the sensitivity of the method. This has been demonstrated with the spatially resolved analysis of fluorine: the formation of the CuF molecule enhances the sensitivity of fluorine so it is possible to detect it clearly in a single shot – a prerequisite for imaging. With all lasers-based methods LIBS, LA-ICP-MS and online-LASIL it was shown to achieve quantitative results even when a matrix matched standard is not available, which can be significant benefit of these methods.

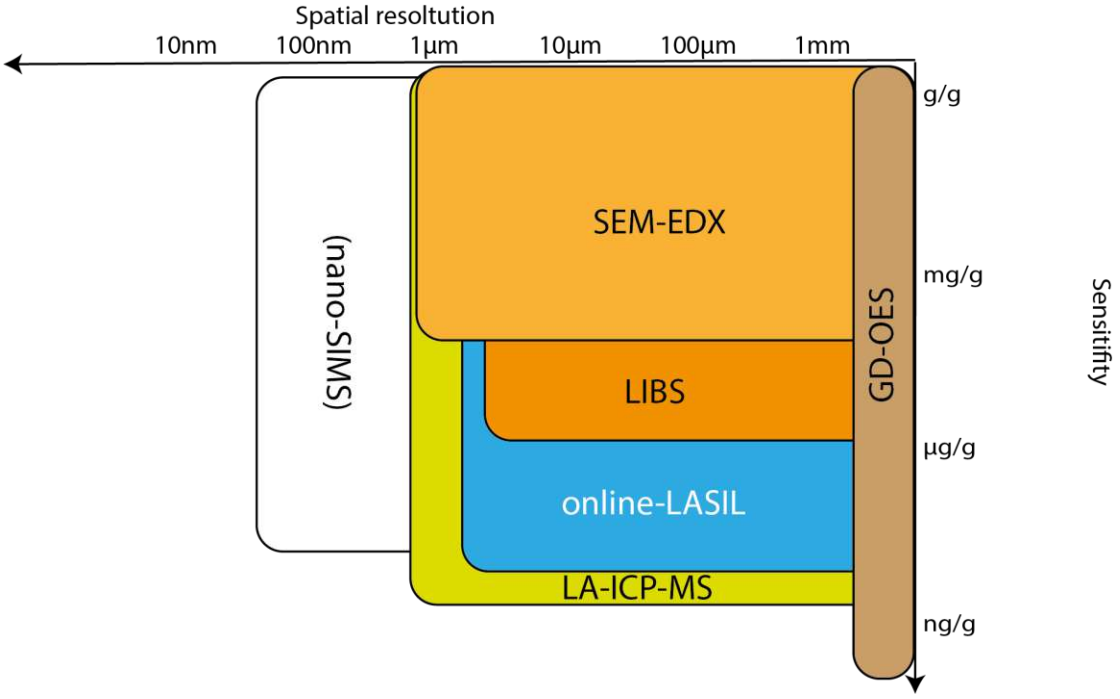

Figure 12: Comparison the sensitivity with the spatial resolution of the methods used in this work with other direct solid sampling methods, axes are logarithmic.[26] after [74]

A special feature of online-LASIL is its boost in sample depth resolution, compared to classical nanosecond laser ablation. In Figure 13 the depth resolution, as well the depth that is reachable at maximum for some common methods are shown. LASIL pushes the capabilities of nanosecond lasers in regions, which were before only reachable with excimer or femtosecond laser equipment an order of magnitude. A further tempting feature is that it put no constrains on the conductivity of the samples compared to other methods. It has however to be noted that the current online-LASIL setup is still restricted on the geometry of the sample, a feature that is in the pipeline for future development of the system.

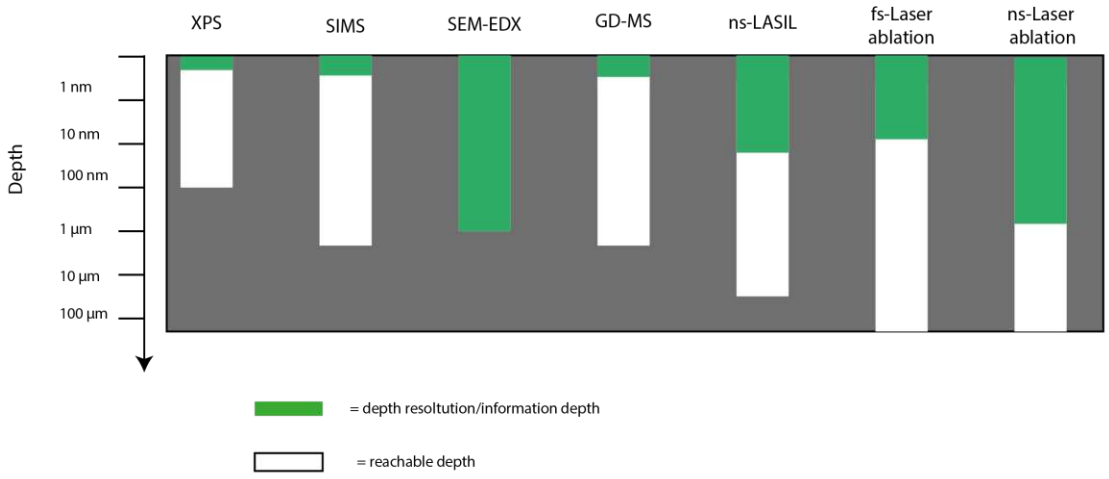

FIGURE 13: Depth resolution and reachable depth for several methods [26, 27]. After [74]

List of Abbreviations

AAS	Atomic absorption spectrometry
AES	Auger electron spectrometry
BAM	Bundesanstalt für Materialprüfung
BN	Boron nitride
CFD	Computational Fluid Dynamics
CRM	Certified Reference Material
CSAAS	Continuous source AAS
EMPA	Electron micro probe analysis
GD	Glow discharge
ICP	Inductively coupled plasma
ICP-MS	Inductively coupled plasma Mass spectrometry Optical emission spectroscopy
ICP-OES	Inductively coupled plasma
IR	Infrared
LA-ICP-MS	Laser abltation ICP-MS
LAMIS	Laser ablation molecular isotopic spectrometry
Laser	Light amplification by stimulated emission of radiation
LASIL	Laser Abaltation of solids in liquids
LIBS	Laser-induced breakdown spectroscopy
LOD	Limit of Detection
MS	Mass spectrometry
Nd:YAG	neodymium-doped yttrium aluminum garnet; Nd:Y3Al5O12
NELIBS	Nanoparticle enhanced LIBS
NIST	National Institute of Standards and Technology
OES	Optical emission spectroscopy
PDMS	Polydimethylsiloxane
PEEK	Polyether ether ketone
PFA	Perfluoroalkoxy alkane
PTFE	Polytetrafluoroethylene
SEM-EDX	Scanning Electron Microscopy (SEM) with Energy Dispersive X-Ray Analysis (EDX)
SiC	Siliconcarbide
SIMS	Secondary ion mass spectrometry
SiN	Siliconnitride
TOF	Time of flight
UV	Ultraviolet
XPS	X-Ray Photoelectron spectroscopy
XRF	X-Ray Fluorescence

Bibliography

[1] H. A. Laitinen. "Editorial. The Seven Ages of an Analytical Method". In: *Analytical Chemistry* 45.14 (2003), pp. 2305–2305. ISSN: 0003-2700 1520-6882. DOI: 10.1021/ac60336a600.

[2] J. D. Winefordner, I. B. Gornushkin, T. Correll, E. Gibb, B. W. Smith, and N. Omenetto. "Comparing several atomic spectrometric methods to the super stars: special emphasis on laser induced breakdown spectrometry, LIBS, a future super star". In: *Journal of Analytical Atomic Spectrometry* 19.9 (2004). ISSN: 0267-9477 1364-5544. DOI: 10.1039/b400355c.

[3] V. N. Ochkin. *Spectroscopy of low temperature plasma*. John Wiley Sons, 2009. ISBN: 3527627510.

[4] T. Belmonte, C. Noël, T. Gries, J. Martin, and G. Henrion. "Theoretical background of optical emission spectroscopy for analysis of atmospheric pressure plasmas". In: *Plasma Sources Science and Technology* 24.6 (2015). ISSN: 0963-0252 1361-6595. DOI: 10.1088/0963-0252/24/6/064003.

[5] D. W. Hahn and N. Omenett. "Laser-Induced-Breakdown Spectroscopy (LIBS), Part I: Review of Basic Diagnostics and Plasma– Particle Interactions: Still-Challenging Issues Within the Analytical Plasma Community". In: *APPLIED SPECTROSCOPY* 64.12 (2010), pp. 335–366.

[6] D. Günther and B. Hattendorf. "Solid sample analysis using laser ablation inductively coupled plasma mass spectrometry". In: *TrAC Trends in Analytical Chemistry* 24.3 (2005), pp. 255–265. ISSN: 01659936. DOI: 10.1016/j.trac.2004.11.017.

[7] M. DellAglio, R. Gaudiuso, O. De Pascale, and A. De Giacomo. "Mechanisms and processes of pulsed laser ablation in liquids during nanoparticle production". In: *Applied Surface Science* 348 (2015), pp. 4–9. ISSN: 01694332. DOI: 10.1016/j.apsusc.2015.01.082.

[8] R. E. Russo, X. Mao, and S. S. Mao. "The physics of laser ablation in microchemical analysis". In: *Anal Chem* 74.3 (2002), 70A–77A. ISSN: 0003-2700 (Print) 0003-2700 (Linking). DOI: 10.1021/ac0219445. URL: https://www.ncbi.nlm.nih.gov/pubmed/11838700.

[9] R. E. Russo, X. Mao, and O. V. Borisov. "Laser ablation sampling". In: *TrAC Trends in Analytical Chemistry* 17.8-9 (1998), pp. 461–469. ISSN: 01659936. DOI: 10.1016/s0165-9936(98)00047-8.

[10] Z. Yan and D. B. Chrisey. "Pulsed laser ablation in liquid for micro-/nanostructure generation". In: *Journal of Photochemistry and Photobiology C: Photochemistry Reviews* 13.3 (2012), pp. 204–223. ISSN: 13895567. DOI: 10.1016/j.jphotochemrev.2012.04.004.

[11] J. Pisonero and D. Gunther. "Femtosecond laser ablation inductively coupled plasma mass spectrometry: fundamentals and capabilities for depth profiling analysis". In: *Mass Spectrom Rev* 27.6 (2008), pp. 609–23. ISSN: 1098-2787 (Electronic) 0277-7037 (Linking). DOI: 10.1002/mas.20180. URL: https://www.ncbi.nlm.nih.gov/pubmed/18636536.

[12] F. Poitrasson and F.-X. d'Abzac. "Femtosecond laser ablation inductively coupled plasma source mass spectrometry for elemental and isotopic analysis: are ultrafast lasers worthwhile?" In: *Journal of Analytical Atomic Spectrometry* 32.6 (2017), pp. 1075–1091. ISSN: 0267-9477 1364-5544. DOI: 10.1039/c7ja00084g.

[13] D. Marla, U. V. Bhandarkar, and S. S. Joshi. "Critical assessment of the issues in the modeling of ablation and plasma expansion processes in the pulsed laser deposition of metals". In: *Journal of Applied Physics* 109.2 (2011). ISSN: 0021-8979 1089-7550. DOI: 10.1063/1.3537838.

[14] S. Musazzi and U. Perini. *Laser-Induced Breakdown Spectroscopy: Theory and Applications*. Springer Berlin Heidelberg, 2014. ISBN: 9783642450853. URL: https://books.google.at/books?id=CNUlBAAAQBAJ.

[15] G. Yang. "Laser ablation in liquids: Applications in the synthesis of nanocrystals". In: *Progress in Materials Science* 52.4 (2007), pp. 648–698. ISSN: 00796425. DOI: 10.1016/j.pmatsci.2006.10.016.

[16] R. E. Russo, X. Mao, J. J. Gonzalez, V. Zorba, and J. Yoo. "Laser ablation in analytical chemistry". In: *Anal Chem* 85.13 (2013), pp. 6162–77. ISSN: 1520-6882 (Electronic) 0003-2700 (Linking). DOI: 10.1021/ac4005327. URL: https://www.ncbi.nlm.nih.gov/pubmed/23614661.

[17] S. Nelms. *Inductively Coupled Plasma Mass Spectrometry Handbook*. CRC Press, 2005. URL: https://books.google.at/books?id=Ov5fvAEACAAJ.

[18] C. Agatemor and D. Beauchemin. "Matrix effects in inductively coupled plasma mass spectrometry: a review". In: *Anal Chim Acta* 706.1 (2011), pp. 66–83. ISSN: 1873-4324 (Electronic) 0003-2670 (Linking). DOI: 10.1016/j.aca.2011.08.027. URL: https://www.ncbi.nlm.nih.gov/pubmed/21995912.

[19] S. D. Tanner, V. I. Baranov, and D. R. Bandura. "Reaction cells and collision cells for ICP-MS: a tutorial review". In: *Spectrochimica Acta Part B: Atomic Spectroscopy* 57.9 (2002), pp. 1361–1452. ISSN: 05848547. DOI: 10.1016/s0584-8547(02)00069-1.

[20] K. L. Linge and K. E. Jarvis. "Quadrupole ICP-MS: Introduction to Instrumentation, Measurement Techniques and Analytical Capabilities". In: *Geostandards and Geoanalytical Research* 33.4 (2009), pp. 445–467. ISSN: 16394488 1751908X. DOI: 10.1111/j.1751-908X.2009.00039.x.

[21] L. Ebdon, M. E. Foulkes, and S. Hill. "Direct atomic spectrometric analysis by slurry atomisation. Part 9. Fundamental studies of refractory samples". In: *Journal of Analytical Atomic Spectrometry* 5.1 (1990). ISSN: 0267-9477 1364-5544. DOI: 10.1039/ja9900500067.

[22] C. C. Garcia, H. Lindner, and K. Niemax. "Transport efficiency in femtosecond laser ablation inductively coupled plasma mass spectrometry applying ablation cells with short and long washout times". In: *Spectrochimica Acta Part B: Atomic Spectroscopy* 62.1 (2007), pp. 13–19. ISSN: 05848547. DOI: 10.1016/j.sab.2006.11.005.

[23] S. J. M. Van Malderen, A. J. Managh, B. L. Sharp, and F. Vanhaecke. "Recent developments in the design of rapid response cells for laser ablation-inductively coupled plasma-mass spectrometry and their impact on bioimaging applications". In: *Journal of Analytical Atomic Spectrometry* 31.2 (2016), pp. 423–439. ISSN: 0267-9477 1364-5544. DOI: 10.1039/c5ja00430f.

[24] C. D. Quarles, J. J. Gonzalez, L. J. East, J. H. Yoo, M. Morey, and R. E. Russo. "Fluorine analysis using Laser Induced Breakdown Spectroscopy (LIBS)". In: *Journal of Analytical Atomic Spectrometry* 29.7 (2014). ISSN: 0267-9477 1364-5544. DOI: 10.1039/c4ja00061g.

[25] A. Limbeck, M. Bonta, and W. Nischkauer. "Improvements in the direct analysis of advanced materials using ICP-based measurement techniques". In: *Journal of Analytical Atomic Spectrometry* 32.2 (2017), pp. 212–232. ISSN: 0267-9477 1364-5544. DOI: 10.1039/c6ja00335d.

[26] G. Friedbacher and H. Bubert. *Surface and Thin Film Analysis*. Wiley-VCH. Weinheim, Germany, 2011. ISBN: 978-3-527-32047-9.

[27] J. Pisonero, B. Fernández, and D. Günther. "Critical revision of GD-MS, LA-ICP-MS and SIMS as inorganic mass spectrometric techniques for direct solid analysis". In: *Journal of Analytical Atomic Spectrometry* 24.9 (2009). ISSN: 0267-9477 1364-5544. DOI: 10.1039/b904698d.

[28] Y. Li, D. Tian, Y. Ding, G. Yang, K. Liu, C. Wang, and X. Han. "A review of laser-induced breakdown spectroscopy signal enhancement". In: *Applied Spectroscopy Reviews* 53.1 (2017), pp. 1–35. ISSN: 0570-4928 1520-569X. DOI: 10.1080/05704928.2017.1352509.

[29] A. De Giacomo, M. Dell'Aglio, R. Gaudiuso, C. Koral, and G. Valenza. "Perspective on the use of nanoparticles to improve LIBS analytical performance: nanoparticle enhanced laser induced breakdown spectroscopy (NELIBS)". In: *Journal of Analytical Atomic Spectrometry* 31.8 (2016), pp. 1566–1573. ISSN: 0267-9477 1364-5544. DOI: 10.1039/c6ja00189k.

[30] B. Mangusson and U. Örnemark. *Eurachem Guide: The Fitness for Purpose of Analytical Methods – A Laboratory Guide to Method Validation and Related Topics*. 2nd ed. 2014. ISBN: 978-91-87461-59-0.

[31] S. Hill. *Inductively Coupled Plasma Spectrometry and its Applications*. Wiley, 2007. ISBN: 9781405135948. URL: https://books.google.at/books?id=ojPVC2jhQHAC.

[32] S. C. Jantzi, V. Motto-Ros, F. Trichard, Y. Markushin, N. Melikechi, and A. De Giacomo. "Sample treatment and preparation for laser-induced breakdown spectroscopy". In: *Spectrochimica Acta Part B: Atomic Spectroscopy* 115 (2016), pp. 52–63. ISSN: 05848547. DOI: 10.1016/j.sab.2015.11.002.

[33] A. Limbeck, P. Galler, M. Bonta, G. Bauer, W. Nischkauer, and F. Vanhaecke. "Recent advances in quantitative LA-ICP-MS analysis: challenges and solutions in the life sciences and environmental chemistry". In: *Anal Bioanal Chem* 407.22 (2015), pp. 6593–617. ISSN: 1618-2650 (Electronic) 1618-2642 (Linking). DOI: 10.1007/s00216-015-8858-0. URL: https://www.ncbi.nlm.nih.gov/pubmed/26168964.

[34] M. Bonta, H. Lohninger, M. Marchetti-Deschmann, and A. Limbeck. "Application of gold thin-films for internal standardization in LA-ICP-MS imaging experiments". In: *Analyst* 139.6 (2014), pp. 1521–31. ISSN: 1364-5528 (Electronic) 0003-2654 (Linking). DOI: 10.1039/c3an01511d. URL: https://www.ncbi.nlm.nih.gov/pubmed/24473070.

[35] Y. Liu, Z. Hu, S. Gao, D. Günther, J. Xu, C. Gao, and H. Chen. "In situ analysis of major and trace elements of anhydrous minerals by LA-ICP-MS without applying an internal standard". In: *Chemical Geology* 257.1-2 (2008), pp. 34–43. ISSN: 00092541. DOI: 10.1016/j.chemgeo.2008.08.004.

[36] J. El Haddad, L. Canioni, and B. Bousquet. "Good practices in LIBS analysis: Review and advices". In: *Spectrochimica Acta Part B: Atomic Spectroscopy* 101 (2014), pp. 171–182. ISSN: 05848547. DOI: 10.1016/j.sab.2014.08.039.

[37] L. Yang, R. E. Sturgeon, and Z. Mester. "Quantitation of trace metals in liquid samples by dried-droplet laser ablation inductively coupled plasma mass spectrometry". In: *Anal Chem* 77.9 (2005), pp. 2971–7. ISSN: 0003-2700 (Print) 0003-2700 (Linking). DOI: 10.1021/ac048275a. URL: https://www.ncbi.nlm.nih.gov/pubmed/15859618.

[38] R. D. Deegan, O. Bakajin, T. F. Dupont, G. Huber, S. R. Nagel, and T. A. Witten. "Capillary flow as the cause of ring stains from dried liquid drops". In: *Nature* 389.6653 (1997), pp. 827–829. DOI: 10.1038/39827.

[39] M. Weiss, H. Riedl, V. Moares, P. H. Mayrhofer, and A. Limbeck. "Laser based analysis of transition metal boride thin films using liquid standards". In: *Microchemical Journal* 152 (2020). ISSN: 0026265X. DOI: 10.1016/j.microc.2019.104449.

[40] F. Horak, A. Nagl, K. Fottinger, and A. Limbeck. "Application of micro-dried droplets for quantitative analysis of particulate inorganic samples with LA-ICP-MS demonstrated on surface-modified nanoparticle TiO2 catalyst materials". In: *Mikrochim Acta* 187.12 (2020), p. 641. DOI: 10.1007/s00604-020-04609-9.

[41] M. Bonta, T. Anderl, A. Cognigni, M. Hejazifar, K. Bica, and A. Limbeck. "Determination of residual chloride content in ionic liquids using LA-ICP-MS". In: *RSC Advances* 6.93 (2016), pp. 90273–90279. ISSN: 2046-2069. DOI: 10.1039/c6ra21203d.

[42] M. Thompson, S. Chenery, and L. Brett. "Calibration studies in laser ablation microprobe-inductively coupled plasma atomic emission spectrometry". In: *Journal*

of Analytical Atomic Spectrometry 4.1 (1989), pp. 11–16. ISSN: 0267-9477. DOI: 10.1039/JA9890400011. URL: http://dx.doi.org/10.1039/JA9890400011.

[43] C. O Connor, B. L. Sharp, and P. Evans. "On-line additions of aqueous standards for calibration of laser ablation inductively coupled plasma mass spectrometry: theory and comparison of wet and dry plasma conditions". In: *Journal of Analytical Atomic Spectrometry* 21.6 (2006). ISSN: 0267-9477 1364-5544. DOI: 10.1039/b600916f.

[44] H. Zeng, X.-W. Du, S. C. Singh, S. A. Kulinich, S. Yang, J. He, and W. Cai. "Nanomaterials via Laser Ablation/Irradiation in Liquid: A Review". In: *Advanced Functional Materials* 22.7 (2012), pp. 1333–1353. ISSN: 1616301X. DOI: 10.1002/adfm.201102295.

[45] E. V. Muravitskaya, V. A. Rosantsev, M. V. Belkov, E. A. Ershov-Pavlov, and E. V. Klyachkovskaya. "Laser ablation in liquids as a new technique of sampling in elemental analysis of solid materials". In: *Spectrochimica Acta Part B: Atomic Spectroscopy* 64.2 (2009), pp. 119–125. ISSN: 05848547. DOI: 10.1016/j.sab.2008.11.003.

[46] D. N. Douglas, J. L. Crisp, H. J. Reid, and B. L. Sharp. "Laser Ablation of a Sample In Liquid—LASIL". In: *Journal of Analytical Atomic Spectrometry* 26.6 (2011). ISSN: 0267-9477 1364-5544. DOI: 10.1039/c0ja00144a.

[47] S. Okabayashi, T. D. Yokoyama, Y. Kon, S. Yamamoto, T. Yokoyama, and T. Hirata. "Evaluation of Laser Ablation in Liquid (LAL) technique as a new sampling technique for elemental and isotopic analysis using ICP-mass spectrometry". In: *Journal of Analytical Atomic Spectrometry* 26.7 (2011). ISSN: 0267-9477 1364-5544. DOI: 10.1039/c0ja00200c.

[48] M. Fujiwara, K. Hirosawa, N. Nonose, S. Nishida, and N. Furuta. "Evaluation of measurement uncertainty in the elemental analysis of sintered silicon carbide using laser ablation in liquid—inductively coupled plasma mass spectrometry with external calibration and isotope dilution". In: *Accreditation and Quality Assurance* 24.5 (2019), pp. 329–339. ISSN: 0949-1775 1432-0517. DOI: 10.1007/s00769-019-01389-5.

[49] R. Machida, R. Nishioka, M. Fujiwara, and N. Furuta. "Determination of Trace Elements in Sintered and Single-Crystal Silicon Carbide by Laser Ablation in Liquid Inductively Coupled Plasma Mass Spectrometry". In: *Anal Sci* 33.4 (2017), pp. 537–544. ISSN: 1348-2246 (Electronic) 0910-6340 (Linking). DOI: 10.2116/analsci.33.537. URL: https://www.ncbi.nlm.nih.gov/pubmed/28392534.

[50] K. Hirosawa and N. Furuta. "Atomization and Changes in Chemical Composition by Laser Ablation in Liquid prior to Determination of Trace Elements in Gallium Nitride". In: *Anal Sci* 35.5 (2019), pp. 557–563. ISSN: 1348-2246 (Electronic) 0910-6340 (Linking). DOI: 10.2116/analsci.18P542. URL: https://www.ncbi.nlm.nih.gov/pubmed/30662017.

[51] R. Machida, T. Nakazawa, Y. Sakuraba, M. Fujiwara, and N. Furuta. "Particle size-related elemental fractionation in laser ablation in liquid inductively coupled plasma mass spectrometry". In: *Journal of Analytical Atomic Spectrometry* 30.12 (2015), pp. 2412–2419. ISSN: 0267-9477 1364-5544. DOI: 10.1039/c5ja00349k.

[52] M. V. Bel'kov, V. S. Burakov, V. V. Kiris, and S. N. Raikov. "New fast spectral analysis method for solid materials". In: *Journal of Applied Spectroscopy* 74.3 (2007), pp. 313–314. ISSN: 0021-9037 1573-8647. DOI: 10.1007/s10812-007-0050-7.

[53] A. Aziz, J. A. C. Broekaert, K. Laqua, and F. Leis. "A Study of Direct Analysis of Solid Samples Using Spark Ablation Combined with Excitation in an Inductively Coupled Plasma". In: *Spectrochimica Acta Part B-Atomic Spectroscopy* 39.9-11 (1984), pp. 1091–1103. ISSN: 0584-8547. DOI: Doi10.1016/0584-8547(84)80195-0. URL: %3CGo%20to%20ISI%3E://WOS:A1984AAA8100005.

[54] E. H. Hansen and M. Miró. "How flow-injection analysis (FIA) over the past 25 years has changed our way of performing chemical analyses". In: *TrAC Trends in Analytical Chemistry* 26.1 (2007), pp. 18–26. ISSN: 01659936. DOI: 10.1016/j.trac.2006.07.010.

[55] M. Bonta, J. Frank, S. Taibl, J. Fleig, and A. Limbeck. "Online-LASIL: Laser Ablation of Solid Samples in Liquid with online-coupled ICP-OES detection for direct determination of the stoichiometry of complex metal oxide thin layers". In: *Anal Chim Acta* 1000 (2018), pp. 93–99. ISSN: 1873-4324 (Electronic) 0003-2670 (Linking). DOI: 10.1016/j.aca.2017.10.025. URL: https://www.ncbi.nlm.nih.gov/pubmed/29289328.

[56] C. Herzig, J. Frank, A. K. Opitz, J. Fleig, and A. Limbeck. "Quantitative analysis of gadolinium doped cerium oxide thin films via online-LASIL-ICP-OES". In: *Journal of Analytical Atomic Spectrometry* (2019). ISSN: 0267-9477 1364-5544. DOI: 10.1039/c9ja00250b.

[57] C. Herzig, J. Frank, A. K. Opitz, J. Fleig, and A. Limbeck. "Quantitative imaging of structured complex metal oxide thin films using online-LASIL-ICP-MS". In: *Talanta* 217 (2020). ISSN: 00399140. DOI: 10.1016/j.talanta.2020.121012.

[58] M. Weiss, C. Riedl, J. Frank, J. Fleig, and A. Limbeck. "Quantitative analysis of the platinum surface decoration on lanthanum strontium iron oxide thin films via online-LASIL-ICP-MS". In: *Microchemical Journal* 166 (2021). ISSN: 0026265X. DOI: 10.1016/j.microc.2021.106236.

[59] V. Amendola and M. Meneghetti. "What controls the composition and the structure of nanomaterials generated by laser ablation in liquid solution?" In: *Phys Chem Chem Phys* 15.9 (2013), pp. 3027–46. ISSN: 1463-9084 (Electronic) 1463-9076 (Linking). DOI: 10.1039/c2cp42895d. URL: https://www.ncbi.nlm.nih.gov/pubmed/23165724.

[60] C. Alvarez-Llamas, J. Pisonero, and N. Bordel. "A novel approach for quantitative LIBS fluorine analysis using CaF emission in calcium-free samples". In: *Journal of Analytical Atomic Spectrometry* 32.1 (2017), pp. 162–166. ISSN: 0267-9477 1364-5544. DOI: 10.1039/c6ja00386a.

[61] S. Mores, G. C. Monteiro, S. Santos Fda, E. Carasek, and B. Welz. "Determination of fluorine in tea using high-resolution molecular absorption spectrometry with electrothermal vaporization of the calcium mono-fluoride CaF". In: *Talanta* 85.5 (2011), pp. 2681–5. ISSN: 1873-3573 (Electronic) 0039-9140 (Linking). DOI: 10.1016/j.talanta.2011.08.044. URL: https://www.ncbi.nlm.nih.gov/pubmed/21962702.

[62] A. A. Bol'shakov, X. Mao, J. J. González, and R. E. Russo. "Laser ablation molecular isotopic spectrometry (LAMIS): current state of the art". In: *Journal of Analytical Atomic Spectrometry* 31.1 (2016), pp. 119–134. ISSN: 0267-9477 1364-5544. DOI: 10.1039/c5ja00310e.

[63] C. Haisch, R. Niessner, O. I. Matveev, U. Panne, and N. Omenetto. "Element-specific determination of chlorine in gases by Laser-Induced-Breakdown-Spectroscopy (LIBS)". In: *Analytical and Bioanalytical Chemistry* 356.1 (1996), pp. 21–6. ISSN: 1618-2650 (Electronic) 1618-2642 (Linking). DOI: 10.1007/s0021663560021. URL: https://www.ncbi.nlm.nih.gov/pubmed/15045253.

[64] A. De Giacomo and J. Hermann. "Laser-induced plasma emission: from atomic to molecular spectra". In: *Journal of Physics D: Applied Physics* 50.18 (2017), p. 183002. ISSN: 0022-3727 1361-6463. DOI: 10.1088/1361-6463/aa6585.

[65] C. Alvarez-Llamas, J. Pisonero, and N. Bordel. "Quantification of fluorine traces in solid samples using CaF molecular emission bands in atmospheric air Laser-Induced

Breakdown Spectroscopy". In: *Spectrochimica Acta Part B: Atomic Spectroscopy* 123 (2016), pp. 157–162. ISSN: 05848547. DOI: 10.1016/j.sab.2016.08.006.

[66] Z. Tang, R. Zhou, Z. Hao, W. Zhang, Q. Li, Q. Zeng, X. Li, X. Zeng, and Y. Lu. "Determination of fluorine in copper ore using laser-induced breakdown spectroscopy assisted by the SrF molecular emission band". In: *Journal of Analytical Atomic Spectrometry* 35.4 (2020), pp. 754–761. ISSN: 0267-9477 1364-5544. DOI: 10.1039/c9ja00407f. URL: https://pubs.rsc.org/en/content/articlelanding/2020/JA/C9JA00407F.

[67] C. Riedl, A. Schmid, A. Nenning, H. Summerer, S. Smetaczek, S. Schwarz, J. Bernardi, A. Optiz, A. Limbeck, and J. Fleig. "Outstanding Oxygen Reduction Kinetics of La0.6Sr0.4FeO3 Surfaces Decorated with Platinum Nanoparticles". In: *Journal of The Electrochemical Society* 167.10 (2020). ISSN: 1945-7111. DOI: 10.1149/1945-7111/ab9c7f.

[68] T. Glechner, R. Hahn, L. Zauner, S. Rißlegger, A. Kirnbauer, P. Polcik, and H. Riedl. "Structure and mechanical properties of reactive and non-reactive sputter deposited WC based coatings". In: *Journal of Alloys and Compounds* 885 (2021). ISSN: 09258388. DOI: 10.1016/j.jallcom.2021.161129.

[69] C. Fuger, B. Schwartz, T. Wojcik, V. Moraes, M. Weiss, A. Limbeck, C. A. Macauley, O. Hunold, P. Polcik, D. Primetzhofer, P. Felfer, P. H. Mayrhofer, and H. Riedl. "Influence of Ta on the oxidation resistance of WB2z coatings". In: *Journal of Alloys and Compounds* (2020). ISSN: 09258388. DOI: 10.1016/j.jallcom.2020.158121.

[70] C. Fuger, R. Hahn, L. Zauner, T. Wojcik, M. Weiss, A. Limbeck, O. Hunold, P. Polcik, and H. Riedl. "Anisotropic super-hardness of hexagonal WB2±z thin films". In: *Materials Research Letters* 10.2 (2022), pp. 70–77. ISSN: 2166-3831. DOI: 10.1080/21663831.2021.2021308.

[71] T. Glechner, H. G. Oemer, T. Wojcik, M. Weiss, A. Limbeck, J. Ramm, P. Polcik, and H. Riedl. "Influence of Si on the oxidation behavior of TM-Si-B2±z coatings (TM=Ti, Cr, Hf, Ta, W)". In: *Surface and Coatings Technology* (2022). ISSN: 02578972. DOI: 10.1016/j.surfcoat.2022.128178.

[72] C. Riedl, M. Siebenhofer, A. Nenning, G. Friedbacher, M. Weiss, C. Rameshan, J. Bernardi, A. Limbeck, M. Kubicek, A. K. Opitz, and J. Fleig. "Performance modulation through selective, homogenous surface doping of lanthanum strontium ferrite electrodes revealed by in situ PLD impedance measurements". In: *Journal*

of Materials Chemistry A (2022). ISSN: 2050-7488 2050-7496. DOI: 10.1039/d1ta08634k.

[73] A. Pekarsky, S. Mihalyi, M. Weiss, A. Limbeck, and O. Spadiut. "Depletion of Boric Acid and Cobalt from Cultivation Media: Impact on Recombinant Protein Production with Komagataella phaffii". In: *Bioengineering (Basel)* 7.4 (2020). ISSN: 2306-5354 (Print) 2306-5354 (Linking). DOI: 10.3390/bioengineering7040161. URL: https://www.ncbi.nlm.nih.gov/pubmed/33322107.

[74] Web Page. URL: http://mcf.tamu.edu/wp-content/uploads/2017/09/EAG_ResolutionVsDetectionLimit.pdf.

Maximilian Weiss

Curriculum Vitae

✉ *maximilian.weiss@tuwien.ac.at*

Education

2018–2022 **Doctoral programme in Engineering Sciences, Dissertation field: Technical Chemistry**, *TU Wien*, Dissertation: New approaches for elemental analysis of advanced solid materials using Laser-Assisted Plasma Spectrochemistry.

2017–2018 **Master's programme Technische Chemie**, *TU Wien*, Specialization: Applied analytical and physical chemistry, Passed with distinction .
Master thesis: Development of a LA-ICP-MS procedure for stoichiometry analysis of ternary boride thin films

2013–2017 **Bachelor programme Technical Chemistry**, *TU Wien*, Passed with distinction .

2004–2012 **Bundesgymnasium Oberschützen**, Matura passed with distinction .

Peer reviewed Publications

2022 **M. Weiss**, Z. Gajarska, H. Lohninger, M. Marchetti-Deschmann, G. Ramer, B. Lendl, and A. Limbeck. Elemental mapping of fluorine by means of molecular laser induced breakdown spectroscopy. *Anal Chim Acta*, volume 1195, page 339422, 2022.

2022 C. Riedl, M. Siebenhofer, A. Nenning, G. Friedbacher, **M. Weiss**, C. Rameshan, J. Bernardi, A. Limbeck, M. Kubicek, A. Karl Opitz, and J. Fleig. Performance modulation through selective, homogenous surface doping of lanthanum strontium ferrite electrodes revealed by in situ pld impedance measurements. *Journal of Materials Chemistry A*, 2022.

2022 T. Glechner, H. G. Oemer, T. Wojcik, **M. Weiss**, A. Limbeck, J. Ramm, P. Polcik, and H. Riedl. Influence of si on the oxidation behavior of tm-si-b2±z coatings (tm=ti, cr, hf, ta, w). *Surface and Coatings Technology*, 2022.

2022 C. Fuger, R. Hahn, L. Zauner, T. Wojcik, **M. Weiss**, A. Limbeck, O. Hunold, P. Polcik, and H. Riedl. Anisotropic super-hardness of hexagonal wb2±z thin films. *Materials Research Letters*, volume 10, pages 70–77, 2022.

2021 **M. Weiss**, C. Riedl, J. Frank, J. Fleig, and A. Limbeck. Quantitative analysis of the platinum surface decoration on lanthanum strontium iron oxide thin films via online-lasil-icp-ms. *Microchemical Journal*, volume 166, 2021.

2020 **M. Weiss**, H. Riedl, V. Moares, Paul H. Mayrhofer, and A. Limbeck. Laser based analysis of transition metal boride thin films using liquid standards. *Microchemical Journal*, volume 152, 2020.

2020 A. Pekarsky, S. Mihalyi, **M. Weiss**, A. Limbeck, and O. Spadiut. Depletion of boric acid and cobalt from cultivation media: Impact on recombinant protein production with komagataella phaffii. *Bioengineering (Basel)*, volume 7, 2020.

2020 C. Fuger, B. Schwartz, T. Wojcik, V. Moraes, **M. Weiss**, A. Limbeck, C. A. Macauley, O. Hunold, P. Polcik, D. Primetzhofer, P. Felfer, P. H. Mayrhofer, and H. Riedl. Influence of ta on the oxidation resistance of wb2z coatings. *Journal of Alloys and Compounds*, 2020.

Scientific conferences

Oral presentations

2022 M. Weiss, Z. Gajarska, H. Lohninger, and A. Limbeck. Fluorine imaging with molecular emission libs. 2022 Winter Conference on Plasma Spectrochemistry, 2022.

2021 M. Weiss, C. Riedl, H. Riedl, J. Frank, P.H. Mayrhofer, J. Fleig, and A. Limbeck. Online laser ablation of solids in liquids (lasil) as a versatile tool for quantitative thin film analysis. AOFKA - Applied Surface and Solid State Analytics, Freiberg, 2021.

2020 M. Weiss, J. Fleig, and A. Limbeck. Quantitative analysis of multi-layer systems with online laser-ablation of solids in liquid (lasil). 2020 Winter Conference on Plasma Spectrochemistry, Tucson, Arizona,US, 2020.

2019 M. Weiss, H. Riedl, P.H. Mayrhofer, and A. Limbeck. Determination of the stochiometric composition of ternary boride thin films via la-icp-ms and libs. ANAKON 2019, Münster, Germany, 2019.

2019 M. Weiss, H. Riedl, P.H. Mayrhofer, J. Fleig, and A. Limbeck. Laser based elemental analysis of multilayer systems. 20. Tagung Festkörperanalytik - 20th Conference on Solid State Analysis, Wien, 2019.

Posters

2022 M. Weiss, M. Podsednik, S. Larisegger, M. Nelhiebel, and A. Limbeck. Characterization of high-tech materials using online-lasi. 2022 Winter Conference on PlasmaSpectrochemistry, 2022.

2021 M. Weiss, Z. Gajarska, J. Lohninger, G. Ramer, B. Lendl, and A. Limbeck. Libs analysis of fluorine in solid samples via measurement of molecular emission bands. AOFKA - Applied Surface and Solid State Analytics, Freiberg, 2021.

2020 M. Weiss, St. Smetaczek, D. Rettenwander, J. Fleig, and A. Limbeck. Characterization of solid lithium ion conductors with libs. 2020 Winter Conference on Plasma Spectrochemistry, Tucson, Arizona, US, 2020.

2019 M. Weiss, D. Wipp, E. Povoden-Karadeniz, and A. Limbeck. La-icp-ms depth profiling of micro-alloyed steels. 20. Tagung Festkörperanalytik - 20th Conference on Solid State Analysis, 2019.

2019 M. Weiss, St. Smetaczek, D. Rettenwander, J. Fleig, and A. Limbeck. Libs as versatile tool for characterization of llzo garnets. EMSLIBS 2019, Brünn, 2019.

2019 M. Weiss, H. Riedl, P.H. Mayrhofer, and A. Limbeck. Quantification strategies for stoichiometry determination of thin films via la-icp-ms. 30th MassSpec-Forum Vienna, Vienna, 2019.

Coauthored conference contributions

2021 A. Limbeck, M. Weiss, Z. Gajarska, G. Ramer, B. Lendl, and J. Lohninger. Analysis of fluorine in polymer samples using libs via measurement of molecular emission bands. SCIX 2021, 2021.

2021 T. Glechner, R. Hahn, A. Bahr, T. Wojcik, M. Weiss, J. Ramm, O. Hunold, S. Kolozsvári, and H. Riedl. Alloying of period vi transition metal boride-based coatings for ultra-high temperature oxidation protection. AVS 67 Virtual Symposium, 2021.

2020 C. Fuger, B. Schwartz, T. Wojcik, V. Moraes, M. Weiss, C. Macauley, O. Hunold, P. Polcik, D. Primetzhofer, P. Felfer, P.H. Mayrhofer, and H. Riedl. Influence of ta on the oxidation resistance of wb2-z coatings. AVS 2020 International Twitter Poster Competition, 2020.

2020 C. Fuger, B. Schwartz, T. Wojcik, V. Moraes, M. Weiss, A. Limbeck, C. Macauley, O. Hunold, P. Polcik, D. Primetzhofer, P. Felfer, P.H. Mayrhofer, and H. Riedl. Oxidation resistance of ta doped wb2-z coatings. 17th International Conference on Plasma Surface Engineering, 2020.

2019 D. Wipp, M. Weiss, A. Limbeck, A. Gramlich, S. Zamberger, M. Galler, and E. Povoden-Karadeniz. Tracing competitive segregation effects in boron containing micro-alloyed steels. Materials Science Technology, 2019.

2019 D. Wipp, L. Volgger, H. Hutter, A. Gramlich, Limbeck A. Weiss, M., S. Zamberger, M. Galler, and E. Povoden-Karadeniz. Successful determination of trace element boron in steel by combined high-resolution analytical techniques. Euromat 2019, 2019.

2019 A. Limbeck, M. Weiss, H. Riedl, and P.H. Mayrhofer. Development of laser based procedures for stoichiometry analysis of ternary boride thin films. 2019 European Winter Conference on Plasma Spectrochemistry, 2019.

Awards

2022 ***Best Poster Award at the 2022 Winter Conference on Plasma Spectrochemistry in Tuscon, Arizona***

2021 ***2nd Best Poster Award at the AOFKA2021 in Freiberg***

2018 ***Performance Scholarship of the TU Wien***

2017 ***Performance Scholarship of the TU Wien***

Professional Experience

2018–2022 **Project Assistant**, *TU Wien, Institute of Chemical Technologies and Analytics*.

July 2014 **Internship at the municipal wastewater treatment facility**, *Gemeinde Rechnitz*.

2012-2013 **Civilian Service as Paramedic**, *Österreiches Rotes Kreuz , Bezirksstelle Oberwart*.

July 2011 **Internship**, *Raiffeisenbezirksbank Oberwart*.

Computer skills

Programming Languages	Python(proficient), C (basic), Arduino(basic), Matlab (basic)
Data Analysis	Microsoft Excel(proficient), OriginLab Origin(very good), R (basic)
Visualization	Adobe Illustrator, Adobe Photoshop, Inkscape, ImageJ
Word Processing	Microsoft Word, LaTex, Adobe Indesign
CAD	Autodesk Inventor

Languages

Mother Language	German
Fluent	English
Very Good	Spanish, Latin